January 2019

Endolysosome Dysfunction And Inter-Organellar Signalling: An 'Iron-Ic' Story

Peter Halcrow

ENDOLYSOSOME DYSFUNCTION AND INTER-ORGANELLAR SIGNALLING:
AN 'IRON-IC' STORY

by

Peter W. Halcrow

Masters of Science: Biophysics

California State University, Dominguez Hills

A Dissertation

Submitted to the Graduate Faculty

of the

University of North Dakota

In partial fulfillment of the requirements

for the degree of Doctor of Philosophy in Biomedical Sciences

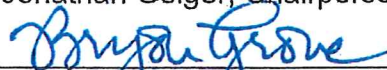Grand Forks, North Dakota

August

2019
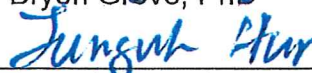
This dissertation, submitted by Peter W. Halcrow in partial fulfillment of the requirements for the Degree of Doctor of Philosophy from the University of North Dakota, has been read by the Faculty Advisory Committee under whom the work has been done and is hereby approved.

Jonathan Geiger, Chairperson

Bryon Grove, PhD

Junguk Hur, PhD

Joyce Ohm, PhD

Marc Basson, MD, Member at Large

This dissertation is being submitted by the appointed advisory committee as having met all of the requirements of the School of Graduate Studies at the University of North Dakota and is hereby approved.

Chris Nelson, PhD
Assoc. Dean of the School of Graduate Studies

7/19/19
Date

iii

PERMISSION

Title: Endolysosome Dysfunction and Inter-Organeller Signalling:
              An 'Iron-ic' Story

Department: Biomedical Sciences

Degree: Doctor of Philosophy

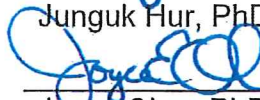In presenting this dissertation in partial fulfillment of the requirements for a graduate degree from the University of North Dakota, I agree that the library of this University shall make it freely available for inspection. I further agree that permission for extensive copying for scholarly purposes may be granted by the professor who supervised my dissertation work, or in his absence, by the Chairperson of the department or the dean of the School of Graduate Studies. It is understood that any copying or publication or other use of this dissertation or part thereof for financial gain shall not be allowed without my written permission. It is also understood that due recognition shall be given to me and to the University of North Dakota in any scholarly use which may be made of any material in my dissertation.

<div align="right">

Peter W. Halcrow
August, 2019

</div>

TABLE OF CONTENTS

ix

LIST OF FIGURES

ACKNOWLEDGMENTS

sharing ideas and thoughts at conferences across the country, and for the others as well. I would like to thank my committee for being a part of my research development and expanding my knowledge of how to conduct experiments and further test exciting research areas that may have clinical applications.

Finally, I would like to thank my loving and caring mother, Dr. Ruth Scott, as well as her late mother Nellie Scott. They have shown me great patience, understanding, and support all these years. For Nellie who taught me to count uncooked beans on her front porch when I was at the age of 3…thank you for your devotion to education, honesty, and sincerity. For Dr. Ruth Scott who has been the complete cornerstone in my life…without you this is not possible.

ABSTRACT

Endosomes and lysosomes (endolysosomes) are acidic organelles that are important both physiologically and pathologically. Implicated in the physiological and pathophysiological processes regulated by endolysosomes are readily releasable stores of cations including ferrous iron (Fe^{2+}); an essential cofactor for the generation of reactive oxygen species (ROS). In determining the extent to which and mechanisms by which Fe^{2+} released from endolysosomes affects cellular functions it was important to determine levels of Fe^{2+} in endolysosomes. In some cells and by other researchers, FeRhoNox-1 was found to detect Fe^{2+} in acidic organelles known as Golgi. Here, using U87MG astrocytoma cells and primary cultures of rat neurons we report that FeRhoNox-1 is highly specific for Fe^{2+}, that FeRhoNox-1 positive stores are largely localized in endolysosomes and not in Golgi, that control levels of Fe^{2+} were 36.3 ± 13.6 µM in endolysosomes, and that the stores of Fe^{2+} in endolysosomes increased to 75 ± 15.7 µM when cells were incubated with ferric ammonium citrate and decreased to 0.08 ± 0.05 µM when cells were incubated with the iron chelator deferoxamine. Furthermore, subpopulations of endolysosomes exist with extensive variability in Fe^{2+} content. Our findings demonstrate the utility of using FeRhoNox-1 to measure Fe^{2+} stores in endolysosomes and suggest that this probe will find important uses in better understanding cellular events downstream of released endolysosome Fe^{2+}.

Mitochondria are subject to iron overload under a variety of conditions and disease states, but it is not clear what are the subcellular origins of this iron nor its consequences. Endolysosomes are storage sites of ferrous iron (Fe^{2+}), and the degree to which and the precise mechanisms by which endolysosome Fe^{2+} contribute to iron-dependent changes to mitochondria and cell injury remains uncertain. Here, our studies were aimed to determine the role of inter-organellar signaling of Fe^{2+} from iron-rich endolysosomes to mitochondria under pharmacologically-induced conditions. We demonstrated, in U87MG astrocytoma cells, mouse primary hepatocytes, and primary cultures of rat cortical neurons, that Fe^{2+} within endolysosomes was translocated to the mitochondria resulting in mitochondrial dysfunction and cell death. The weak-base chloroquine and the vacuolar-ATPase inhibitor bafilomycin A1 both de-acidify endolysosomes and both induced the release of Fe^{2+} and this resulted in increased concentrations of Fe^{2+} in the cytoplasm and in mitochondria. Furthermore, the endocytosed iron chelator, deferoxamine, inhibited the release of bafilomycin A1- and chloroquine-induced release of endolysosome stores of Fe^{2+} and prevented the induced increases of ROS in cytoplasm and mitochondria. These findings demonstrate that redox-active Fe^{2+} in endolysosomes plays a key upstream role in mitochondrial iron accumulation and dysfunction, and deferoxamine might be potential adjunctive therapeutic strategies in preventing neurotoxicity and enhancing therapeutic outcomes of disease.

Drugs of abuse including the opioid morphine increase levels of reactive oxygen species (ROS) and predispose cells to insult-induced cell death.

However, it remains uncertain as to the underlying mechanisms. Iron has long been known to be required for the generation of mitochondrial ROS and endolysosomes are major storage sites of ferrous iron (Fe^{2+}). Yet, the degree to which and the precise mechanisms by which endolysosome iron plays a role in mitochondrial dysfunction remains uncertain. Here, our studies were aimed to determine the effects of morphine on inter-organellar signaling of Fe^{2+} from iron-rich endolysosomes to mitochondria. We demonstrated, in U87MG astrocytoma cells, that endolysosome Fe^{2+} is translocated to mitochondria and results in mitochondrial dysfunction. Morphine de-acidification of endolysosomes caused the release of Fe^{2+} from endolysosomes and increased levels of Fe^{2+} in cytosol and in. The morphine-induced effects on endolysosome Fe^{2+} appeared to be regulated through mu opioid receptors because naloxone blocked the de-acidification of endolysosomes by morphine and the release of endolysosome iron. Furthermore, the endocytosed iron chelator, deferoxamine, inhibited the release of redox-active Fe^{2+} into the cytosol and the morphine-induced increases in mitochondrial ROS. These findings demonstrate that redox-active Fe^{2+} in endolysosomes plays a key upstream role in mitochondrial dysfunction, and deferoxamine might be a potentially useful therapeutic strategy associated with opioid use disorders.

HIV-associated neurocognitive disorder (HAND) affects 50% of people living with HIV-1 despite viral suppression achieved by antiretroviral therapies. Pathologically, brain tissue from HAND patients has shown morphological changes to intracellular organelles including endolysosomes and mitochondria.

Moreover, people living with HIV-1 show elevated iron serum levels and iron chelators have been suggested as an adjuvant therapy to antiretroviral therapeutics. Mechanistically, soluble factors including the HIV-1 coat protein gp120 have been implicated in HAND pathogenesis. Here, we tested the hypothesis that HIV-1 gp120-induced de-acidification of endolysosomes leads to an efflux of iron from endolysosomes and a subsequent increase in levels of cytosolic and mitochondrial reactive oxygen species (ROS). We used U87MG glioblastoma cells and time-lapse confocal microscopy to measure gp120-induced changes in endolysosome pH, endolysosome iron, cytosolic and mitochondrial iron, and ROS levels. HIV-1 gp120 de-acidified endolysosomes, reduced endolysosome iron levels, increased levels of cytosolic and mitochondrial iron, and increased levels of cytosolic and mitochondrial ROS. These effects were all attenuated significantly by the iron chelator deferoxamine that only enters cells via endocytosis. These results suggest that cellular and subcellular effects of HIV-1 gp120 can be downstream of its ability to de-acidify endolysosomes and increase the release of iron from endolysosomes. Thus, endolysosomes might represent an early and upstream target for therapeutic strategies against HAND.

CHAPTER 1

INTRODUCTION

Endosomes and Lysosomes

The discovery and functional significance of endosomes and lysosomes were honored with Nobel prizes for lysosomes in 1955 by Christian de Duve (de Duve, 2005) and for endosomes and endocytosis in 1985 (Motulsky, 1986). Endosomes are membrane-bound compartments involved in the endocytic transport pathway, and molecules or ligands internalized from the plasma membrane follow this pathway to lysosomes for degradation. Alternatively, endocytosed materials and endosomes themselves can be recycled back to the plasma membrane from which they can release their contents extracellularly (Stoorvogel et al., 1991). The endomembrane system includes endosomes, lysosomes, the Golgi apparatus, endoplasmic reticulum, nuclear membranes; endosomes are known as sorting compartments of this system (Mellman, 1996). Endosomes are classified as early, sorting, or late, and as endosomes mature their lumen becomes more acidic where, eventually, they fuse with lysosomes as shown in Figure 1.1 (Futter et al., 1996, Luzio et al., 2000, Lafourcade et al., 2008). This transition from late endosomes to lysosomes is unidirectional since late endosomes are consumed in the process of fusing with lysosomes. Thus,
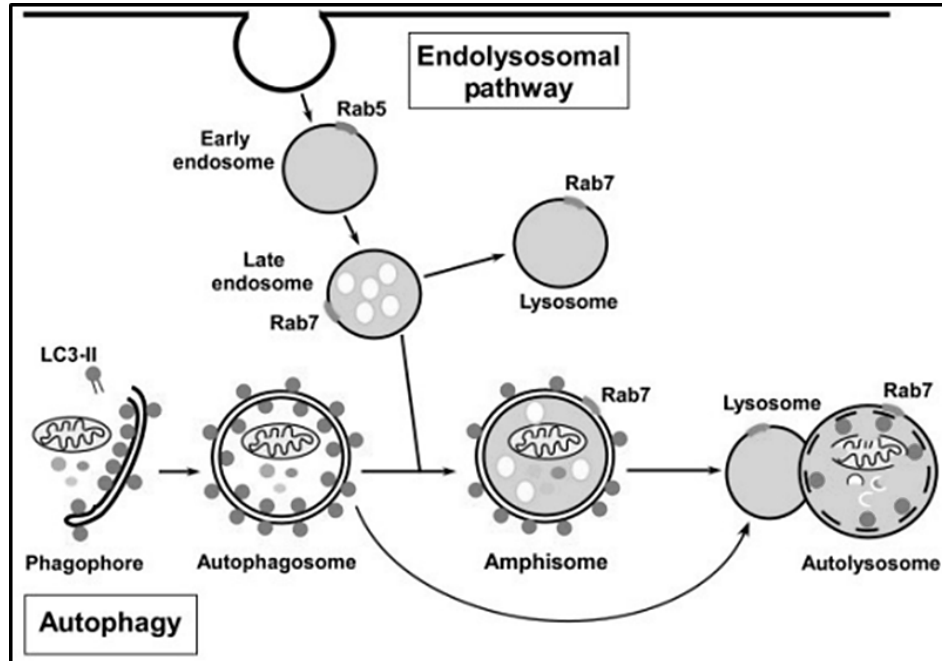
Figure 1. 1.   The endolysosomal pathway: Schematic diagram showing early endosomes maturing into lysosomes. Also, the autophagy process is followed by fusion of autophagosomes either with lysosomes to form autophagosomes, or to late endosomes in which amphisomes fuse with lysosomes to form autolysosomes. (Cited from Hansen, T. BMC Biology (2011)).

molecules in the lumen of endosomes transition into lysosomes. Because

endosomes fuse with lysosomes as a part of the endomembrane pathway and

the two are not distinguished in this study, the term "endolysosomes" will be used

hereafter.

Endolysosomes have many key physiological functions including plasma

membrane repair, cell homeostasis, energy metabolism, signal transduction, and

immune responses (Settembre et al., 2013, Perera and Zoncu, 2016). The main

function of endolysosomes is to process molecules taken in by cells and to

recycle damaged cellular components, both of which are conducted by the

hydrolytic enzymes within the lumen of endolysosomes (Perera and Zoncu,

2016). A defining feature of endolysosomes is their acidic internal pH, which ranges from 4.5 to 5.5. The acidic nature of endolysosomes is established and maintained by vacuolar H^+ ATPase (v-ATPase) that pumps protons into the lumen of endolysosomes in conjunction with counterflux of other ion species such as Cl-, Na+, and K+ through membrane channels (Forgac, 2007, Ishida et al., 2013, Mindell, 2012B). The acidic luminal pH of endolysosomes provides an optimal environment for hydrolases that catalyze the degradation of macromolecules and the production of amino acids, monosaccharides, and free fatty acids, which are exported throughout the cell via permeases (Jezegou et al., 2012, Rong et al., 2012, Liu et al., 2012, Sagne et al., 2001). The multiple endocytic pathways, including phagocytosis, macropinocytosis, clathrin and caveolin-dependent and -independent endocytosis, import macromolecules from the extracellular space to the endolysosome system for degradation (Conner and Schmid, 2003, Di Fiore and von Zastrow, 2014, Goldstein and Brown, 2015). It is through the self-catabolic process of autophagy that cytoplasmic macromolecules, damaged or misfolded proteins, and even entire organelles are captured and delivered to endolysosomes (Kaur and Debnath, 2015, Mizushima and Komatsu, 2011). Hence, endolysosomal processing of a variety of cargo is essential for the removal of cellular components, the elimination of damaged organelles, the termination of signal transduction, and the maintenance of metabolic homeostasis. These functions underscore the fundamental role of endolysosomes in maintaining cellular health.

Endolysosomes are storage sites for ions including H^+, Na^+, K^+, Cl^-, Ca^{2+}, Zn^{2+}, Fe^{3+}, and Fe^{2+} (Xu and Ren, 2015, Xiong and Zhu, 2016b) as they integrate and digest materials compartmentalized by endocytosis, phagocytosis or autophagy. These endolysosome ions have key roles in cellular functions. As known, H^+ ions are important in maintaining the acidic environment, which provides an optimal environment for the activity of endolysosomal digestive enzymes (Mindell, 2012a). Ca^{2+} plays a role in vesicle trafficking (Wong et al., 2012), and Na^+ is important in the function of endolysosome transporters, including the SLC38 family transporters (Mackenzie and Erickson, 2004, Wang et al., 2015). K^+ is known to regulate the membrane potential of endolysosomes as well as the Ca^{2+} homeostasis of endolysosomes (Cang et al., 2015, Cao et al., 2015). Cl^- regulates the membrane potential of endolysosomes as a counter-ion and also facilitates acidification of endolysosomes (Kasper et al., 2005, Lange et al., 2006). Fe^{2+} catalyzes the hydrolysis of H_2O_2 and produces reactive oxygen species (Dixon et al., 2012, Fenton, 1894). And, Zn^{2+} serves as a key coenzyme for many proteins (Tapiero and Tew, 2003). In addition, there are ion channels and transporters that mediate the flux or transport of these ions across endolysosomal membranes. As an example, two pore channels (TPCs) conduct Na^+ and Ca^{2+} release from endolysosomes (Ishibashi et al., 2000, Calcraft et al., 2009, Wang et al., 2012), and transient receptor potential mucolipin (TRPML) channels form non-selective cation channels on endolysosome membranes that are permeable to many types of positively charged ions (Dong et al., 2008, Eichelsdoerfer et al., 2010). Furthermore, defects in ion exchange can lead to

abnormal endolysosome morphology, defective vesicle trafficking, impaired autophagy, and diseases such as neurodegeneration and lysosomal storage disorders (Wong et al., 2012, Kasper et al., 2005, Cang et al., 2015, Lange et al., 2006). Therefore, ions within endolysosomes play critical roles in maintaining endolysosomal function and these same ions can regulate cell survival.

Drug-induced de-acidification of the endolysosomes causes an efflux of cations such as Ca^{2+} from endolysosomes into the cytosol (Christensen et al., 2002, Fernández et al., 2016b). These released cations then play crucial roles in exploiting cellular signaling pathways including endolysosomal exocytosis (Cheng et al., 2014, Medina et al., 2011). Thus, it has been important to determine the concentrations of endolysosomal ions to fully understand the roles they play in cellular function and dysfunction, as well as drug-induced ramifications due to altered ion homeostasis within endolysosomes. In endolysosomes, Na^+ concentrations are in the range of 20-140 mM and K^+ concentrations are in the range of 2-50 mM; both play key roles in controlling endolysosome acidification (Steinberg et al., 2010, Wang et al., 2012). Ca^{2+} concentration in endolysosomes is about 0.5 mM (Christensen et al., 2002, Lloyd-Evans et al., 2008), and Ca^{2+} efflux from endolysosomes is known to be important for signal transduction, organelle homeostasis, and organelle acidification (Luzio et al., 2000, Dong et al., 2010, Luzio et al., 2007, Morgan et al., 2011). Cl^- concentrations within endolysosomes are about 80 mM (Stauber and Jentsch, 2013) and affect the function of catabolite exporters and regulate Ca^{2+} release (DeFelice and Goswami, 2007, Saito et al., 2007). Although

endolysosomes are the intracellular source of ferric iron (Fe^{3+}) and ferrous iron (Fe^{2+}), little to nothing is known about the level of ferrous iron stored within endolysosomes. One review article stated that Fe^{2+} ions within endolysosomes are in the low micromolar range (2-5 µM) because a higher ferrous iron concentration would lead to elevated ROS causing cell damage (Kiselyov et al., 2011, Mills et al., 2010). However, the referred to study used the cytosolic iron stain Phen-Green to measure intracellular labile iron, which is not a measurement of endolysosome iron concentrations. Upon a further literature search, the Fe^{2+} concentration within endolysosomes was not found, possibly due to a lack of available probes. With ferrous iron being important in the formation of reactive oxygen species and oxidative damage, it is important to determine endolysosome levels of ferrous iron.

Fenton Reaction, Haber-Weiss Reactions, and Reactive Oxygen Species

In 1894, H.J.H Fenton discovered that several metals have a special oxygen transfer property which improves the use of hydrogen peroxide. Since this discovery the iron-catalyzed production of hydrogen peroxide has been called Fenton's reaction (Fenton, 1894). In addition, Fritz Haber and his student Joshua Weiss in 1932 developed the Haber-Weiss reaction in which hydroxyl radicals are generated from hydrogen peroxide and superoxide (Weiss, 1934). The main finding by Haber and Weiss was that hydrogen peroxide is decomposed by a chain reaction (Koppenol, 2001) and it proceeds by successive steps as shown below in Figure 1.2. Ferrous iron within the cell, known as free labile iron or chelatable iron, is a key reactant in the formation of the highly

---

Fenton and Haber-Weiss Reactions

The Haber-Weiss chain is initiated by the Fenton reaction:

$Fe^{2+} + H_2O_2 \rightarrow Fe^{3+} + HO^- + HO^•$ (step 1: initiation)
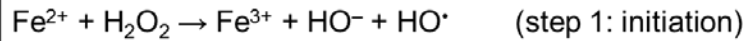
Then, the reaction chain propagates by means of two successive steps:

$HO^• + H_2O_2 \rightarrow H_2O + O_2^{•-} + H^+$ (step 2: propagation)

$O_2^{•-} + H^+ + H_2O_2 \rightarrow O_2 + HO^• + H_2O$ (step 3: propagation)
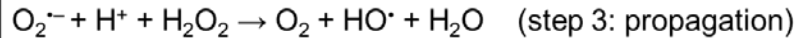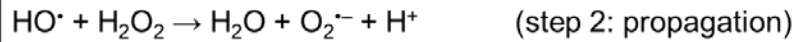
Finally, the chain is terminated when the hydroxyl radical is scavenged:

$Fe^{2+} + HO^• + H^+ \rightarrow Fe^{3+} + H_2O$ (step 4: termination)
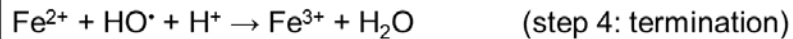
Of note, ferrous iron can generate a superoxide:

$Fe^{2+} + O_2 \rightarrow Fe^{3+} + O_2^{•-}$
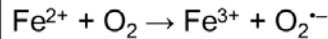
Figure 1. 2.   Fenton and Haber-Weiss Reactions: H.J.H Fenton discovered that iron catalyzed hydrogen peroxide, and Haber and Weiss discovered hydroxyl radicals are generated from hydrogen peroxide and superoxide.

reactive hydroxyl radical ($HO^•$) from H_2O_2 and superoxide (O_2^-) from O_2, which damages DNA, proteins, and membranes (Fenton, 1894) (Kehrer, 2000). The generation of reactive oxygen species (ROS) contributes to cellular dysfunction and cell death from oxidative stress and ischemia or reperfusion (Jaeschke et al., 2002, Videla et al., 2003, Schwabe and Brenner, 2006). In 1970, there was an emerging interest for the effect of free radicals on ageing mechanisms of living cells due to oxygen (O_2), so it was proposed that the Haber–Weiss reaction was a source of radicals responsible for cellular oxidative stress. However, this hypothesis was later disproved (Koppenol, 2001). The oxidative stress toxicity is

not caused by the Haber–Weiss reaction as a whole, but by the Fenton reaction, which is one specific part of it (Koppenol, 2001).

Mitochondria, ROS, and Cellular Dysfunction

The term "mitochondria" was coined by Carl Benda in 1898 (Benda, 1898, Ernster and Schatz, 1981). Friedrich Meves made the first recorded observation of mitochondria in plants in 1904, and in 1925 the respiratory chain was described when David Keilin discovered cytochromes (Ernster and Schatz, 1981). A mitochondrion is a double-membrane bound organelle in eukaryotic cells that generates most of the cell's adenosine triphosphate (ATP) as a chemical source of energy; thus, mitochondria are termed the "powerhouse" of the cell (Siekevitz, 1957). In addition, mitochondria have key roles in signaling, cellular differentiation, cell death, and controlling the cell cycle and cell growth (McBride et al., 2006). Therefore, it is not surprising that mitochondrial dysfunction has been implicated in human disease including cardiac dysfunction (Lesnefsky et al., 2001), heart failure (Dorn et al., 2015), autism (Griffiths and Levy, 2017), and neurodegenerative diseases (Johri and Beal, 2012).

Mitochondria are an important source of ROS and they participate in redox signaling throughout cells (Andreyev et al., 2005, Muller, 2000, Balaban et al., 2005). The first report that the respiratory chain produced ROS came in 1966 (Jensen, 1966), which was followed by the pioneering work of Chance and his colleagues in 1979 who showed that isolated mitochondria produce H_2O_2 (Chance et al., 1979). Later, it was confirmed that H_2O_2 generated within mitochondria was catalyzed from the dismutation of superoxide (Loschen et al.,

1974). Near the same time, it was discovered that mitochondria contain their own SOD (superoxide dismutase) and MnSOD (manganese superoxide dismutase), which confirmed the biological significance of mitochondrial superoxide production (Weisiger and Fridovich, 1973). Since then, the literature has further elucidated the sources and consequences of mitochondrial ROS production and how it contributes to cellular dysfunction and a range of pathologies (Balaban et al., 2005, Droge, 2002). Specifically, it is now known that ROS production leads to oxidative damage of proteins, membranes, lipids, and DNA, as well as impairing mitochondria from synthesizing ATP and conducting normal metabolic functions such as amino acid metabolism, the tricarboxylic acid cycle, the urea cycle, and Fe-S assembly as shown in Figure 1.3 (Murphy, 2009).

Mitochondria have important functions in iron metabolism that includes the synthesis of iron-sulfur clusters (ISCs) and heme; both are vital for normal cell function. Iron is an important molecule involved in the electron transport chain because 12 proteins contain ISCs and 8 proteins contain heme in their active centers (Rouault and Tong, 2005). Further, mitochondria have a readily-available pool of redox-active iron (Petrat et al., 2002), and an increase in this iron pool directly associates with an increase in oxidative damage (Pelizzoni et al., 2011, Kumfu et al., 2012). Thus, mitochondrial iron levels are tightly regulated because a shortage affects processes that require iron as a co-factor such as the electron transport chain, whereas an excess of redox-active iron promotes the generation of elevated levels of ROS. Not surprisingly, mitochondrial iron accumulation has been associated with diseases including cancer and neurodegenerative diseases
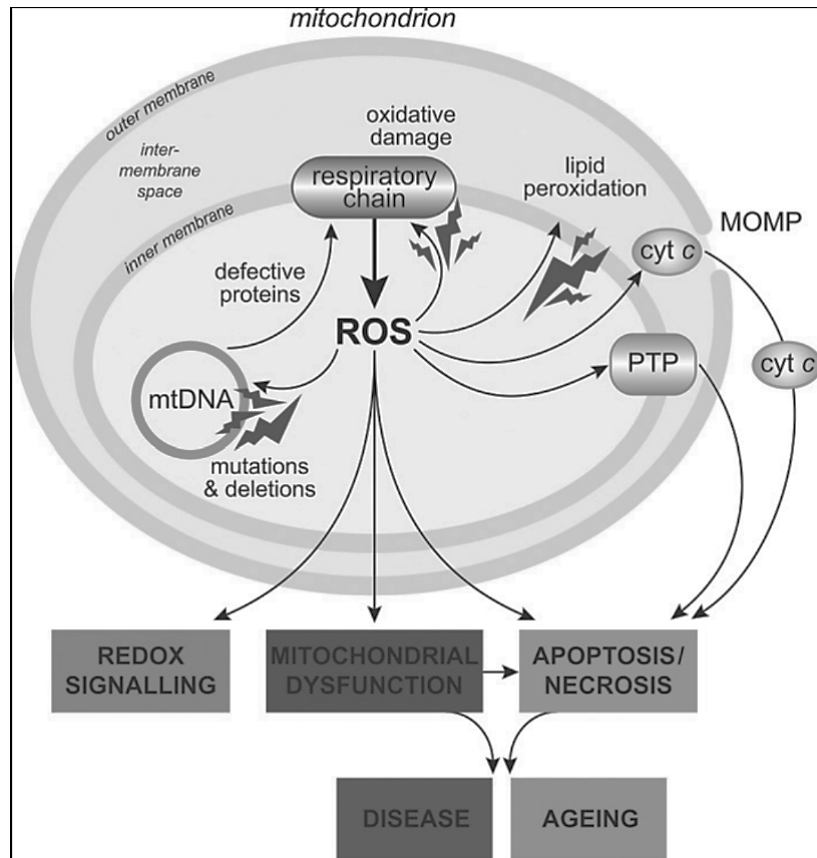
Figure 1. 3.   Effects of mitochondrial ROS on cell physiology. ROS production within mitochondria leads to oxidative damage to proteins, membranes, lipids, and DNA, as well as impair mitochondria to synthesize ATP and carry out normal metabolic functions. Oxidative damage within mitochondria causes the release of cytochrome c to the cytosol and activating apoptosis, thus, mitochondrial damage contributes to a wide range of diseases. (Cited from Murphy, M., Biochemical Journal, 2009)

(Zecca et al., 2004, Andersen et al., 2014, Urrutia et al., 2014, Enns, 2003).

Cancer cells have a much higher requirement for iron and are sensitive to iron depletion (Richardson et al., 2009), and studies have shown that iron chelators induce apoptosis in cancer cells in vitro and reduce tumor size in vivo (Richardson et al., 2009, Kalinowski and Richardson, 2007). However, the mechanism of action by which iron chelators affect physiological and pathological processes are not fully understood (Bystrom et al., 2014). Although iron

10

metabolism and mitochondrial iron has been studied extensively, it still remains unclear where the excess iron in mitochondria is coming from and whether or not mitochondrial iron accumulation is a downstream or upstream event of disease.

Deferoxamine (DFO)

Deferoxamine (DFO), otherwise known as Desferal or desferoxamine, is an iron chelator that was approved for medical use in 1968 (Ballas et al., 2018). Clinically, it is the only iron chelator proven of benefit and is used as adjunctive therapy for patients with acute iron overload or hemochromatosis (Mobarra et al., 2016). DFO binds ferric and ferrous iron tightly rendering the molecule inactive and incapable of catalyzing redox reactions. DFO is used to treat iron overload because it has a large preference for iron over other ions such as calcium ($K_d=10^{-31}$ M for iron, $K_d=10^{-9}$ M for calcium) (Keberle, 1964). Iron ions have six electrochemical coordination sites, and a chelator molecule that binds all six sites completely inactivates labile iron. These chelators are termed hexidentate, and DFO is an example that chelates iron in a one-to-one ratio (Keberle, 1964). Furthermore, it has been shown that DFO cannot enter the cell by passive diffusion but enters the cell by endocytosis and remains within endolysosomes (Doulias et al., 2003, Lloyd et al., 1991b).

Rationale, Purpose, and Hypotheses

Previous studies have emphasized the importance of measuring the concentration of ferrous iron in endolysosomes, which could lead to determining the extent to which and the mechanisms by which endolysosome Fe^{2+} plays a role in cellular processes (Xiong and Zhu, 2016b). However, to-date there are no

available probes with which to assess endolysosome Fe^{2+}. Therefore, the purpose of the first study, outlined in Chapter 2, is to characterize a fluorescence probe that might be specific for ferrous iron within endolysosomes and that might find use as a probe to measure the iron concentrations in various types of cells. The hypothesis to be tested in our first study was that FeRhonox-1 is highly specific for Fe^{2+} molecules, localizes to endolysosomes, and it can be used to determine the role of endolysosome Fe^{2+} in cellular mechanisms.

Previous studies have shown that de-acidification of endolysosomes induced by certain drugs such as bafilomycin A1 and chloroquine causes a release of Ca^{2+} from endolysosomes into the cytosol (Christensen et al., 2002, Fernández et al., 2016b). In addition, previous works have determined the significant role iron plays in mitochondrial damage without the knowledge of where excess iron is coming from (Stehling et al., 2013, Carroll et al., 2011). Therefore, the purpose of the second study, outlined in Chapter 3, is to determine the role of endolysosome ferrous iron in inter-organelle communication with mitochondria. The hypothesis of this study is that ferrous iron within endolysosomes is translocated to the mitochondria induced by the pharmacological agents' chloroquine and bafilomycin A1 that de-acidify the endolysosomes. The increase in mitochondrial iron leads to increased ROS levels and cell death.

The third study, outlined in Chapter 4, is an extension of the second study but looking at drugs of abuse. Drugs of abuse have been associated with neurodegenerative disorders, and, more specifically, evidence shows that drugs

of abuse increase free radicals and mitochondrial dysfunction such as decreased cellular energy production (Xu et al., 2011, Cunha-Oliveira et al., 2013). The purpose of this study is to determine if a drug of abuse, morphine, causes mitochondrial dysfunction due to endolysosome communication by Fe^{2+}. The hypothesis of this study is that morphine de-acidifies endolysosome pH releasing Fe^{2+} into the cytosol and then taken up by the mitochondria leading to mitochondrial ROS.

The fourth study, outlined in Chapter 5, which is also an extension of the second study looks at HIV-1 associated proteins and their effect on endolysosomes and mitochondrial communication by exploiting iron. Previous studies have shown that the HIV-1 associated proteins glycoprotein (gp120) and trans-activator of transcription protein (Tat) exploit endolysosome Ca^{2+} and pH (Nath et al., 1995, Hui et al., 2012b)). Thus, the purpose of this study is to determine the role of gp120 in endolysosome and mitochondria communication by iron. The hypothesis of this study is that gp120 de-acidifies endolysosome, releases endolysosome iron into the cytosol, and this iron is taken up by the mitochondria.

CHAPTER 2

IDENTIFICATION AND MEASUREMENT OF FERROUS IRON IN ENDOLYSOSOMES USING FERHONOX-1, A FLUORESCENT PROBE FOR DETECTING LABILE FE^{2+} IN LIVING CELLS

Peter W. Halcrow, Gaurav Datta, Nicole Miller, Nabab Khan, Koffi L. Lakpa, Xuesong Chen and Jonathan D. Geiger

Department of Biomedical Sciences
University of North Dakota School of Medicine and Health Sciences
Grand Forks, North Dakota, 58202

Abstract

Endosomes and lysosomes (endolysosomes) are acidic organelles that are important both physiologically and pathologically. Implicated in the physiological and pathophysiological processes regulated by endolysosomes are readily releasable stores of cations including ferrous iron (Fe^{2+}); an essential cofactor for the generation of reactive oxygen species (ROS). In determining the extent to which and mechanisms by which Fe^{2+} released from endolysosomes affects cellular functions it was important to determine levels of Fe^{2+} in endolysosomes. In some cells and by other researchers, FeRhoNox-1 was found to detect Fe^{2+} in acidic organelles known as Golgi. Here, using U87MG astrocytoma cells and primary cultures of rat neurons we report that FeRhoNox-1 is highly specific for Fe^{2+}, that FeRhoNox-1 positive stores are largely localized in endolysosomes and not in Golgi, that control levels of Fe^{2+} were 36.3 ± 13.6 µM in endolysosomes, and that the stores of Fe^{2+} in endolysosomes increased to 75 ± 15.7 µM when cells were incubated with ferric ammonium citrate and decreased to 0.08 ± 0.05 µM when cells were incubated with the iron chelator deferoxamine. Furthermore, subpopulations of endolysosomes exist with extensive variability in Fe^{2+} content. Our findings demonstrate the utility of using FeRhoNox-1 to measure Fe^{2+} stores in endolysosomes and suggest that this probe will find important uses in better understanding cellular events downstream of released endolysosome Fe^{2+}.

Introduction

The existence and functional significance of lysosomes and endosomes was honored with Nobel prizes for lysosomes in 1955 (de Duve, 2005) and for endosomes and endocytosis in 1985 (Motulsky, 1986). Endosomes and lysosomes (here after referred to as endolysosomes) are now known to regulate many physiological functions including plasma membrane repair, cell homeostasis, energy metabolism, nutrient-dependent signal transduction, and immune responses (Perera and Zoncu, 2016, Settembre and Ballabio, 2013). Pathologically, morphological and functional changes to endolysosomes have been described for a wide spectrum of diseases including cancer and neurodegenerative diseases (Colacurcio and Nixon, 2016).

A defining feature of endolysosomes is their acidic luminal pH; a discovery that predates the description of lysosomes by 60 years (Lellouch, 1993). Endolysosome acidification is mainly regulated by vacuolar-ATPase that drives protons against their electrochemical gradients into the lumen of endolysosomes (Perera and Zoncu, 2016). Such transmembrane proton gradients are well known to exist in endolysosomes as well as in mitochondria, Golgi complex, secretory granules, and plasma membranes (Mindell, 2012a). Endolysosome acidity is also essential for the functionality of 60 different hydrolase enzymes and the fusing of autophagosomes with lysosomes to form autophagolysosomes (Ktistakis and Tooze, 2016).

Endolysosomes are known to contain high levels of transition metals including iron, copper and zinc as well as readily releasable stores of calcium

(Hui et al., 2015, Xu and Ren, 2015). Iron, in particular, is essential for a variety of important biological events and iron overload has been implicated in such diseases as cancer and neurodegenerative diseases. Ferric iron (Fe^{3+}) bound to transferrin enters cells by endocytosis whereupon it is reduced to unbound labile ferrous iron (Fe^{2+}). Because of the importance of Fe^{2+} as a catalyst of Fenton and Haber-Weiss reactions that generate potentially toxic levels of reactive oxygen species (ROS), it is important to know the extent to which and the mechanisms by which Fe^{2+} exits endolysosomes and enters the cytosol and mitochondria.

About five years ago, the fluorescence 'turn-on' probe FeRhoNox-1 was found to have pronounced specificity for Fe^{2+} versus other biologically relevant metal ions (Mukaide et al., 2014). It was also shown that FeRhoNox-1 labels Fe^{2+} stores in acidic Golgi organelles at least in some cells (Hirayama et al., 2013). However, to date, no reports have appeared determining whether FeRhoNox-1 labels Fe^{2+} alternatively in endolysosomes and whether FeRhoNox-1 can be used to quantitatively measure levels of Fe^{2+} in endolysosomes. Here, we report that FeRhoNox-1 was highly specific for Fe^{2+} versus other cations such as calcium, magnesium, copper and zinc. Further, FeRhoNox-1 positive stores were selectively localized in endolysosomes and that subpopulations of endolysosomes exist with extensive variability in Fe^{2+} content. And, finally as a proof of principle for quantitative measurements of labile iron stores, endolysosome Fe^{2+} stores were increased with ferric ammonium citrate supplementation and were decreased with the iron chelator deferoxamine. It is

likely that FeRhoNox-1 will find extensive use for better understanding the physiological relevance and pathological significance of Fe^{2+} in living cells.

Materials and Methods

Cultures of U87MG Astrocytoma Cells

U87MG cells were cultured in DMEM (Invitrogen) supplemented with 10% fetal calf serum and penicillin/streptomycin (Invitrogen). Cells were grown to about 40% confluence (~15,000 cells) in 35 mm^2 plastic culture dishes coated with poly-D-lysine in a 37°C and 5% CO_2 environment.

Primary Cultures of Rat Neurons

Primary neuronal cultures were prepared with cortical tissue from male and female Holtzman E17 rat embryos, as we have previously described (Festa et al., 2015, Sengupta et al., 2009, Pitcher et al., 2014). We prepare two different types of primary neuronal cultures, which allow for isolation of cortical neurons in the presence or absence of glia. Most of the experiments used primary cortical neurons grown in the absence of glia (neurobasal cultures), as originally described by (Brewer et al., 1993). Briefly, dissected cortical neurons were plated in Neurobasal medium containing 2% heat inactivated horse serum (Hyclone), 2% B-27 supplement 50X (Gibco), 1% GlutaMAX (Gibco), and X uM L-Glutamic acid (Tocris 0218) for the first four hours of culture. Next, cultures were washed with neurobasal medium, before replacement with the same neurobasal medium formula, without horse serum. On fifth day in vitro (DIV 5), medium was replaced with neurobasal, containing 2% B27 and 1% Glutamax; the medium was changed every four days for the rest of the culture. Select experiments used

primary cortical neurons cultured in the presence of a glial feeder layer (bilaminar cultures), as we described previously (Shimizu et al., 2011). The bilaminar culture system is more similar to the *in vivo* environment due to the presence of glia during neuronal maturation and throughout the culture; however, it still enables direct investigation of neurons, as they can be separated from the glial layer. Dissected primary neurons were plated in DMEM with 10% heat inactivated horse serum (Hyclone) for four hours. Following a wash with DMEM, culture media was changed to DMEM containing 1% N2.1 supplement (Gibco), and X mg Ovalbumin (Sigma). One-half of the culture medium was replaced every 7 DIV. Neurons were typically used for experiments from day 9-14 *in vitro*.

FeRhoNox-1 Specificity for Fe^{2+}

To determine the specificity of FeRhoNox-1 for Fe^{2+}, we first used a cell-free system and a LSM800 laser scanning microscope system (Zeiss). FeRhoNox-1 was added to plates at a final concentration of 10 µM, and $FeCl_2$, $FeCl_3$, $MgCl_2$, $CaCl_2$, and $ZnCl_2$ were added at final concentrations ranging from 1 to 1000 µM in water. Following the addition of the reagents, plates were incubated at room temperature for 1 h and then analyzed at an excitation wavelength of 537 nm and an emission wavelength of 569 nm.

Identification of FeRhoNox-1 Positive Organelles in U87MG Cells

Individual culture dishes containing U87MG cells were incubated with FeRhoNox-1 (10 µM) for 1 h, washed 3-times with PBS, and then imaged using a LSM800 laser scanning microscope system (Zeiss) at excitation and emission wavelengths of 537 and 569 nm, respectively. U87MG cells were incubated with

the late endosome/lysosome marker LysoTracker Green DND-26 (10 µM, Invitrogen) for 30 min at 37°C. Fields were chosen at random and at least five images from every experimental condition were acquired by confocal microscopy (LSM800, Zeiss). Pearson correlation coefficients were then determined for the colocalization of FeRhoNox-1 positive and LysoTracker-positive endolysosomes after the images were merged. Using Imaris software the LisICQ was determined for colocalization of FeRhonox-1 positive and LysoTracker-positive endolysosomes.

Identification of Golgi-Positive Organelles in U87MG Cells

CellLight™ Golgi-GFP, BacMam 2.0 (ThermoFisher) was used to stain Golgi. Golgi-GFP was added to dishes of U87MG cells at a concentration of 1×10^8 CellLight® particles/mL and after incubating cells overnight at 37°C in a 5% CO_2 environment, cells were washed 3-times with PBS and then imaged using confocal microscopy (LSM800, Zeiss) at excitation and emission wavelengths 488 and 510 nm, respectively. Pearson correlation coefficients were then determined for the colocalization of FeRhoNox-1 positive and LysoTracker-positive endolysosomes after the images were merged.

Materials

FeRhoNox-1 was purchased from Goryo Chemical Company (Japan). All other reagents including $FeCl_2$, $FeCl_3$, $MgCl_2$, $CaCl_2$, and $ZnCl_2$ were obtained from standard sources (Millipore Sigma and ThermoFisher).

Statistical Analysis

All data were presented as means $\pm$ standard deviation (SD). Statistical significance between two groups was analyzed with a Student's t-test, and statistical significance among multiple groups was analyzed with one-way ANOVA plus a Tukey post-hoc test. $p < 0.05$ was accepted to be statistically significant. Pearson Correlation Coefficients were performed using ImageJ software.

Results

FeRhoNox-1 specificity for Fe^{2+}

We first determined the specificity with which FeRhoNox-1 labels Fe^{2+}. FeRhoNox-1 at a concentration of (5 µM) was incubated for 1 h in the absence or presence of $FeCl_2$, $FeCl_3$, $MgCl_2$, $CaCl_2$, and $ZnCl_2$ at final concentrations ranging from 1 to 1000 µM. Following the incubations, aliquots were imaged by confocal microscopy. FeRhoNox-1 fluorescence was found to be highly specific for Fe^{2+} and not Fe^{3+} (Figure 2.1). FeRhoNox-1 fluorescence did not increase significantly in the presence of $MgCl_2$, $CaCl_2$ or $ZnCl_2$ at any of the concentrations tested (see Supplemental Figure S.2.A.).

FeRhoNox-1 labels endolysosome stores of Fe^{2+}

We next determined the extent to which FeRhoNox-1 positive stores of Fe^{2+} colocalized with LysoTracker-positive endolysosomes. Confocal microscope images of FeRhoNox-1 positive staining showed a normally distributed pattern of endolysosome staining (Figure 2.2). The late endosome/lysosome marker LysoTracker showed a staining pattern similar to that observed for FeRhoNox-1

in U87MG cells (Figure 2) and in primary cultures of rat neurons (Data not shown). When the images for FeRhoNox-1 and LysoTracker were merged, the staining patterns showed a very high degree of colocalization; the Pearson correlation coefficient for the colocalization was 0.84 $\pm$ 0.03.

To further differentiate the observed localization of FeRhoNox-1 in endolysosomes, we determined next the extent to which FeRhoNox-1 staining colocalized with EEA1-positive early endosomes and LAMP1-positive late endosomes/lysosomes. As expected, confocal microscope images of FeRhoNox-1 positive staining showed a normally distributed pattern of staining (Figure 2.3). The FeRhoNox-1-positive staining showed a very high degree of colocalization with EEA1-positive endosomes; the Pearson correlation coefficient for RhoNox-1 and EEA1 colocalization was 0.86 $\pm$ 0.04. The FeRhoNox-1-positive staining also showed a moderate degree of colocalization with the LAMP1-positive late endosomes/lysosomes; the Pearson correlation coefficient for FeRhoNox-1 and LAMP1 colocalization was 0.56 $\pm$ 0.05.

FeRhoNox-1 Positive Stores of Fe^{2+} Were Not Highly Expressed in Golgi

Having observed FeRhoNox-1 positive staining in endosomes and lysosomes, we next wanted to specifically determine the extent to which FeRhoNox-1 positive staining might also be co-localized in Golgi. FeRhoNox-1-positive and Golgi Tracker-positive Golgi staining was observed in U87MG cells, but the staining patterns showed distinct differences (Figure 2.4). When the images were merged, FeRhoNox-1-positive staining a weak degree of

colocalization with Golgi Tracker-positive staining (Figure 2.4); the Pearson

correlation coefficient for the colocalization was 0.13 $\pm$ 0.06.

FeRhoNox-1 Fluorescence Intensity Increased with Ferric Ammonium Citrate (FAC) and Decreased with Deferoxamine (DFO)

As a proof of principle for the utility of FeRhoNox-1 to measure

quantitatively labile levels of iron, we next determined the extent to which

increasing or decreasing levels of Fe^{2+} in endolysosomes were reflected by

changes in FeRhoNox-1 fluorescence intensity. Incubation of U87MG cells for

1 h with FAC (50 µM) to increase levels of endolysosome Fe^{2+} resulted in

statistically significant (p<0.001) increases in FeRhoNox-1 fluorescence intensity

to 146 $\pm$ 6 % from that of normal control cells of 101 $\pm$ 5 % (Figure 5B,D).

Incubation of U87MG cells for 1 h with the iron chelator DFO (25 µM) to decrease

levels of Fe^{2+} in endolysosomes resulted in statistically significant (p<0.0001)

decreases in FeRhoNox-1 fluorescence intensity to 51 $\pm$ 5 % of control values

(Figure 5C,D). Because little is known about quantitative levels of Fe^{2+} in

endolysosomes we next developed a standard curve of the FeRhoNox-

1/Lysotracker ratios at concentrations of Fe^{2+} ranging from 10 to 100 µM. We

observed a very strong linear relationship between FeRhoNox-1/Lysotracker

ratios and Fe^{2+}; the Pearson correlation coefficient for the colocalization was

0.92 $\pm$ 0.02 (Figure 5E). Using this standard curve, we determined that levels of

Fe^{2+} under normal conditions were 36.3 $\pm$ 13.6 µM, and that levels of Fe^{2+} were

75.0 + 15.7 µM in cells pretreated with FAC and were 0.08 + 0.05 µM in cells

pretreated with DFO (Figure 5E).

Intracellular Endolysosome Fe^{2+} Concentration Variability

Qualitatively, it appeared that concentrations of Fe^{2+} varied greatly among endolysosomes in individual cells. In order to measure quantitatively, the range of Fe^{2+} contained in subpopulations of endolysosomes we first developed a standard concentration-response relationship of the FeRhonox-1/LysoTracker ratio using a cell-free system. Individual endolysosome Fe^{2+} levels were measured and the data were separated into bins of 0-25, 26-50, 51-75, 76-100, and 100-150 μM (Figure 6). Although the average concentration of Fe^{2+} under normal conditions was 36.3 $\pm$ 13.6 μM, the concentrations of Fe^{2+} in endolysosomes varied greatly and ranged from undetectable to over 100 μM.

Discussion

Intracellular labile iron regulates a variety of physiological functions and increased levels of intracellular Fe^{2+} have been implicated in the genesis of a number of pathological conditions including cancer and neurodegenerative diseases (Rockfield et al., 2017, Padmanabhan et al., 2015). In non-intestinal cells, virtually all Fe^{3+} is endocytosed bound to transferrin whereupon it is reduced in endolysosomes to Fe^{2+} (Kurz et al., 2011). Thus, it is very important to be able to measure levels of Fe^{2+} in endolysosomes to appreciate its physiological roles and pathological relevance. However, due in part to the lack of probes with which to study endolysosome stores of Fe^{2+}, it has been difficult to determine the degree to which and the mechanisms by which endolysosome Fe^{2+} affects physiologically- and pathologically-relevant processes. One such

probe is FeRhoNox-1; a highly selective turn-on fluorescence compound capable of detecting levels of Fe^{2+} in acidic organelles (Hirayama et al., 2013).

In agreement with previous studies (Hirayama et al., 2013, Mukaide et al., 2014) we found that FeRhoNox-1 was highly selective for Fe^{2+}; no significant increases in fluorescence were observed with Fe^{3+}, zinc, copper, magnesium or calcium. When studies were conducted by others with human hepatocellular carcinoma cells (HepG2) and human breast cancer cells (MCF-7), a staining pattern consistent with FeRhoNox-1 positive staining of Golgi was reported (Hirayama et al., 2013). However, no co-distribution studies were conducted with markers for endolysosomes. Here, we report that FeRhoNox-1 stained endolysosome-positive stores of Fe^{2+} with very high correlation coefficients for the co-localization with markers for endolysosomes (LysoTracker), early endosomes (EEA1), and late endosomes/lysosomes (LAMP1). For example, the high correlation between LysoTracker and FeRhoNox-1 staining of 0.84 ± 0.03 that we found in U87MG astrocytoma cells and in primary cultures of rat neurons is virtually identical to that just reported for a different endolysosome-specific Fe^{2+} probe (Hirayama, 2018). On the other hand, we found a low correlation between FeRhoNox-1 staining and Golgi staining. Even qualitatively, the FeRhoNox-1 staining we observed was consistent with the punctate nature of endolysosomes and was very different from the wispy nature of Golgi.

Although it has been reported that FeRhoNox-1 can exhibit marked background fluorescence signals (Niwa et al., 2014), in our studies the background fluorescence was limited and easily corrected for. With this

technique, we were able to detect increased levels of endolysosome Fe^{2+} following incubation of U87 cells with FAC and decreased levels following incubation with the Fe^{2+} chelating compound DFO that is known to specifically enter cells by endocytosis and once endocytosed DFO resides in endolysosomes for extended periods of time (Lloyd et al., 1991). We also noted that subpopulations of endolysosomes exist and can be differentiated on the basis of their Fe^{2+} content. While it is unclear why the Fe^{2+} content is so variable, one possibility is related to the differences noted in endolysosome pH depending on their positions in cells and findings that endolysosome de-acidification causes Fe^{2+} to be released from endolysosomes (Uchiyama et al., 2008). However, FeRhoNox-1 staining was not sensitive to changes in pH (see Supplemental Figure S.2.B.) and so the differences in staining were likely due to the content of Fe^{2+} and not the pH of the endolysosome. Thus, FeRhoNox-1 is a useful probe with which to detect relative and absolute levels of endolysosome Fe^{2+} and with this probe others and we can investigate further the physiological and pathological roles of this releasable and biologically-active store of Fe^{2+}.
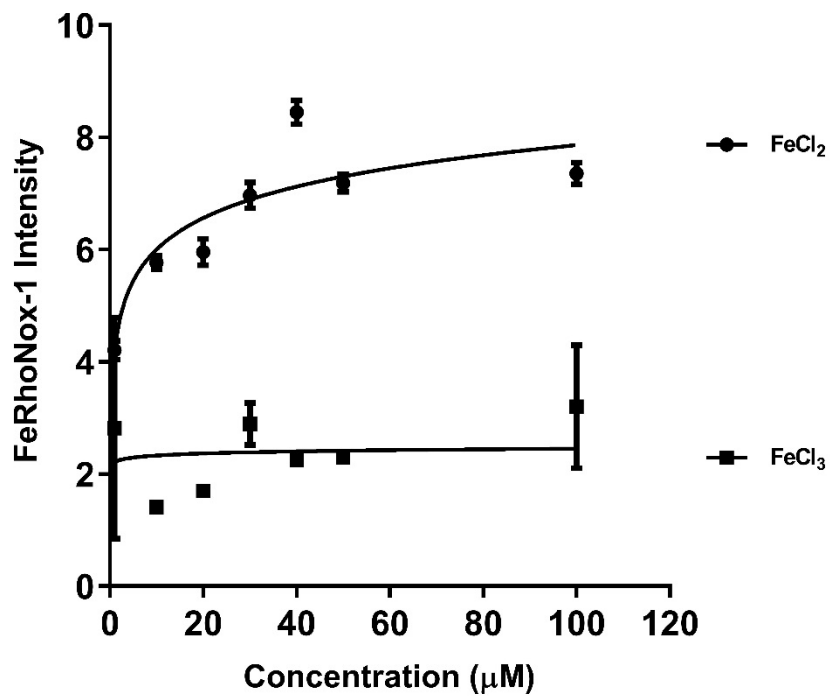
Figure 2. 1.   FeRhoNox-1 fluorescence intensity increased with increased concentrations of $FeCl_2$. $FeCl_2$ (closed circles) and $FeCl_3$ (closed squares) were incubated at concentrations ranging from 1 to 100 µM and FeRhoNox-1 (10 µM) in a cell-free environment. Solutions were incubated for 1 h and aliquots were imaged by confocal microscopy (LSM800, Zeiss) with a 63X oil objective lens. Data shown are means $\pm$ SD from experiments performed on triplicate.
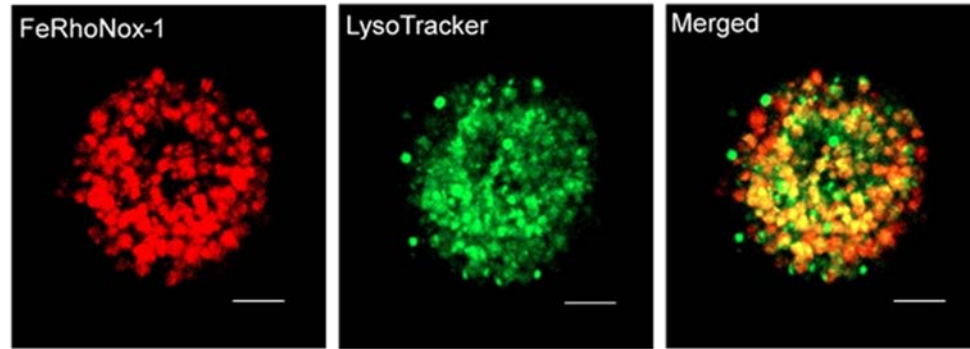
Figure 2. 2.   FeRhoNox-1 labeled endolysosome stores of Fe^{2+}. FeRhoNox-1-positive stores (red) of Fe^{2+} (FeRhoNox-1) and LysoTracker-positive (green) endolysosomes (LysoTracker) were observed in U87MG cells. The FeRhoNox-1 positive staining showed a very high degree of colocalization with the LysoTracker-positive endolysosomes when the images were merged (Merged). The Pearson correlation coefficient for the colocalization determined from three independent experiments was 0.84 $\pm$ 0.03. Scale bar is 2 μm.
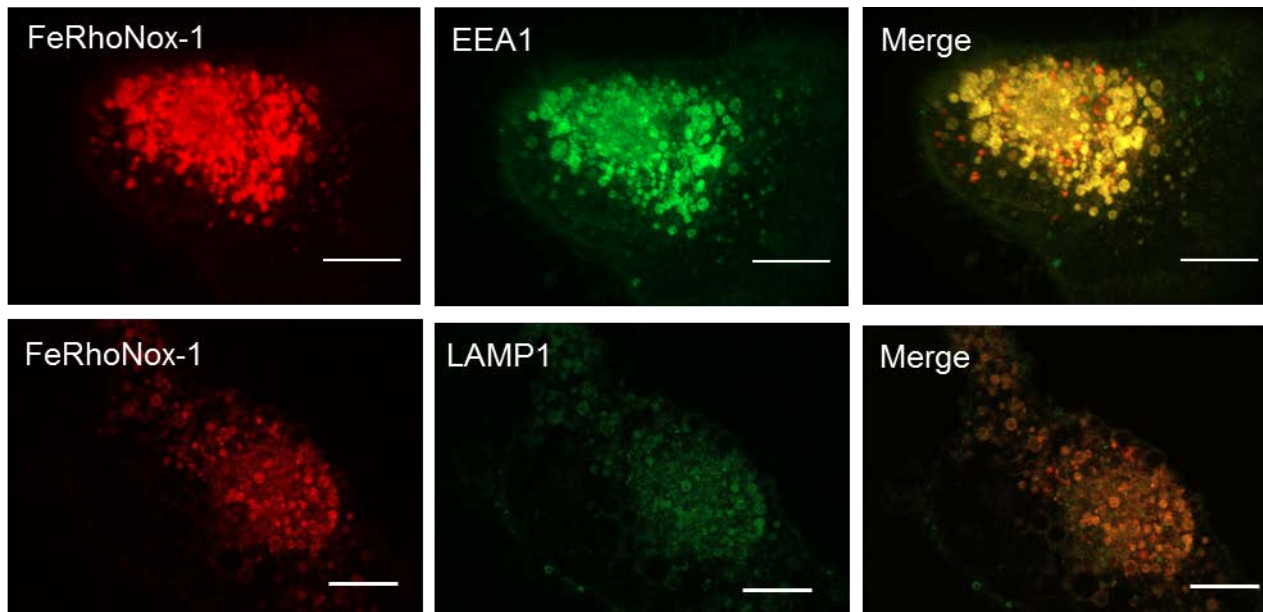
Figure 2. 3.   FeRhoNox-1 labeled Fe^{2+} stores in endosomes and lysosomes. FeRhoNox-1-positive stores of Fe^{2+} (FeRhoNox-1, red), EEA1-positive early endosomes (EEA1, green), and LAMP1-positive late endosomes/lysosomes (LAMP1, yellow) were observed in U87MG cells. The FeRhoNox-1 positive staining showed a very high degree of colocalization with the EEA1-positive endosomes and a high degree of colocalization with the LAMP1-positive lysosomes when the images were merged (Merged). The Pearson correlation coefficients determined from three independent experiments for FeRhoNox-1 and EEA1 colocalization was 0.86 + 0.04 and for FeRhoNox-1 and LAMP1 colocalization was 0.56 + 0.05. Scale bar is 5 μm.
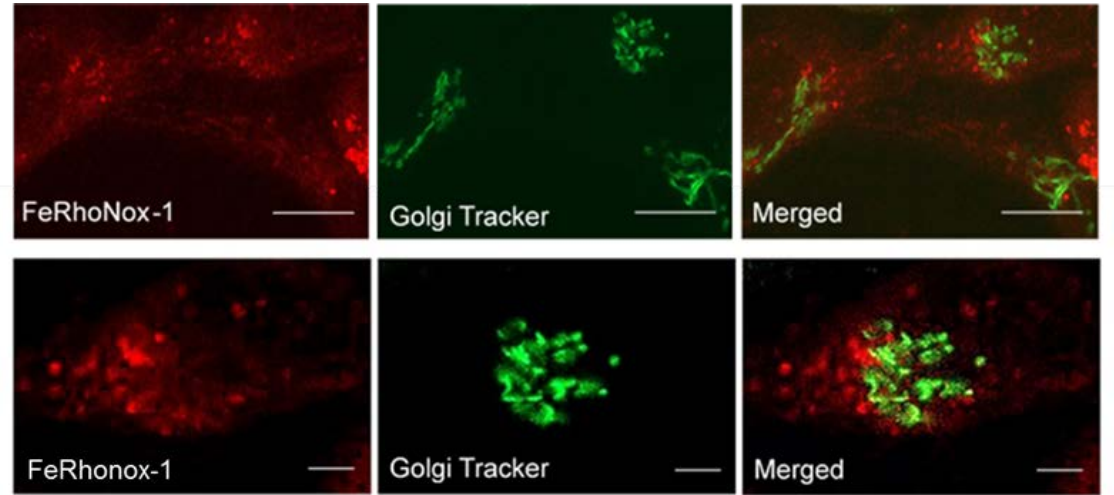
Figure 2. 4. FeRhoNox-1 positive staining was not strongly correlated with Golgi staining. FeRhoNox-1 positive stores of Fe^{2+} (FeRhoNox-1, red) and Golgi Tracker-positive Golgi (Golgi Tracker, green) were observed in U87MG cells. The FeRhoNox-1 positive staining showed a low degree of colocalization with the Golgi Tracker-positive staining when the images were merged (Merged). The upper three images were observed at a lower magnification (scale bar is 5 μm) than were the lower three images (scale bar is 2 μm). The Pearson correlation coefficient for the colocalization determined from three independent experiments performed in triplicate was 0.13 $\pm$ 0.06.

Figure 2. 5.   FeRhoNox-1 fluorescence intensity increased with FAC and
                 decreased with deferoxamine.
                 (A.) As expected, we observed a high level of colocalization
                 between FeRhoNox-1 and LysoTracker staining of
                 endolysosomes (Control).
                 (B.) Preincubation of U87MG cells with 50 µM ferric ammonium
                 citrate (FAC) for 1 h increased FeRhoNox-1 fluorescence
                 staining in endolysosomes.
                 (C.) Preincubation of U87MG cells with 25 µM deferoxamine
                 (DFO) for 1 h reduced FeRhoNox-1 fluorescence staining in
                 endolysosomes.
                 (D.) The quantification of FeRhoNox-1 fluorescence intensity for
                 control cells, and cells treated with FAC and DFO.
                 (E.) A standard dose-response relationship for FeRhoNox-1 and
                 Lysotracker staining was developed in a cell-free system. The
                 dose-response relationship was then used to quantify Fe^{2+} levels
                 in endolysosomes of normal cells (square box) as well as in cells
                 pretreated with FAC or DFO.

A. Control FeRhoNox-1 | LysoTracker | Merged

B. FAC FeRhoNox-1 | LysoTracker | Merged

C. DFO FeRhoNox-1 | LysoTracker | Merged

D

E

Endolysosome [Fe^{2+}] Variability
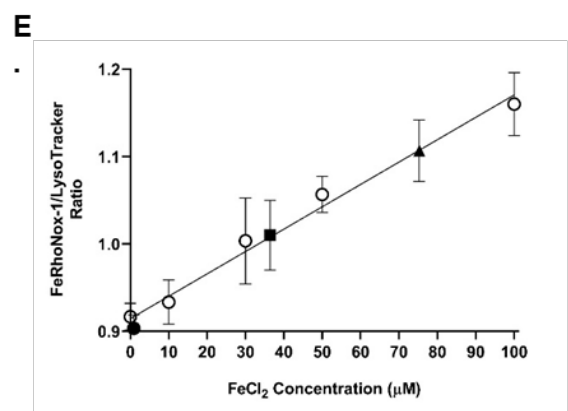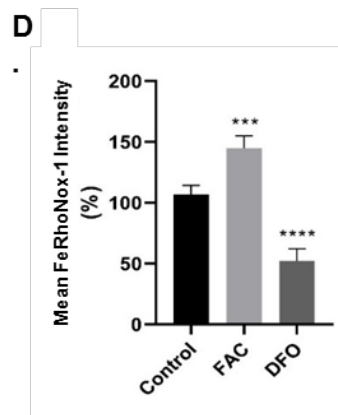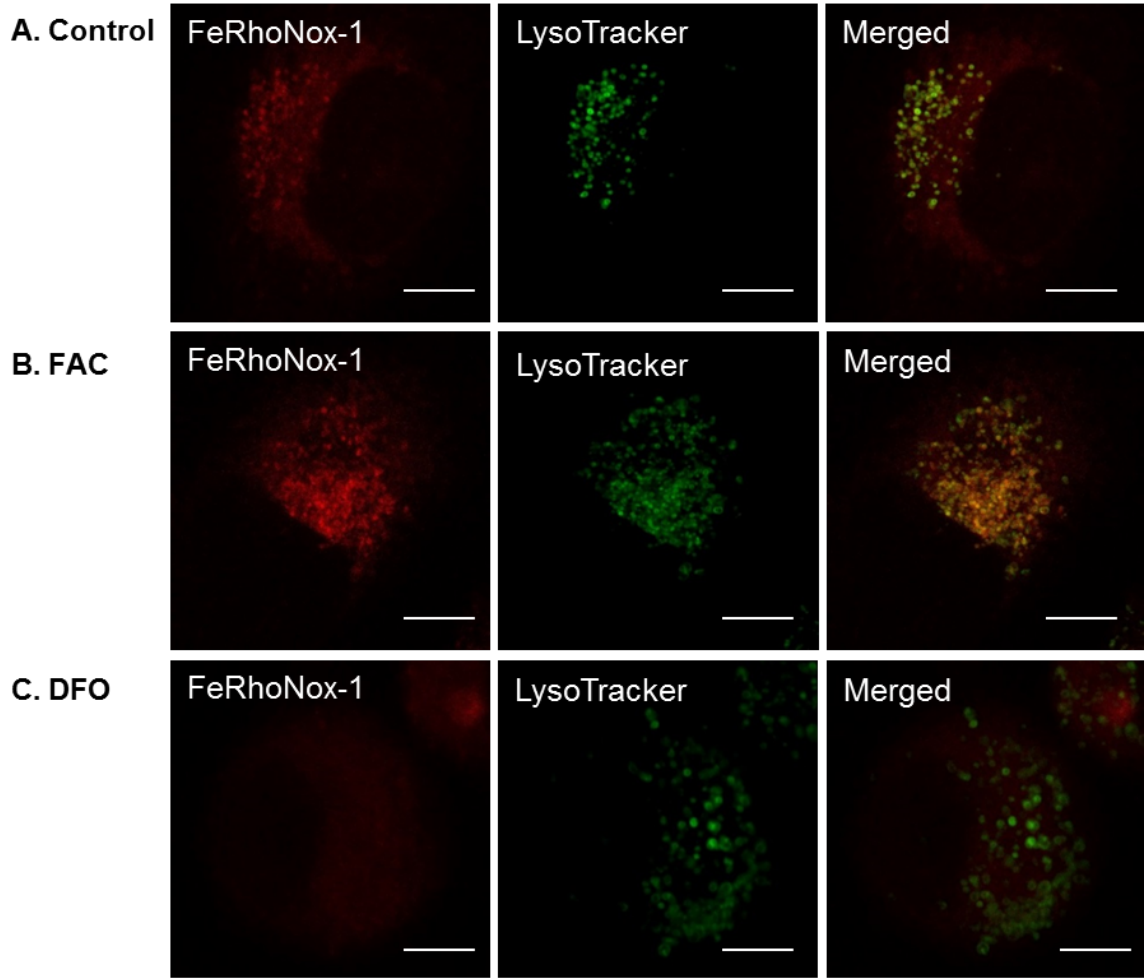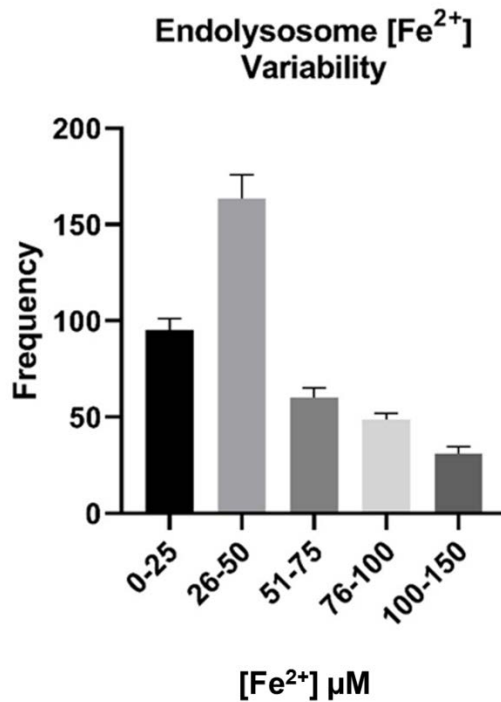
Figure 2. 6.   Intracellular endolysosome Fe^{2+} concentration variability: Qualitatively, it appeared that concentrations of Fe^{2+} varied greatly among endolysosomes in individual cells. In order to measure quantitatively, the range of Fe^{2+} contained in subpopulations of endolysosomes, we first developed a standard concentration-response relationship of the FeRhonox-1/LysoTracker ratio using a cell-free system. Individual endolysosome Fe^{2+} levels were measured and the data were separated into bins of 0-25, 26-50, 51-75, 76-100, and 100-150 µM. Although the average concentration of Fe^{2+} under normal conditions was 36.3 $\pm$ 13.6 µM, the concentrations of Fe^{2+} in endolysosomes varied greatly and ranged from undetectable to over 100 µM.
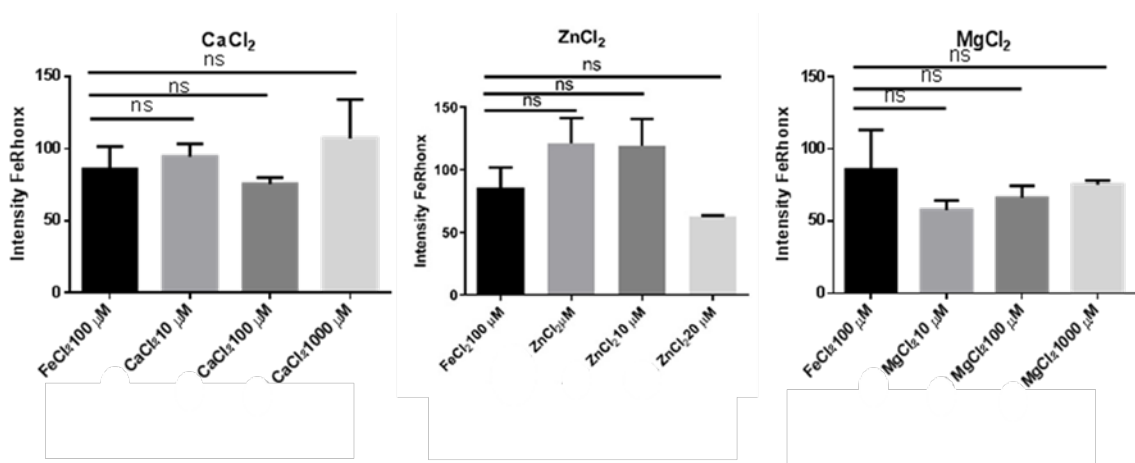
Figure 2. A.   *Supplemental Figure*: RhoNox-1 does not increase with increased concentrations of $ZnCl_2$, $CaCl_2$, or $MgCl_2$. $ZnCl_2$, $CaCl_2$, and $MgCl_2$ were used at different concentrations along with FeRhoNox-1 (10 µM) in a cell free environment. The concentrations were incubated in a 1 ml tube for 1 hour and then added to an empty plate and imaged with a 63X oil objective and a Zeiss LSM800 confocal microscope (Zeiss).
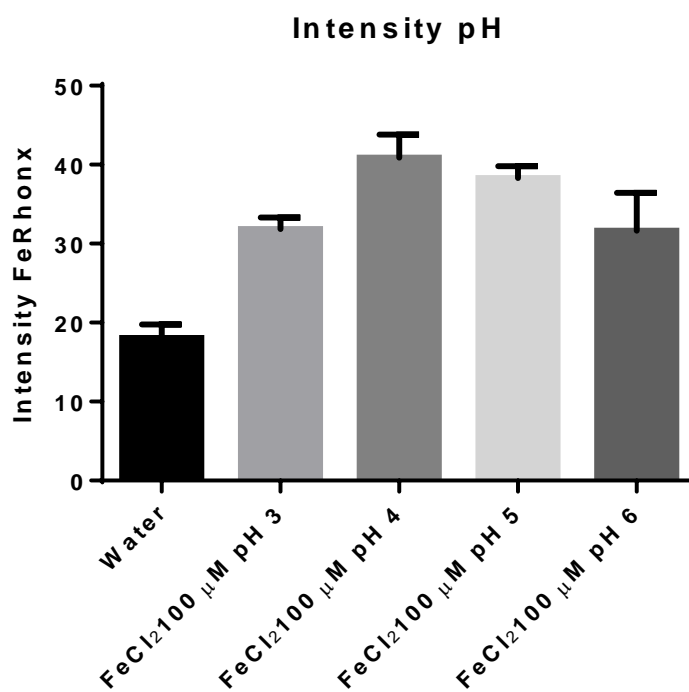
Intensity pH

Figure 2. B.   *Supplemental Figure*: FeRhoNox-1 does not significantly change with pH: In a cell free system with changing pH values from 3 to 6, the FeRhonox-1 fluorescent intensity does not significantly change. This illustrates that FeRhoNox-1 intensity is independent of pH changes.

References

COLACURCIO, D. J. & R. A. NIXON (2016). "Disorders of lysosomal acidification-The emerging role of v-ATPase in aging and neurodegenerative disease." <u>Ageing Res Rev</u> 32: 75-88.

DE DUVE, C. (2005). "The lysosome turns fifty." <u>Nature Cell Biology</u> 7: 847.

HIRAYAMA, T. (2018). "Development of Chemical Tools for Imaging of Fe(II) Ions in Living Cells: A Review." <u>Acta Histochem Cytochem</u> 51(5): 137-143.

HIRAYAMA, T., K. OKUDA & H. NAGASAWA (2013). <u>A highly selective turn-on fluorescent probe for iron(II) to visualize labile iron in living cells</u>. Chem. Sci. 4: 1250-1256.

HUI, L., N. H. GEIGER, D. BLOOR-YOUNG, G. C. CHURCHILL, J. D. GEIGER & X. CHEN (2015). "Release of calcium from endolysosomes increases calcium influx through N-type calcium channels: Evidence for acidic store-operated calcium entry in neurons." <u>Cell Calcium</u> 58(6): 617-627.

KTISTAKIS, N. T. & S. A. TOOZE (2016). "Digesting the Expanding Mechanisms of Autophagy." <u>Trends Cell Biol</u> 26(8): 624-635.

KURZ, T., J. W. EATON & U. T. BRUNK (2011). "The role of lysosomes in iron metabolism and recycling." <u>Int J Biochem Cell Biol</u> 43(12): 1686-1697.

LELLOUCH, A. (1993). "[Metchnikoff (1845-1916) and aging]." <u>Hist Sci Med</u> 27(1): 13-22.

MINDELL, J. A. (2012). "Lysosomal acidification mechanisms." <u>Annu Rev Physiol</u> 74: 69-86.

MOTULSKY, A. G. (1986). "The 1985 Nobel Prize in physiology or medicine." <u>Science</u> 231(4734): 126-129.

MUKAIDE, T., Y. HATTORI, N. MISAWA, S. FUNAHASHI, L. JIANG, T. HIRAYAMA, H. NAGASAWA & S. TOYOKUNI (2014). "Histological detection of catalytic ferrous iron with the selective turn-on fluorescent probe RhoNox-1 in a Fenton reaction-based rat renal carcinogenesis model." <u>Free Radic Res</u> 48(9): 990-995.

NIWA, M., T. HIRAYAMA, K. OKUDA & H. NAGASAWA (2014). "A new class of high-contrast Fe(II) selective fluorescent probes based on spirocyclized scaffolds for visualization of intracellular labile iron delivered by transferrin." <u>Org Biomol Chem</u> 12(34): 6590-6597.

PADMANABHAN, H., M. J. BROOKES & T. IQBAL (2015). "Iron and colorectal cancer: evidence from in vitro and animal studies." <u>Nutr Rev</u> 73(5): 308-317.

PERERA, R. M. & R. ZONCU (2016). "The Lysosome as a Regulatory Hub." <u>Annu Rev Cell Dev Biol</u> 32: 223-253.

ROCKFIELD, S., J. RAFFEL, R. MEHTA, N. REHMAN & M. NANJUNDAN (2017). "Iron overload and altered iron metabolism in ovarian cancer." <u>Biol Chem</u> 398(9): 995-1007.

SETTEMBRE, C. & A. BALLABIO (2013). "New targets for old diseases: lessons from mucolipidosis type II." <u>EMBO Mol Med</u> 5(12): 1801-1803.

CHAPTER 3

**ENDOLYSOSOME DE-ACIDIFICATION-INDUCED IRON RELEASE CAUSES
MITOCHONDRIAL DYSFUNCTION AND CELL DEATH**

Peter W. Halcrow, Nabab Khan, Xuesong Chen, and Jonathan D. Geiger

Department of Biomedical Sciences
University of North Dakota School of Medicine and Health Sciences
Grand Forks, ND 58202, USA

Abstract

Mitochondria are subject to iron overload under a variety of conditions and disease states, but it is not clear what are the subcellular origins of this iron nor its consequences. Endosomes and lysosomes, referred to as endolysosomes, are storage sites of ferrous iron (Fe^{2+}), and the degree to which and the precise mechanisms by which endolysosome Fe^{2+} contribute to iron-dependent changes to mitochondria and cell injury remains uncertain. Here, our studies were aimed to determine the role of inter-organellar signaling of Fe^{2+} from iron-rich endolysosomes to mitochondria under pharmacologically-induced conditions. We demonstrated, in U87MG astrocytoma cells, mouse primary hepatocytes, and primary cultures of rat cortical neurons, that Fe^{2+} within endolysosomes was translocated to the mitochondria resulting in mitochondrial dysfunction and cell death. The weak-base chloroquine and the vacuolar-ATPase inhibitor bafilomycin A1 both de-acidify endolysosomes and both induced the release of Fe^{2+} and this resulted in increased concentrations of Fe^{2+} in the cytoplasm and in mitochondria. Furthermore, the endocytosed iron chelator, deferoxamine, inhibited the release of bafilomycin A1- and chloroquine-induced release of endolysosome stores of Fe^{2+} and prevented the induced increases of ROS in cytoplasm and mitochondria. These findings demonstrate that redox-active Fe^{2+} in endolysosomes plays a key upstream role in mitochondrial iron accumulation and dysfunction, and deferoxamine might be potential adjunctive therapeutic strategies in preventing neurotoxicity and enhancing therapeutic outcomes of disease.

Introduction

Although iron is an essential nutrient for cellular processes such as the electron transport chain, in excess it is a toxicant that can lead to acute cellular necrosis and injury (Christ et al., 1995). Excess iron may promote diseases such as diabetes, cancer, cardiovascular disease, and neurodegeneration (Swanson, 2003, Petersen, 2005, Brewer, 2007, Imeryuz et al., 2007), and disrupted iron homeostasis appears to play an important role in disease pathogenesis (Enns, 2003, Jellinger, 2009). These findings are further strengthened by observations that the iron chelator, deferoxamine (DFO), protects against the deleterious effects of iron in various models of oxidative stress and hypoxic/ischemic injury suggests a role for iron in the pathogenesis of variety of disorders and diseases (Starke and Farber, 1985). However, the intracellular source of excess iron and the precise mechanisms by which iron is mobilized to contribute to cellular injury remain poorly understood.

Ferrous iron (Fe^{2+}), known as labile or chelatable iron, is a key reactant in the formation of the highly reactive hydroxyl radicals ($HO^.$) from H_2O_2 and superoxide (O_2^-) radical from O_2, both of which damage DNA, proteins, and membranes (Fenton, 1894) (Kehrer, 2000). The generation of reactive oxygen species (ROS), including O_2^- and HO, contribute to cellular dysfunction and cell death from oxidative stress, ischemia and ischemia-reperfusion (Jaeschke et al., 2002, Videla et al., 2003, Schwabe and Brenner, 2006). The most important source of ROS is mitochondria through mechanisms linked to ATP production (Loschen et al., 1971, Loschen et al., 1974, Boveris and Cadenas, 1975).

40

Mitochondria have a constitutive presence of ROS from the electron transport chain, thus iron levels must be tightly regulated. However, the intracellular source of excess iron that leads to mitochondrial iron accumulation remains poorly understood. Furthermore, it is unclear whether mitochondrial iron accumulation causes or is a consequence of upstream events including ROS production and cell death (Mena et al., 2015).

Endosomes and lysosomes, referred to as endolysosomes, have many physiological roles including plasma membrane repair, cell homeostasis, cell adhesion and migration, apoptotic cell death, and metabolic signaling (Perera and Zoncu, 2016, Settembre et al., 2013). And it is well-known that endolysosomes are storage sites for readily-releasable cations including Ca^{2+}, Zn^{2+}, Fe^{3+}, and Fe^{2+} (Xu and Ren, 2015, Xiong and Zhu, 2016). Furthermore, endolysosome-associated conductive cation channels like vacuolar-ATPase, transient receptor mucolipin type 1 channels (TRPML1), and two-pore channels (TPCs) regulate the homeostasis of cations and cation-based inter-organellar communication. The acidic pH of endolysosomes is maintained through the influx of protons via vacuolar-ATPases in conjunction with ion channels (TRPML1, TPCs and BK channels) and pH is known to affect cation concentrations in endolysosomes (Pu et al., 2016). The proton force generated by the vacuolar-ATPase drives the movement of ions and small molecules across membranes, creating a voltage gradient which is sustained through counter-ions including Na^+, K^+, and Cl^- (Mindell, 2012). Studies have shown endolysosome de-acidification by bafilomycin A1 and chloroquine cause an efflux of cations such

as Ca^{2+} into the cytosol (Christensen et al., 2002, Fernández et al., 2016), and these released Ca^{2+} cations play crucial roles in exploiting cellular signaling pathways. However, little is known about the role of readily-releasable redox-active Fe^{2+} in endolysosomes in inter-organellar signaling and cell death.

In this study, we showed that bafilomycin A1- and chloroquine-de-acidification of endolysosomes causes an efflux of Fe^{2+} from endolysosomes and that this Fe^{2+} can accumulate in the cytoplasm and in mitochondria where it can contribute to ROS production and cell death. In addition, we demonstrated that DFO chelated endolysosome Fe^{2+} and blocked cytosolic and mitochondrial ROS induced by bafilomycin A1 and chloroquine as well as chloroquine- and bafilomycin A1-induced cell death. Furthermore, we demonstrated the involvement of two-pore channels in the release of Fe^{2+} cations from endolysosomes upon de-acidification and that mitochondrial permeability transition pores (MPTPs) uptake Fe^{2+} into mitochondria.

Materials and Methods

Cell Cultures

U87MG glioblastoma cells were cultured in 1x DMEM (Invitrogen) supplemented with 10% fetal calf serum and 1% penicillin/streptomycin (Invitrogen). Cells were grown to confluence in T75 flasks or 35 mm^2 dishes to about 40% confluence in an environment of 5% CO_2 at 37°C. Cells were only used at passage numbers of 10 or less.

Endolysosome pH

As previously described (Chen et al., 2013, Hui et al., 2012a, Hui et al., 2012b), endolysosome pH was measured using a ratiometric indicator-dye, LysoSensor Yellow/Blue DND-160; a dual excitation dye that allows for the measurement of acidic organelles independent of dye loading efficiency. U87MG cells were loaded with 10 µM DND-160 for 5 minutes at 37°C. Post-incubation, dye-containing media was removed and PBS was added to the cells prior to them being taken for imaging. CellLight Lysosome-RFP (Thermosfisher), incubated in cells overnight, was used to label lysosomes in combination with LysoSensor DND-160 for selectivity of lysosomal labeling. Light emitted at 520 nm in response to excitation at 340 nm and 380 nm was measured for 2 msec every 10 seconds using a filter-based imaging system (Zeiss, Germany). The ratios of light excited (340/380 nm) versus light emitted (520 nm) were converted to pH using a calibration curve established with 10 µM of the H^+/Na^+ ionophore monensin, and 20 µM of the H^+/K^+ ionophore nigericin; both were dissolved in 20 mM 2-(N-morpholino) ethane sulfonic acid (MES), 110 mM KCl, and 20 mM NaCl adjusted to pH 3.0 to 7.0 with HCl/NaOH; the linear range was found to be 4.5 to 6.0 pH.

Endolysosome Iron

FeRhonox-1 (10 µM) (Goryo Chemical), which is highly specific for Fe^{2+}, was incubated with cells for 1 h, washed with PBS, then measured using a confocal microscope at absorption and emission wavelengths 537 nm and 569 nm, respectively. As reported elsewhere (see Chapter 2), FeRhonox-1 staining

colocalized with endolysosomes in U87MG cells and primary cultures of rat

cortical neurons. Experiments were conducted on a LSM800 confocal laser-

scanning microscope (ZEISS).

Cytosolic Iron

Cells were incubated with PhenGreen™ FL diacetate (10 µM) for

30 minutes at 37°C. Cells were washed with PBS and analyzed (Alexa Fluor 488)

using a ThermoFisher Attune flow cytometry and an Axiovert 200M (Zeiss)

microscope. Alexa Fluor 488 is absorbed at 495 nm and emitted at 519 nm. The

x-mean value of emission was recorded on flow cytometry.

Mitochondrial Iron

Mitochondrial iron levels were measured using rhodamine

B-[2,2'-bipyridine-4-yl)-aminocarbonyl]benzyl ester (RDA) dye (Squarix), a

Fe^{2+} specific fluorescent sensor that is localized within mitochondria. Cells were

treated with RDA (100 nM) for 10 minutes at 37°C, then washed with PBS

followed by experiments conducted on a confocal laser scanning microscope

(ZEISS). RDA absorbance is 562 nm and emission is 598 nm. Fluorescent

intensity was measured across 30 mitochondria per cell per individual treatments

for control cells and drug treated cells. The change in fluorescence for control

cells was insignificant compared to chloroquine and bafilomycin A1 treated cells.

Iron Chelation

Deferoxamine (50 µM), a Fe^{2+} chelator that is endocytosed (Doulias et al.,

2003), was incubated in cells for 1 h prior to analysis and administering other

compounds. It is known that DFO does not enter cells by passive diffusion, that it

does enter cells by endocytosis, and that following endocytosis it resides in endolysosomes for extended periods of time (Lloyd et al., 1991). This make DFO a particular useful agent to determine roles for endolysosome Fe^{2+}.

ROS Measurements

Cytosolic ROS was measured using H_2DCFDA, 2,7-dichlorodihydrofluoroscein diacetate (10 µM) (Thermofisher), and mitochondrial ROS was measured using MitoSox Red (5 µM) (Thermofisher). Cells were incubated with the respective dyes at 37ºC for 30 minutes in serum free media and then washed with PBS prior to analysis by flow cytometry.

Generation of TPCN2-Knock Down U87MG Cells

In U87MG cells, expression levels of TPCN2 channels were knocked down using 1 µg/ml shRNA (Santa Cruz) against TPCN2 (Sc-); scrambled shRNA (Sc-108060) was used as a control. Jet prime reagent (2 µl) was used for transfection. Following 36 h incubation, 25 µg/ml puromycin (Invitrogen) was added to activate the shRNA promoter. After incubation for 2 to 3 days, cells were passaged to remove the dead and dying cells; the remaining living cells were cultured for an additional 36 h prior to being taken for experimentation. Knockdown efficiency was confirmed by immunoblotting using antibodies against TPCN2 (Novus, NBP1-30670).

Cell Death Measurements

Cell death was measured using 20 ug/ml of propidium iodide (PI) staining (Sigma-Aldrich). Cells were treated with the various compounds for 24 h, then incubated with propidium iodide for 30 minutes, washed with PBS, and then

measurements were acquired by flow cytometry (Attune NxT). The positive

control was methanol (10 µM) incubated for 2 hours. PI excitation/emission is

493 nm/636 nm. Cells treated with only PI were gated on flow cytometry and

used as a baseline for sample treated cells.

Statistical Analysis

All results are expressed as mean ± SD. Data were analyzed using

GraphPad Prism Version 6 (GraphPad Software, Inc., La Jolla, CA). Statistical

significance between two groups was analyzed with a Student's t-test, and

statistical significance among multiple groups was analyzed with one-way

ANOVA plus a Tukey post-hoc test. $p < 0.05$ was considered to be statistically

significant.

Results

Bafilomycin A1 and chloroquine de-acidify endolysosome pH:

Cultured U87MG cells were incubated with CellLight Lysosome-RFP and

Lysosensor DND-160, which is a ratiometric excitation dye that allows for the

measurement of acidic organelles. Cells were treated with bafilomycin A1 (80 nM

and 200 nM) and chloroquine (100 µM and 200 µM). Bafilomycin A1 is a known

inhibitor of vacuolar-ATPase and chloroquine is a weak base; both are known to

increase the pH of endolysosomes (Tapper and Sundler, 1995, Steinman et al.,

1983). Bafilomycin A1 and chloroquine de-acidified endolysosomes within

seconds of being added to cells as shown in Figure 3.1A. In addition, the de-

acidification of endolysosomes by bafilomycin A1 and chloroquine was dose-

dependent (Figure 3.1B). Furthermore, cells were stained with Lysosensor

DND-189; an alternate method for measuring endolysosome pH. As with DND-160, bafilomycin A1 and chloroquine de-acidified endolysosome pH as determined using DND-189, time-dependently (Figure 3.1C). For ease of illustration, data were represented as a reciprocal of the mean fluorescent intensity so that the increases in pH were readily apparent.

Bafilomycin A1 and Chloroquine Release Fe^{2+} from Endolysosomes into the Cytosol

The FeRhonox-1 dye was previously determined to be highly specific for Fe^{2+} and endolysosomes (see Chapter 2). In addition, it has been shown that the iron chelator DFO inhibits FeRhonox-1 fluorescent intensity because it is endocytosed and chelates Fe^{2+} (see Chapter 2). U87MG cells were co-stained with FeRhonox-1 and LysoTracker for 1 h prior to experimentation. The dual dye method was used to ensure measurement of endolysosome iron as well as to be more indicative of iron release from endolysosomes rather than just an efflux of the FeRhonox-1 dye from non-descript sources. Therefore, the FeRhoNox-1/LysoTracker ratio was used as a method of analysis. In addition, these experiments were conducted at times ranging from 0 to 10 min; intervals that are consistent with time intervals for de-acidification of endolysosomes by bafilomycin A1 and chloroquine (Figure 3.1). FeRhonox-1 colocalized with LysoTracker with a Pearson Correlation Coefficient of 0.84 (Figure 3.2A) as previously determined (see Chapter 2). In control cells treated with PBS, the FeRhonox-1/LysoTracker ratio did not change significantly (Figure 3.2B). Chloroquine significantly decreased (**$P < 0.001$) the FeRhonox-1/LysoTracker from 1.0 to 0.91 (Figure 3.2C). Quantification of the FeRhonox-1/LysoTracker

ratios within endolysosomes for control and chloroquine treated cells is shown in

Figure 3.2D, and the quantification of the cytosolic FeRhonox-1/LysoTracker ratio

for control and chloroquine treated cells is shown in Figure 3.2E. Similar

experiments were conducted with bafilomycin A1. In control cells treated with

0.1% DMSO the FeRhonox-1/LysoTracker ratio was not affected significantly

(Figure 3.3A). However, bafilomycin A1 significantly decreased (**P < 0.001) the

FeRhonox-1/LysoTracker from 1.0 to 0.89 (Figure 3.3B). Quantification of the

FeRhonox-1/LysoTracker ratio within endolysosomes for control and bafilomycin

A1 treated cells is shown in Figure 3.3C, and the quantification of the cytosolic

FeRhonox-1/LysoTracker ratio for control and bafilomycin A1 treated cells is

shown in Figure 3.3D.

To determine whether iron was released into the cytosol, Phen-Green FL

was used; a dye whose fluoresence quenches in the presence of metals such as

zinc, copper, and ferrous iron. Because Phen Green is a quenching stain, the

reciprocal of the mean fluorescent intensity was calculated to illustrate more

easily de-acidification induced increase in cytosolic iron. Deferoxamine is a

ferrous iron chelator that is endocytosed (Doulias et al., 2003), and DFO

significantly decreased the quenching of Phen-Green, indicating there is a

constitutive leak of Fe^{2+} from endolysosomes into the cytosol as shown in

Figure 4. Bafilomycin A1 and chloroquine significantly quenched Phen-Green.

Pretreatment with DFO, prior to bafilomycin A1 and chloroquine treatment,

blocked the quenching of Phen-Green, indicating a release of Fe^{2+} from

endolysosomes into the cytosol by bafilomycin A1 and chloroquine as shown in Figure 3.4 by flow cytometry.

Endolysosome Iron is Taken up by Mitochondria

Rhodamine B 4-[(2,2'-bipyridin-4-yl)aminocarbonyl]benzyl ester (RDA) is a dye specific to Fe^{2+} and the mitochondria, and RDA fluorescence is stoichiometrically (3:1) quenched by Fe^{2+} ions (Rauen et al., 2007). U87MG cells were stained with RDA (100 nM) and MitoTracker (10 µM); the two dyes colocalized with a Pearson Correlation Coefficient of 0.97 as shown in Figure 3.5A. The following RDA experiments were conducted using incubation intervals ranging from 0 to 10 min; a time frame consistent with de-acidification of endolysosomes by bafilomycin A1 and chloroquine (Figure 3.1) and the release of Fe^{2+} from endolysosomes (Figures 3.2 and 3.3). Control cells treated with PBS and DMSO which did not yield significant changes to RDA fluorescence (Figure 3.5B), and DFO did not significantly change the fluorescence intensity of RDA (Figure 3.5C). Bafilomycin A1 and chloroquine quenched RDA fluorescence as shown in Figure 3.5D and 3.5F, and DFO pretreatment blocked RDA quenching induced by bafilomycin A1 and chloroquine treatment (Figure 3.5E and 3.5G). These data indicate that endolysosome iron was translocated to mitochondria. Quantification of these mitochondrial iron experiments is shown in Figure 3.5H. An increase in mitochondrial iron was dose-dependent for bafilomycin A1 and chloroquine (Figure 3.5I and 3.5J) as were changes in endolysosome pH (Figure 3.1). The compound dipeptide glycyl-l-phenylalanine 2-naphthylamide (GPN) is a lysosomotropic agent that disrupts endolysosome membranes and

49

releases contents of endolysosomes into the cytosol (Berg et al., 1994); as such

GPN was used to induce non-selectively the release of Fe^{2+} from

endolysosomes. GPN quenched RDA in a dose-dependent manner as shown in

Figure 3.5K. These data taken together demonstrate inter-organellar signaling of

Fe^{2+} from endolysosomes to mitochondria.

Bafilomycin A1 and Chloroquine-Induced Fe^{2+} Release from Endolysosomes Increases Cytosolic ROS and Mitochondrial ROS

Ferrous iron is a key reactant in the formation of the highly reactive

hydroxyl and superoxide radicals (Fenton, 1894). U87MG cells were stained with

2′,7′-dichlorofluorescin diacetate (H_2DCFDA), which is a measure of cytosolic

ROS. Bafilomycin A1 and chloroquine both increased cytosolic ROS, and DFO

blocked bafilomycin and chloroquine-induced increases in cytosolic ROS

(Figure 3.6A). U87MG cells were stained with MitoSox, a mitochondrial measure

of ROS. Bafilomycin A1 and chloroquine both increased mitochondrial ROS, and

DFO blocked bafilomycin and chloroquine-induced increases in mitochondrial

ROS (Figure 3.6B).

Two-pore Channels are Involved in Fe^{2+} Release from Endolysosomes

Two-pore channels have been shown to be involved in the release of

divalent cations including calcium from endolysosomes (Rivero-Rios et al., 2016).

Therefore, TPCs were analyzed as an endolysosome channel for Fe^{2+} release.

Nicotinic acid adenine dinucleotide phosphate (NAADP) is a TPC activator

(Boccaccio et al., 2014), and NED-19 is a known inhibitor of TPCs (Zharkich et

al., 2016). U87MG cells were stained with RDA and treated with NAADP-AM,

which caused a dose-dependent increase in mitochondrial iron as shown in

Figure 3.7A. Pretreatment with NED-19 for 30 minutes significantly reduced

mitochondrial iron uptake induced by chloroquine or bafilomycin A1 treatment

(Figure 3.7B and 3.7C). TPCN2 knockdown cells (Figure 3.7D) significantly

reduced mitochondrial iron uptake (Figure 3.7B and 3.7C).

Mitochondrial Permeability Transition Pores (MPTPs) Uptake Fe^{2+} into the Mitochondria

Mitochondrial permeability transition pores are known to regulate

mitochondrial iron (Sripetchwandee et al., 2014), and auranofin is a known

activator of MPTPs (Rigobello et al., 2002). Cyclosporin A and TRO19622 inhibit

MPTP (Sripetchwandee et al., 2014, Bordet et al., 2010). GPN (1 µM) plus

auranofin (1 µM) increased mitochondrial uptake of iron, and CSA and

TRO19622 blocked mitochondrial iron uptake (Figure 3.8A). As for GPN, similar

findings were found with bafilomycin A1 and chloroquine as shown in Figure 3.8B

and 3.8C.

Deferoxamine Protects Cells from Chloroquine and Bafilomycin A1-Induced Cell Death

U87MG cells were treated with chloroquine and bafilomycin A1 for 24 h,

stained with propidium iodide (PI) (20 ug/ml), and analyzed for cell death using

flow cytometry. The positive control for cell death was cells treated with methanol

(10 µM) for 2 h. In addition, cells were pretreated with DFO (50 µM) for 1 hr prior

to chloroquine and bafilomycin A1 treatment. Chloroquine and bafilomycin A1

induced cell death after 24 h and DFO protected cells from chloroquine- and

bafilomycin A1-induced cell death (Figure 3.9).

Schematic Diagram of Overall Cellular Mechanisms

The schematic diagram of the proposed involved cellular mechanisms is illustrated in Figure 3.10. According to this scheme, chloroquine and bafilomycin A1 de-acidification of endolysosomes causes the release of iron from endolysosomes into the cytosol where it can be up-taken by mitochondria. The iron released from endolysosomes leads to increased ROS in the cytosol and in mitochondria. DFO chelates endolysosome iron and inhibits levels of ROS induced by chloroquine and bafilomycin A1 as well as cell death.

Discussion

Intracellular labile iron has key roles in many physiological functions and excess levels of intracellular Fe^{2+} have been implicated in the pathogenesis of cancer and neurodegenerative diseases (Padmanabhan et al., 2015, Rockfield et al., 2017). Disrupted iron homeostasis may be an important factor in disease initiation and progression (Enns, 2003, Jellinger, 2009) and it is well-known that endolysosomes are storage sites for readily-releasable redox-active Fe^{2+} cations (Xu and Ren, 2015, Xiong and Zhu, 2016b). However, due at least in part to the lack of available probes with which to study endolysosome Fe^{2+}, it has been difficult to determine the degree to which and the mechanisms by which endolysosome Fe^{2+} affects such physiologically and pathologically relevant processes as inter-organellar signaling, production of ROS, and disease pathogenesis.

In agreement with previous studies by others and us, we demonstrated that chloroquine and bafilomycin A1 de-acidified endolysosomes (Yoshimori et al., 1991) (Steinman et al., 1983), and de-acidification is known to cause an efflux of Ca^{2+} into the cytosol (Christensen et al., 2002, Fernández et al., 2016b, Xiong and Zhu, 2016b, Hui et al., 2015). Using the FeRhonox-1 probe, we demonstrated that bafilomycin A1 and chloroquine decreased levels of Fe^{2+} in endolysosomes.

To determine if the deacidification-induced decreases in endolysosome Fe^{2+} resulted in increases in the cytosol, we used Phen Green Diacetate, which is a cell permeant dye that quenches when exposed to ions including Cu^{2+}, Fe^{2+}, Pb^{2+}, Cd^{2+}, Zn^{2+} and Ni^{2+}. However, a study has shown using external metals that only Fe^{2+} and Cu^{2+} produced significant fluorescent quenching of Phen Green, and the other metals produced very little change in dye fluorescence (Chavez-Crooker et al., 2001). Furthermore, previous studies have used calcein as a measurement of Fe^{2+} (Uchiyama et al., 2008), but recent studies have shown that calcein binds Fe^{3+} and not Fe^{2+} (Thomas et al., 1999). We demonstrated that bafilomycin A1 and chloroquine quenched Phen-Green, and even though Cu^{2+} can quench Phen-Green, the quenching induced by chloroquine and bafilomycin A1 was prevented by pretreatment with DFO, which is highly specific for iron and not copper (Liu and Hider, 2002). Thus, Phen Green quenching is most likely from an increase in chelatable ferrous iron. Interestingly, pretreatment of DFO increased PhenGreen fluorescence which indicates a constitutive leak of Fe^{2+} from endolysosomes into the cytosol.

53

Rhodamine B 4-[(2,2'-bipyridin-4-yl)aminocarbonyl]benzyl ester (RDA) is a dye specific for Fe^{2+} and mitochondria, and RDA fluorescence is stoichiometrically (3:1) quenched by Fe^{2+} (Rauen et al., 2007). We confirmed this with RDA and MitoTracker, which colocalized with a Pearson Correlation Coefficient of 0.97. After chloroquine and bafilomycin A1 treatment, RDA fluorescence quenched, which signifies an increase of chelatable ferrous iron within the mitochondria. Moreover, DFO pretreatment suppressed mitochondrial RDA quenching after chloroquine and bafilomycin A1 treatment. Thus, Fe^{2+} released from endolysosomes into the cytosol by chloroquine and bafilomycin A1 was being taken up by mitochondria. These findings suggest that there is inter-organellar signaling of the ferrous iron cation between endolysosomes and mitochondria.

In the presence of H_2O_2 and O_2, Fe^{2+} catalyzes hydroxyl radicals and superoxides (Fenton, 1894), and the presence of H_2O_2 and O_2 in the cytosol and mitochondria is well studied (Halliwell et al., 2000, Veal et al., 2007). After chloroquine and bafilomycin A1 treatment, cytosolic ROS and mitochondrial ROS significantly increased; findings that suggest that ferrous iron catalyzed ROS formation. Furthermore, DFO blocked bafilomycin and chloroquine-induced cytosolic and mitochondrial ROS. These findings indicate that endolysosome ferrous iron is responsible for ROS production in the cytosol and mitochondria.

Two-pore channels have been shown to be involved in the release of calcium from endolysosomes (Rivero-Rios et al., 2016). Therefore, we studied the possible involvement of TPCN2 in the release of Fe^{2+} from endolysosomes.

Nicotinic acid adenine dinucleotide phosphate (NAADP) a TPC activator

(Boccaccio et al., 2014) caused a dose-dependent increase in mitochondrial iron.

On the other hand, NED-19 a known inhibitor of TPCs (Zharkich et al., 2016)

significantly decreased mitochondrial iron uptake induced by chloroquine or

bafilomycin A1. Furthermore, knocking down expression levels of TPCN2

significantly reduced mitochondrial iron uptake, which is consistent with the NED-

19 experiments.

Mitochondrial permeability transition pores are known to regulate levels of

mitochondrial iron (Sripetchwandee et al., 2014). Auranofin is a known activator

of mPTPs ((Rigobello et al., 2002) and we showed that auranofin increased

mitochondrial uptake of iron. On the other hand, cyclosporin A and TRO19622

both inhibit mPTPs (Sripetchwandee et al., 2014, Bordet et al., 2010) and we

found that CSA and TRO19622 blocked mitochondrial iron uptake.

Lastly, chloroquine (100 µM) and bafilomycin A1 (200 nM) treatment

induced cell death after 24 h, and DFO protected cells against chloroquine- and

bafilomycin A1-induced cell death. These findings are consistent with chloroquine

and bafilomycin A1 inducing mitochondrial iron overload leading to increased

ROS production which irreversibly damages the cells to the point of cell death.

DFO prevented mitochondrial iron overload induced by chloroquine and

bafilomycin A1 and thereby protected cells against the induced cytotoxicity.

In conclusion, excess iron is a known toxicant that can lead to acute

cellular injury (Christ et al., 1995), and excess iron may promote diseases such

as diabetes, cancer, cardiovascular disease, and neurodegeneration (Swanson,

2003, Petersen, 2005, Brewer, 2007, Imeryuz et al., 2007). With recent studies showing there is more ferrous iron in endolysosomes than previously thought (see Chapter 2), it is important to determine the role of endolysosome iron in cellular functions. This study reveals that Fe^{2+} stored in endolysosomes is mobilized into the cytosol and mitochondria following endolysosome deacidification and that this can ultimately lead to mitochondrial dysfunction and cell death. These data support the idea that mitochondrial iron accumulation is downstream of changes to endolysosomes. Thus, possible treatments against disease states might best include strategies against endolysosomes as well as mitochondria.
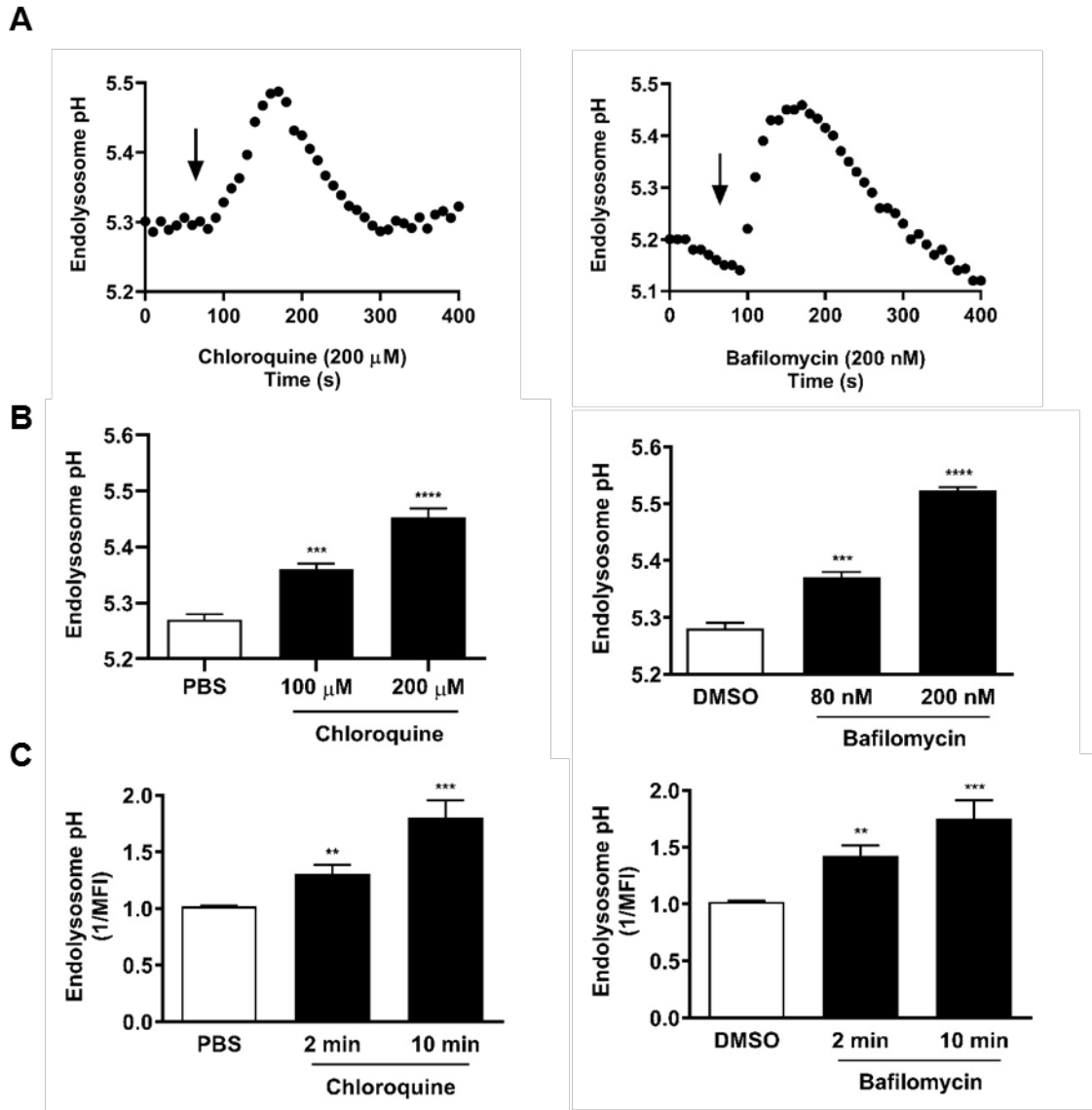
Figure 3. 1   Chloroquine and bafilomycin A1 de-acidified endolysosomes:
(**A**) Chloroquine and bafilomycin A1 increased endolysosome pH
as measured using LysoSensor DND-160.
(**B**) Treatment with different concentrations of bafilomycin A1 and
chloroquine resulted in an increase in endolysosome pH.
(**C**) Using Lysosensor DND-189, bafilomycin A1 and chloroquine
de-acidified endolysosomes in a time-dependent manner as
shown here using the reciprocal of 1 to illustrate an increase in
pH.
(Vehicle for bafilomycin A1 was 0.1% DMSO and vehicle for CQ
was PBS. n=30; ** $P < 0.01$, *** $P < 0.001$, **** $P < 0.0001$).

Figure 3. 2.   Chloroquine reduced Fe^{2+} levels in endolysosomes:
(A) FeRhoNox-1 colocalized with LysoTracker with a Pearson Correlation Coefficient of 0.84.
(B) Control treatment with PBS did not significantly change fluorescent intensity.
(C) Treatment with chloroquine (100 µM) resulted in a significant decrease in FeRhoNox-1 fluorescence intensity at 10 minutes.
(D) Quantification of FeRhoNox-1/Lysotracker ratio in endolysosomes.
(E). Quantification of FeRhoNox-1/Lysotracker ratio in the cytosol. FeRhoNox-1 fluorescence intensity decreased faster than LysoTracker fluorescence intensity in endolysosomes upon treatment, which is indicative of a reduction of iron.
(n=30; * $P < 0.05$, *** $P < 0.001$).

A. Colocalization
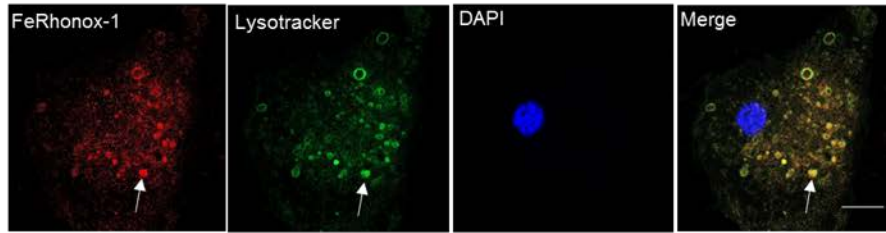
B. Control (PBS)
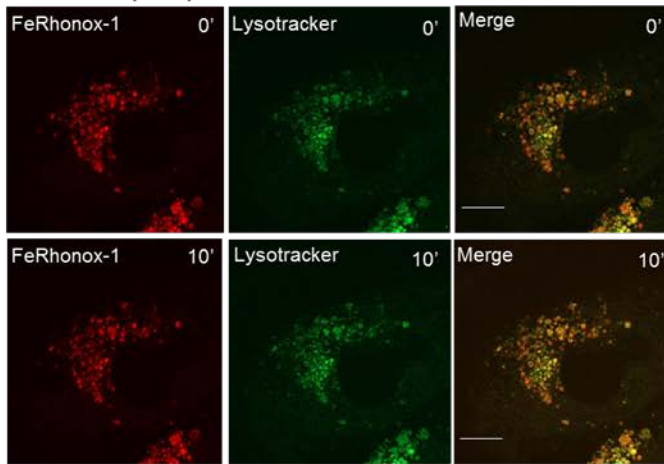
C. Chloroquine
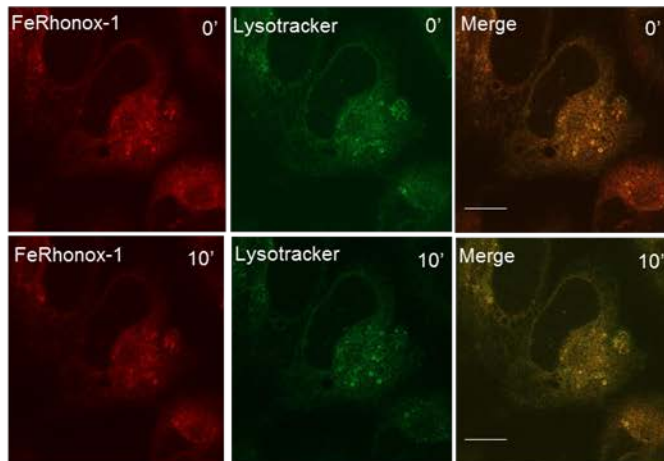
D.
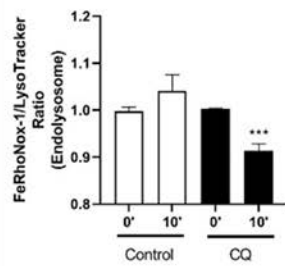
E.
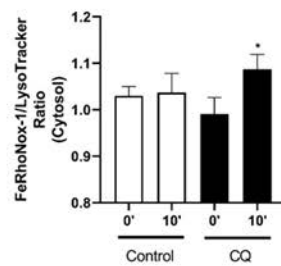
Figure 3. 3.   Bafilomycin A1 reduced Fe^{2+} levels in endolysosomes:
(A) Treatment of U87MG cells with vehicle (DMSO 0.1%) did not significantly change fluorescence intensity.
(B) Treatment with bafilomycin A1 (200 nM) resulted in a significant decrease in FeRhoNox-1 fluorescence intensity.
(C) Quantification of FeRhoNox-1/Lysotracker ratios in endolysosomes.
(D) Quantification of FeRhonox-1/Lysotracker ratios in the cytosol. FeRhoNox-1 fluorescence intensity is decreasing faster than LysoTracker fluorescent intensity in endolysosomes upon treatment, which is indicative of a reduction in iron content. (n=30; * $P < 0.05$, *** $P < 0.001$).

A. Control (DMSO)
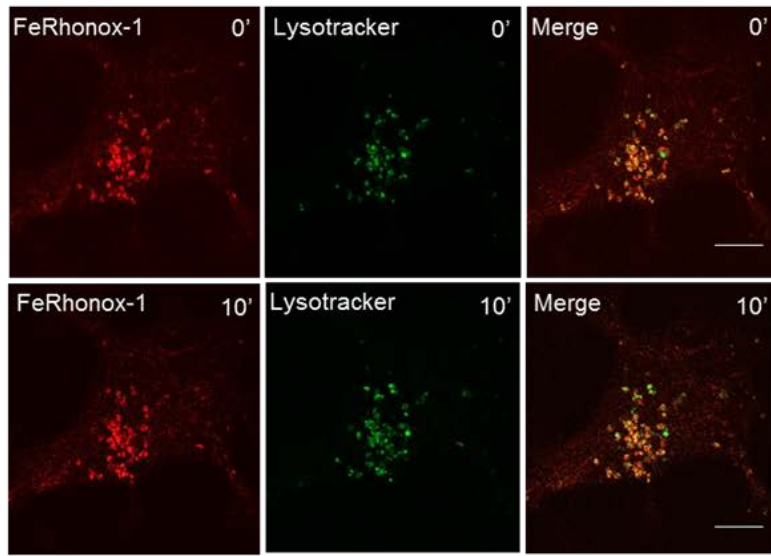
B. Bafilomycin
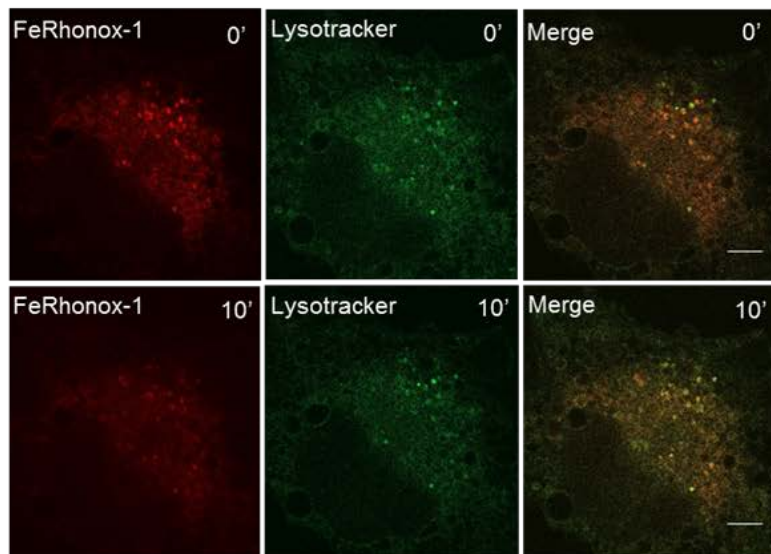
C.
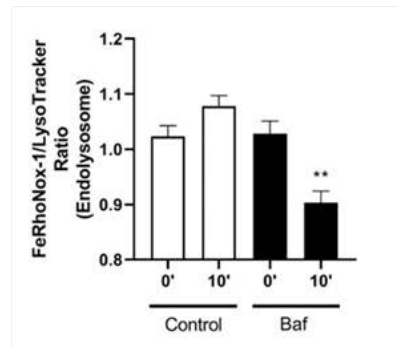
D.
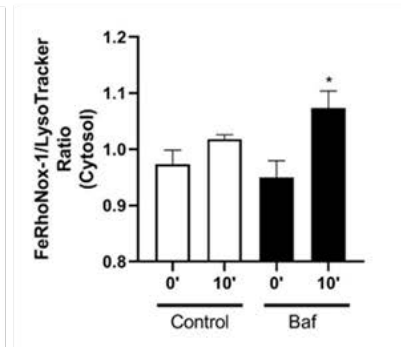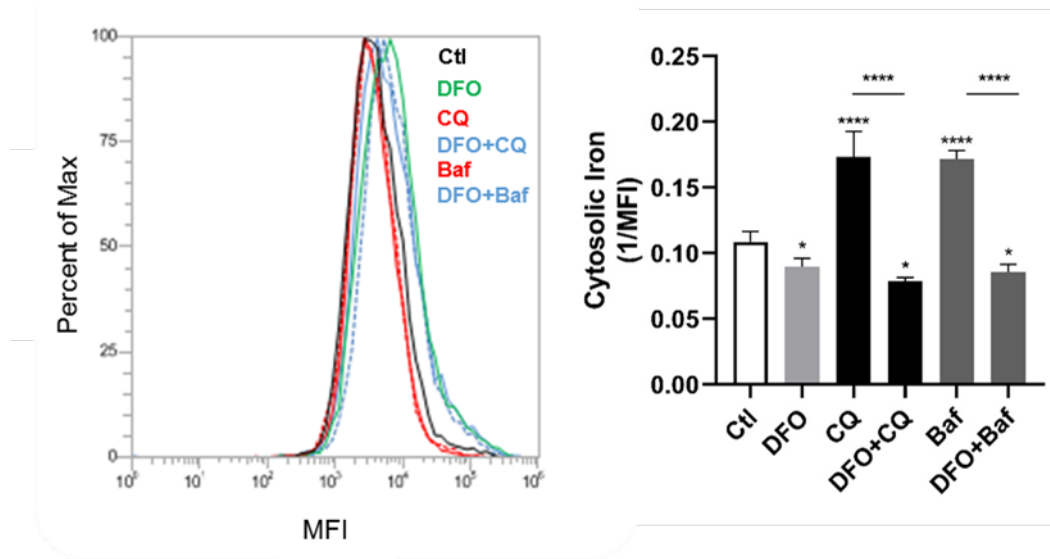
Figure 3. 4.   Chloroquine and bafilomycin A1 increased cytosolic Fe^{2+}: Chloroquine (100 µM) and bafilomycin A1 (200 nM) quenched Phen-Green; data were illustrated as a reciprocal of the Mean Fluorescent Intensity (MFI) to illustrate more clearly the increase in cytosolic iron. DFO blocked chloroquine and bafilomycin A1-induced quenching of Phen-Green. DFO alone suppressed Phen-Green quenching a finding that suggests the presence of a constitutive leak of Fe^{2+}.
(n=5; ** P < 0.01, *** P < 0.001, **** P < 0.0001).

Figure 3. 5.   Chloroquine and bafilomycin A1 increased mitochondrial Fe^{2+}:
(A) Colocalization of the mitochondrial iron stain (RDA) and MitoTracker with a Pearson Correlation Coefficient of 0.97.
(B) Control cells stained with RDA treated with PBS (DMSO yielded similar results as PBS).
(C) DFO (100 µM) did not alter fluorescence intensity.
(D-G) Chloroquine (100 µM) and bafilomycin A1 (200 nM) quenched RDA fluorescence and DFO blocked chloroquine and bafilomycin A1-induced quenching as quantified in (**H**).
(I-K) Mitochondrial iron uptake is dose-dependent on GPN, chloroquine, and bafilomycin A1.
(n=30; * $P < 0.05$, ** $P < 0.01$, *** $P < 0.001$, **** $P < 0.0001$).

A. Colocalization

RDA

Mitotracker

Merge

B. Control   0'   10'

C. DFO   0'   10'

D. CQ   0'   10'

E. DFO + CQ   0'   10'

F. Baf   0'   10'

G. DFO + Baf   0'   10'

H.

Mitochondrial Iron (1/ΔMFI)

Control   DFO   CQ   DFO+CQ   Baf   DFO+Baf

****   ****   ****   ****   ****

I.

Mitochondrial Iron (1/ΔMFI)

DMSO   0.1 μM   0.5 μM   1 μM   2 μM

GPN

***   ****

J.

Mitochondrial Iron (1/ΔMFI)

PBS   10 μM   50 μM   100 μM

Chloroquine

*   ***   ****

K.

Mitochondrial Iron (1/ΔMFI)

DMSO   10 nM   100 nM   200 nM

Bafilomycin A1

*   ***   ****

64
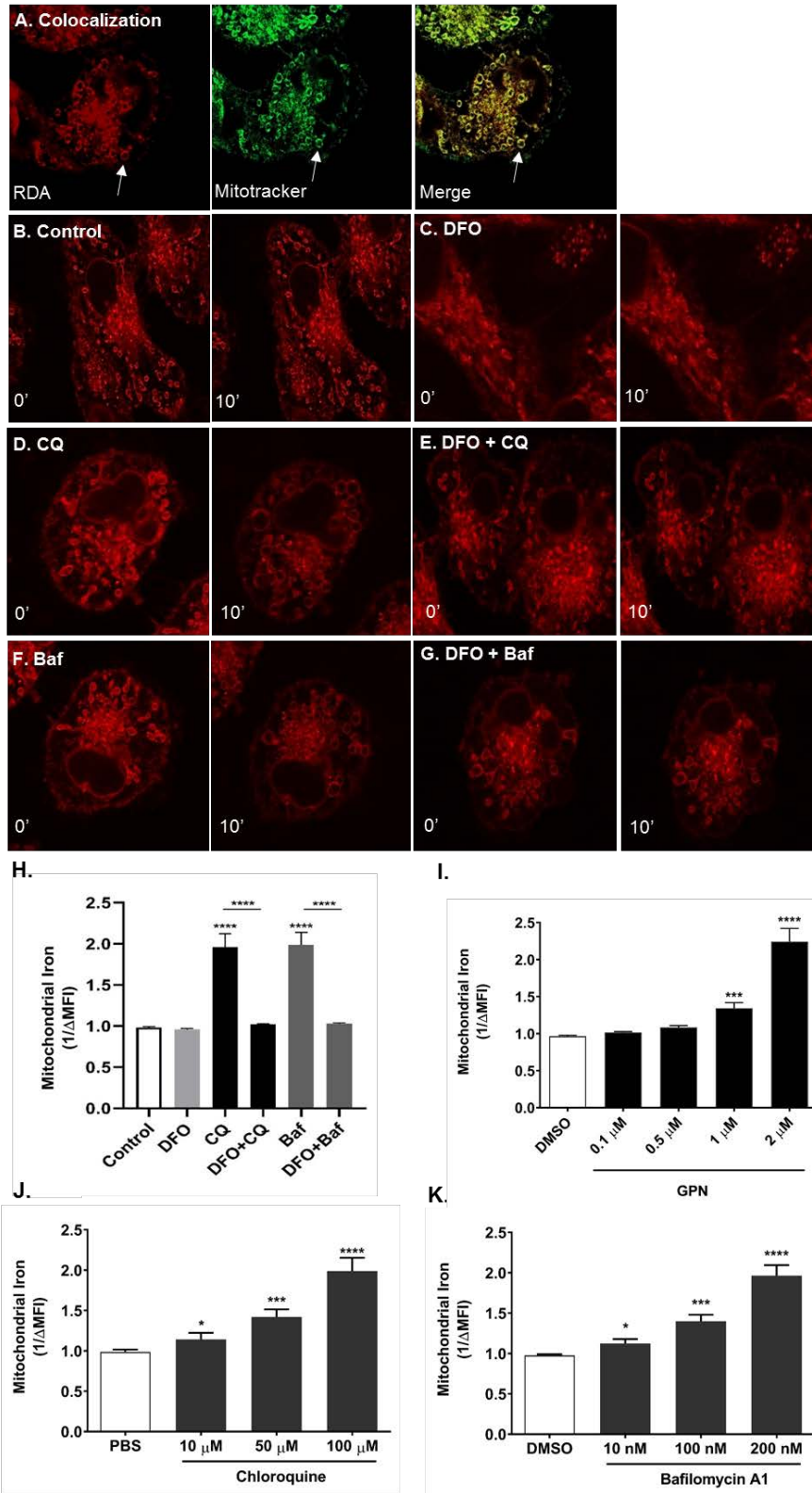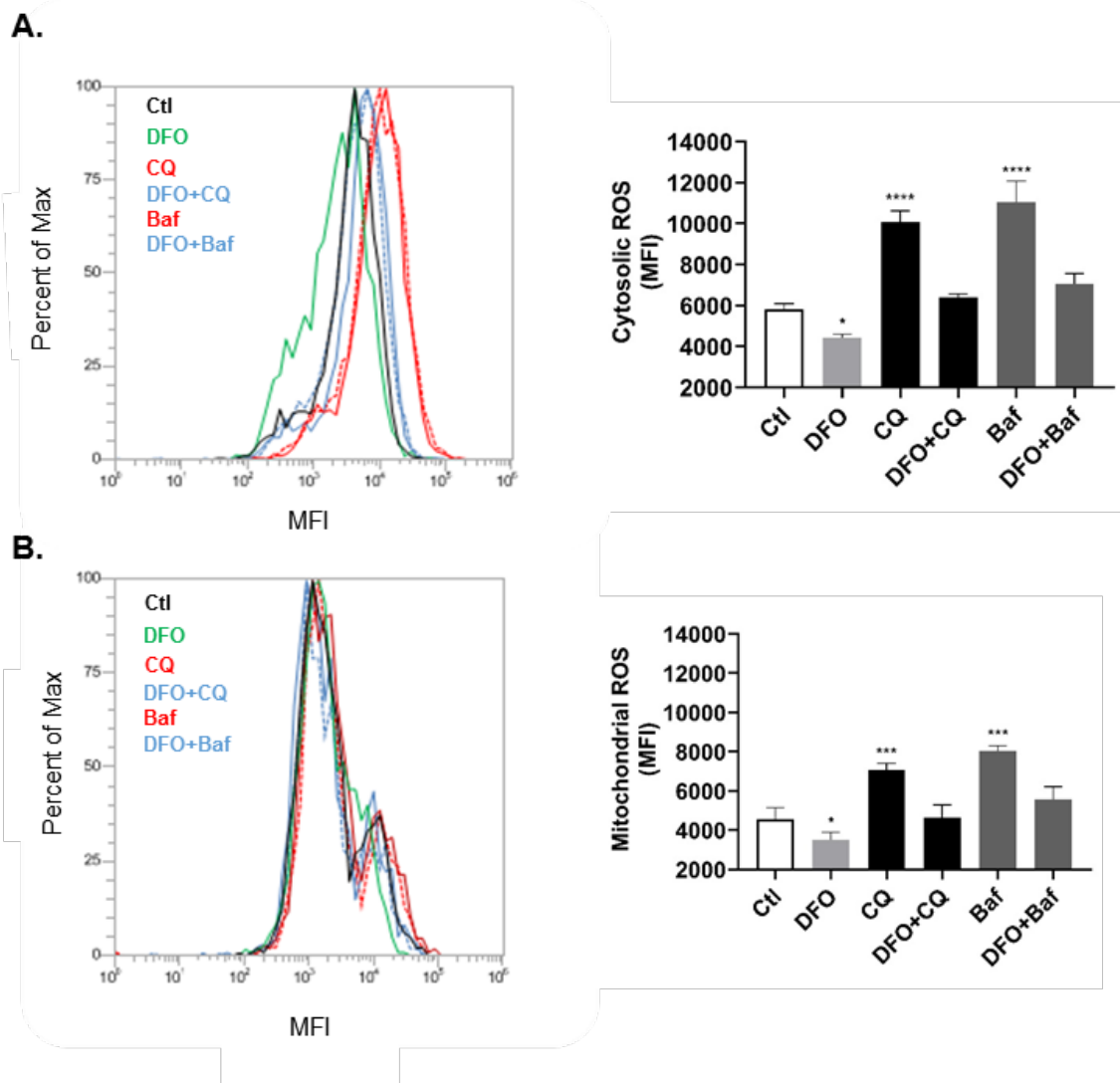
Figure 3. 6. Chloroquine and bafilomycin A1 increased cytosolic ROS and mitochondrial ROS:
(A) Using H$_2$DCFDA for measures of cytosolic ROS, chloroquine (100 µM) and bafilomycin A1 (200 nM) increased ROS, and these increases were inhibited by DFO.
(B) Using MitoSox for measures of mitochondrial ROS, chloroquine (100 µM) and bafilomycin A1 (200 nM) increased ROS, and these increases were inhibited by DFO.
(n=5; * P < 0.05, ** P < 0.01, *** P < 0.001, **** P < 0.0001).
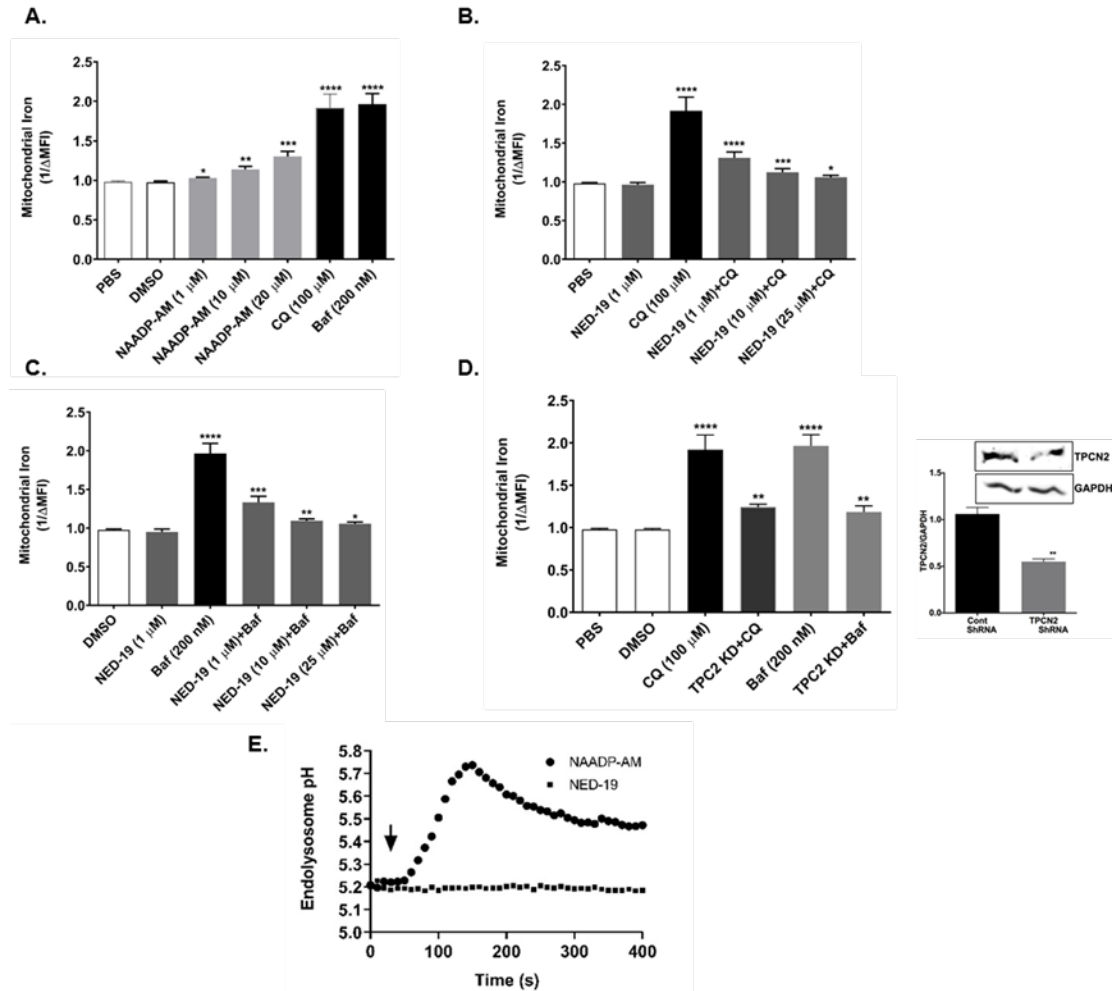
Figure 3. 7.   Mitochondrial iron uptake was regulated by two-pore channels on endolysosomes:
(A) The TPC activator, NAADP-AM, dose-dependently increased mitochondrial iron.
(B-C) The TPC antagonist, NED-19, dose-dependently blocked mitochondrial iron uptake induced by chloroquine (100 μM) and bafilomycin A1 (200 nM).
(D) TPCN2 knockdown cells significantly decreased mitochondrial iron uptake induced by bafilomycin A1 and chloroquine.
(E) Interestingly, NAADP-AM (20 μM) significantly de-acidifies endolysosomes whereas NED-19 remains unchanged.
(n=30; * $P < 0.05$, ** $P < 0.01$, *** $P < 0.001$, **** $P < 0.0001$).
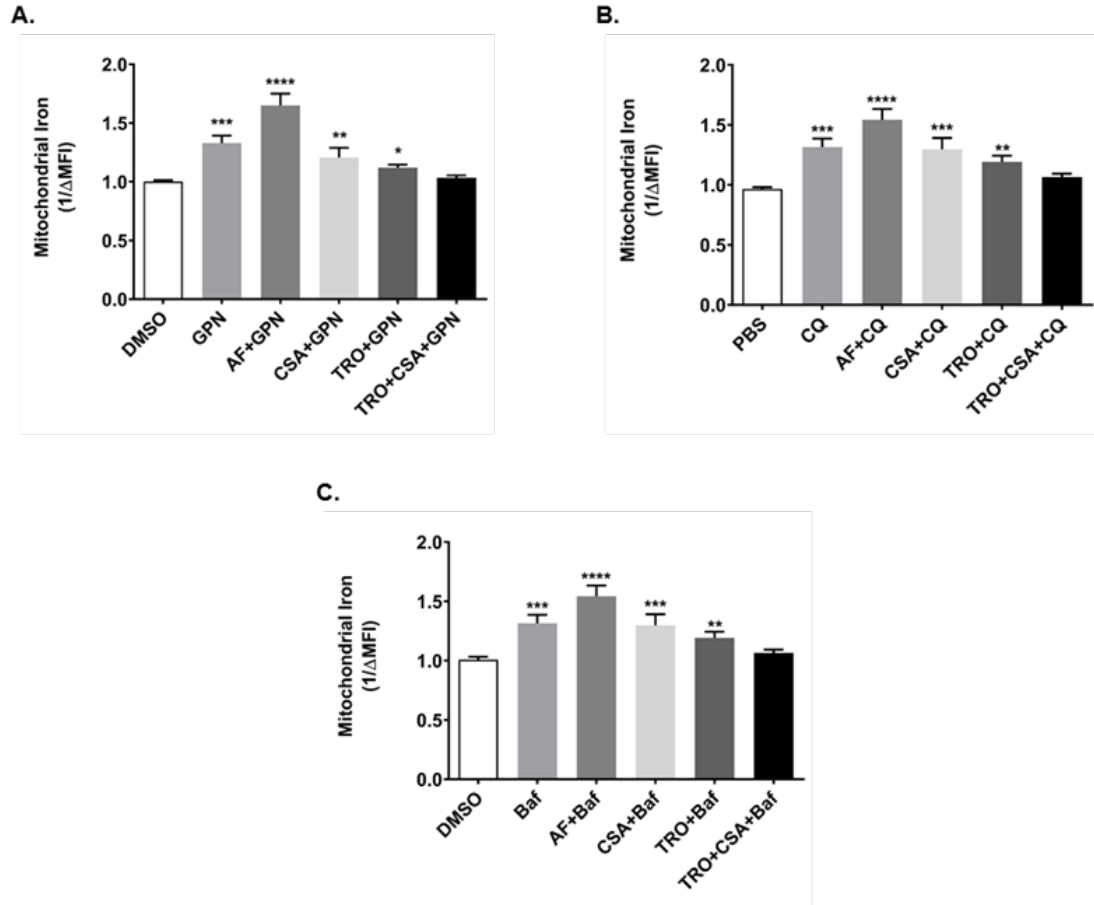
Figure 3. 8.   Mitochondrial permeability transition pores (mMPTP) regulated
                iron uptake:
                (A) Auranofin (AF) increased GPN-induced mitochondrial iron
                uptake, and cyclosporine A (CSA) in combination with
                TRO19622 (TRO) inhibited GPN-induced mitochondrial iron
                uptake.
                (B-C) AF increased chloroquine- and bafilomycin A1-induced
                mitochondrial iron uptake, and CSA and TRO inhibited
                mitochondrial iron uptake.
                (n=30; * $P < 0.05$, ** $P < 0.01$, *** $P < 0.001$, **** $P < 0.0001$).
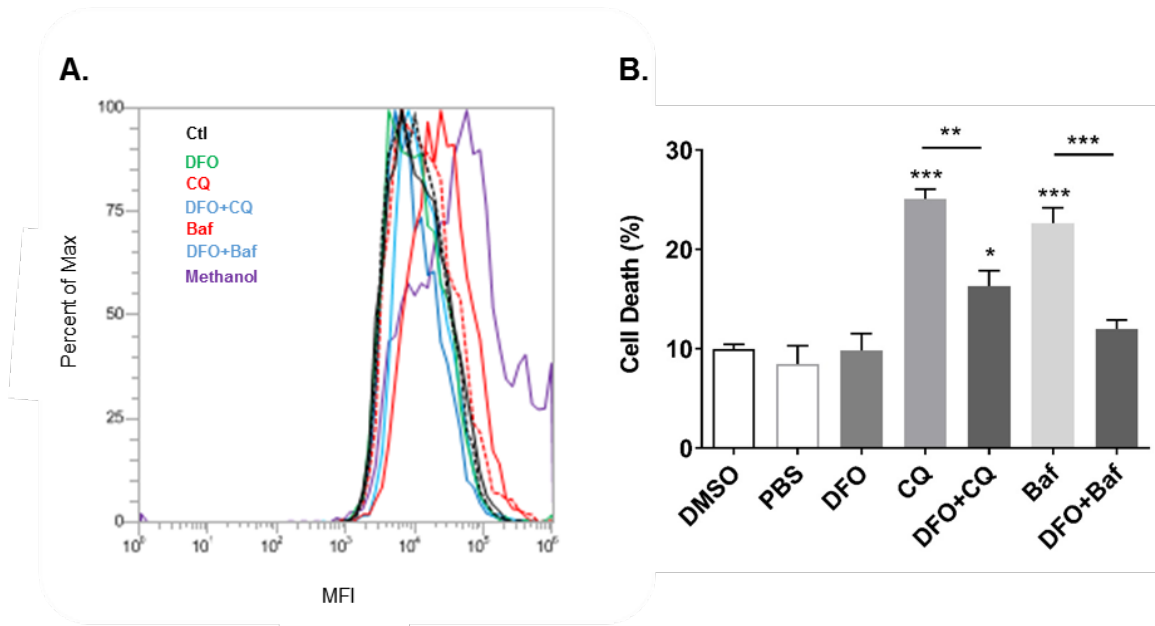
Figure 3. 9.   Deferoxamine protected against chloroquine- and bafilomycin
A1-induced cell death:
(A) Histogram of cell death experiment with propidium iodide.
Methanol (10 µM) caused 80% cell death after 2 h and was used
as a positive control.
(B) Chloroquine (100 µM) and bafilomycin A1 (200 nM)
increased cell death after 24 hours, and DFO pretreatment
protected cells against chloroquine- and bafilomycin A1-induced
cell death.
(n=5; * $P < 0.05$, ** $P < 0.01$, *** $P < 0.001$, **** $P < 0.0001$).
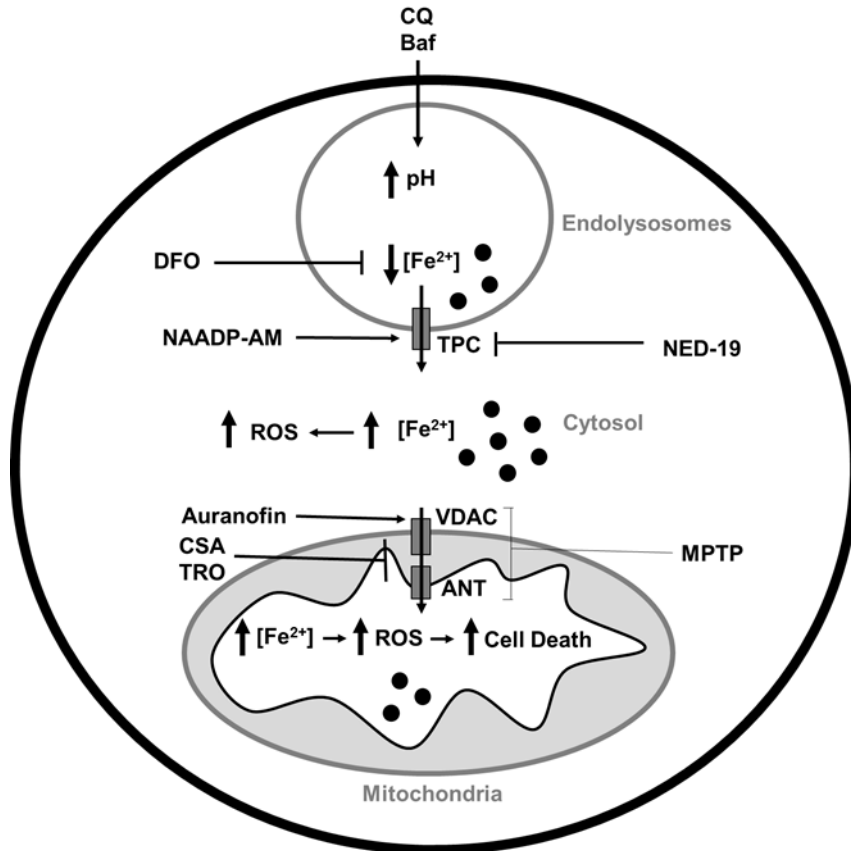
Figure 3. 10.   Schematic diagram of cellular mechanisms: De-acidification of endolysosomes can cause the release of iron from endolysosomes and this released iron can accumulate in the cytoplasm and in mitochondria. The iron released from endolysosomes leads to increased levels of ROS in the cytosol and in mitochondria. DFO chelates endolysosome iron and inhibits ROS and cell death induced by chloroquine and bafilomycin A1.

References

BERG, T. O., STRØMHAUG, P. E., LØVDAL, T., SEGLEN, P. O. & BERG, T. 1994. Use of glycyl-L-phenylalanine 2-naphthylamide, a lysosome-disrupting cathepsin C substrate, to distinguish between lysosomes and prelysosomal endocytic vacuoles. Biochemical Journal, 300, 229.

BOCCACCIO, A., SCHOLZ-STARKE, J., HAMAMOTO, S., LARISCH, N., FESTA, M., GUTLA, P. V., COSTA, A., DIETRICH, P., UOZUMI, N. & CARPANETO, A. 2014. The phosphoinositide PI(3,5)P(2) mediates activation of mammalian but not plant TPC proteins: functional expression of endolysosomal channels in yeast and plant cells. Cell Mol Life Sci, 71, 4275-83.

BORDET, T., BERNA, P., ABITBOL, J.-L. & PRUSS, R. M. 2010. Olesoxime (TRO19622): A Novel Mitochondrial-Targeted Neuroprotective Compound. Pharmaceuticals (Basel, Switzerland), 3, 345-368.

CHAVEZ-CROOKER, P., GARRIDO, N. & AHEARN, G. A. 2001. Copper transport by lobster hepatopancreatic epithelial cells separated by centrifugal elutriation: measurements with the fluorescent dye Phen Green. J Exp Biol, 204, 1433-44.

CHEN, X., HUI, L., GEIGER, N. H., HAUGHEY, N. J. & GEIGER, J. D. 2013. Endolysosome involvement in HIV-1 transactivator protein-induced neuronal amyloid beta production. Neurobiol Aging, 34, 2370-8.

CHRISTENSEN, K. A., MYERS, J. T. & SWANSON, J. A. 2002. pH-dependent regulation of lysosomal calcium in macrophages. J Cell Sci, 115, 599-607.

DOULIAS, P. T., CHRISTOFORIDIS, S., BRUNK, U. T. & GALARIS, D. 2003. Endosomal and lysosomal effects of desferrioxamine: protection of HeLa cells from hydrogen peroxide-induced DNA damage and induction of cell-cycle arrest. Free Radic Biol Med, 35, 719-28.

ENNS, G. M. 2003. The contribution of mitochondria to common disorders. Molecular Genetics and Metabolism, 80, 11-26.

FENTON, H. J. H. 1894. LXXIII.—Oxidation of tartaric acid in presence of iron. Journal of the Chemical Society, Transactions, 65, 899-910.

FERNÁNDEZ, B., FDEZ, E., GÓMEZ-SUAGA, P., GIL, F., MOLINA-VILLALBA, I., FERRER, I., PATEL, S., CHURCHILL, G. C. & HILFIKER, S. 2016. Iron overload causes endolysosomal deficits modulated by NAADP-regulated 2-pore channels and RAB7A. Autophagy, 12, 1487-1506.

HUI, L., CHEN, X. & GEIGER, J. D. 2012a. Endolysosome involvement in LDL cholesterol-induced Alzheimer's disease-like pathology in primary cultured neurons. Life Sci, 91, 1159-68.

HUI, L., CHEN, X., HAUGHEY, N. J. & GEIGER, J. D. 2012b. Role of endolysosomes in HIV-1 Tat-induced neurotoxicity. ASN Neuro, 4, 243-52.

JELLINGER, K. A. 2009. Recent advances in our understanding of neurodegeneration. J Neural Transm (Vienna), 116, 1111-62.

LIU, Z. D. & HIDER, R. C. 2002. Design of clinically useful iron(III)-selective chelators. Med Res Rev, 22, 26-64.

MYHRE, O., ANDERSEN, J. M., AARNES, H. & FONNUM, F. 2003. Evaluation of the probes 2′,7′-dichlorofluorescin diacetate, luminol, and lucigenin as indicators of reactive species formation. Biochemical Pharmacology, 65, 1575-1582.

PADMANABHAN, H., BROOKES, M. J. & IQBAL, T. 2015. Iron and colorectal cancer: evidence from in vitro and animal studies. Nutr Rev, 73, 308-17.

RAUEN, U., SPRINGER, A., WEISHEIT, D., PETRAT, F., KORTH, H. G., DE GROOT, H. & SUSTMANN, R. 2007. Assessment of chelatable mitochondrial iron by using mitochondrion-selective fluorescent iron indicators with different iron-binding affinities. Chembiochem, 8, 341-52.

RIGOBELLO, M. P., SCUTARI, G., BOSCOLO, R. & BINDOLI, A. 2002. Induction of mitochondrial permeability transition by auranofin, a gold(I)-phosphine derivative. British journal of pharmacology, 136, 1162-1168.

RIVERO-RIOS, P., FERNANDEZ, B., MADERO-PEREZ, J., LOZANO, M. R. & HILFIKER, S. 2016. Two-Pore Channels and Parkinson's Disease: Where's the Link? Messenger (Los Angel), 5, 67-75.

ROCKFIELD, S., RAFFEL, J., MEHTA, R., REHMAN, N. & NANJUNDAN, M. 2017. Iron overload and altered iron metabolism in ovarian cancer. Biol Chem, 398, 995-1007.

SRIPETCHWANDEE, J., KENKNIGHT, S. B., SANIT, J., CHATTIPAKORN, S. & CHATTIPAKORN, N. 2014. Blockade of mitochondrial calcium uniporter prevents cardiac mitochondrial dysfunction caused by iron overload. Acta Physiol (Oxf), 210, 330-41.

STEINMAN, R. M., MELLMAN, I. S., MULLER, W. A. & COHN, Z. A. 1983. Endocytosis and the recycling of plasma membrane. J Cell Biol, 96, 1-27.

STEREA, A. M., ALMASI, S. & EL HIANI, Y. 2018. The hidden potential of lysosomal ion channels: A new era of oncogenes. Cell Calcium, 72, 91-103.

TAPPER, H. & SUNDLER, R. 1995. Bafilomycin A1 inhibits lysosomal, phagosomal, and plasma membrane H(+)-ATPase and induces lysosomal enzyme secretion in macrophages. J Cell Physiol, 163, 137-44.

THOMAS, F., SERRATRICE, G., BEGUIN, C., AMAN, E. S., PIERRE, J. L., FONTECAVE, M. & LAULHERE, J. P. 1999. Calcein as a fluorescent probe for ferric iron. Application to iron nutrition in plant cells. J Biol Chem, 274, 13375-83.

UCHIYAMA, A., KIM, J. S., KON, K., JAESCHKE, H., IKEJIMA, K., WATANABE, S. & LEMASTERS, J. J. 2008. Translocation of iron from lysosomes into mitochondria is a key event during oxidative stress-induced hepatocellular injury. Hepatology, 48, 1644-54.

XIONG, J. & ZHU, M. X. 2016. Regulation of lysosomal ion homeostasis by channels and transporters. Science China. Life sciences, 59, 777-791.

XU, H. & REN, D. 2015. Lysosomal Physiology. Annual Review of Physiology, 77, 57-80.

YOSHIMORI, T., YAMAMOTO, A., MORIYAMA, Y., FUTAI, M. & TASHIR, Y. 1991. Bafilomycin AI, a Specific Inhibitor of Vacuolar-type H+-ATPase, Inhibits Acidification and Protein Degradation in Lysosomes of Cultured Cells. THE JOURNAL OF BIOLOGICAL CHEMISTRY. 266(26):17707-12.

ZHARKICH, I. L., NADEEV, A. D., TSITRIN, E. B., GONCHAROV, N. V. & AVDONIN, P. V. 2016. Suppression of Histamine-Induced Relaxation of Rat Aorta and Calcium Signaling in Endothelial Cells by Two-Pore Channel Blocker trans-NED19 and Hydrogen Peroxide. Izv Akad Nauk Ser Biol, 430-438.

CHAPTER 4

MORPHINE DE-ACIDIFICATION OF ENDOLYSOSOMES INDUCES IRON RELEASE RESULTING IN MITOCHONDRIAL DYSFUNCTION

Peter W. Halcrow[1], Nabab Khan[1], Xuesong Chen[1],
Olimpia Meucci[2], and Jonathan D. Geiger[1]

Department of Biomedical Sciences[1]
University of North Dakota School of Medicine and Health Sciences
Grand Forks, ND 58203, USA

Department of Pharmacology & Physiology[2]
Drexel University College of Medicine
Philadelphia, PA 19102

Abstract

Drugs of abuse including the opioid morphine increase levels of reactive oxygen species (ROS) and predispose cells to insult-induced cell death. However, it remains uncertain as to the underlying mechanisms. Iron has long been known to be required for the generation of mitochondrial ROS and endosomes and lysosomes, referred to as endolysosomes, are major storage sites of ferrous iron (Fe^{2+}). Yet, the degree to which and the precise mechanisms by which endolysosome iron plays a role in mitochondrial dysfunction remains uncertain. Here, our studies were aimed to determine the effects of morphine on inter-organellar signaling of Fe^{2+} from iron-rich endolysosomes to mitochondria. We demonstrated, in U87MG astrocytoma cells, that endolysosome Fe^{2+} is translocated to mitochondria and results in mitochondrial dysfunction. Morphine de-acidification of endolysosomes caused the release of Fe^{2+} from endolysosomes and increased levels of Fe^{2+} in cytosol and in. The morphine-induced effects on endolysosome Fe^{2+} appeared to be regulated through mu opioid receptors because naloxone blocked the de-acidification of endolysosomes by morphine and the release of endolysosome iron. Furthermore, the endocytosed iron chelator, deferoxamine, inhibited the release of redox-active Fe^{2+} into the cytosol and the morphine-induced increases in mitochondrial ROS. These findings demonstrate that redox-active Fe^{2+} in endolysosomes plays a key upstream role in mitochondrial dysfunction, and deferoxamine might be a potentially useful therapeutic strategy associated with opioid use disorders.

Introduction

Drugs of abuse including the opioid morphine have been associated with the pathogenesis of neurological diseases; mechanistically this had been linked through increases in reactive oxygen species (ROS), mitochondrial dysfunction, and bioenergetic failure (Imam and Ali, 2000, Imam and Ali, 2001, Stephans et al., 1998, Cunha-Oliveira et al., 2013, Xu et al., 2011). Drugs of abuse-induced decreases in levels of ATP and increased levels of ROS (Acikgoz et al., 1998, Binienda et al., 1998) and such measures of neurotoxicity can be blocked by the antioxidants (Fosslien, 2001, Imam and Ali, 2000). However, mechanisms by which opioids (and other drugs of abuse) increase levels of ROS remain unclear.

Iron plays a crucial role in cellular functions such as the iron-sulfur clusters in the electron transport chain and iron in excess is toxic and leads to cellular injury and death (Christ et al., 1995). Excess iron can promote neurodegeneration (Swanson, 2003, Petersen, 2005, Brewer, 2007, Imeryuz et al., 2007) and iron dyshomeostasis has been linked to disease initiation and progression (Enns, 2003, Jellinger, 2009). Even though various models of oxidative stress and hypoxia have pointed to a role for iron in their pathogenesis (Jellinger, 2009), the intracellular source of excess iron and the precise mechanisms by which iron is mobilized intracellularly to contribute to cellular injury remain poorly understood.

A key reactant in the formation of ROS is ferrous iron (Fe^{2+}) (Fenton, 1894, Kehrer, 2000, Weiss, 1934). In the presence of H_2O_2 and O_2, Fe^{2+} generates highly reactive hydroxyl radicals (HO) and superoxides (O_2^-) that

75

ultimately damage DNA and proteins (Kehrer, 2000). It is well established that ROS contributes to cellular dysfunction and cell death (Jaeschke et al., 2002, Videla et al., 2003, Schwabe and Brenner, 2006). Furthermore, the most important source of ROS happens in the mitochondria because that is where ATP is produced (Loschen et al., 1974, Boveris and Cadenas, 1975). Because mitochondria have a constitutive presence of ROS generated by the electron transport chain, the levels of mitochondrial iron must be tightly regulated. The accumulation of iron in the mitochondria has been observed in neurogenerative diseases, but the source of excess iron and how mitochondrial iron accumulation is a downstream effect remains undetermined (Mena et al., 2015).

Endosomes and lysosomes, referred to as endolysosomes, have key physiological roles including plasma membrane repair, cell homeostasis, cell adhesion and migration, apoptotic cell death, and metabolic signaling (Perera and Zoncu, 2016, Settembre et al., 2013). And, it is well-established that endolysosomes store readily-releasable cations including Ca^{2+}, Zn^{2+}, Fe^{3+}, and Fe^{2+} (Xu and Ren, 2015, Xiong and Zhu, 2016b). The acidic pH of endolysosome lumens is maintained through the influx of protons via v-ATPases in conjunction with ion channels (TRPML1, TPCs, and BK) regulating cation concentrations within endolysosomes (Pu et al., 2016). The v-ATPase mechanism generates a proton force that drives ions across endolysosome membranes creating a voltage gradient which is sustained by counter-ions including Na^+, K^+, and Cl^- (Mindell, 2012a). The efflux of cations such as Ca^{2+} from endolysosomes into the cytosol has been demonstrated with drugs that de-acidify endolysosomes, and

76

these released cations play crucial roles in cellular signaling pathways (Christensen et al., 2002). However, very little is known about the role of the redox-active Fe^{2+} cation within endolysosomes in inter-organellar signaling and cell death.

In this study, we show morphine de-acidifies endolysosomes causing an efflux of Fe^{2+} out of endolysosomes into the cytosol and into mitochondria increasing. As well, morphine increased levels of ROS and these effects of morphine were controlled by mu opioid receptors because naloxone blocked morphine-induced de-acidification of endolysosomes and morphine-induced release of iron from endolysosomes. In addition, we demonstrate that the iron chelator DFO blocked morphine-induced increases in cytosolic and mitochondrial Fe^{2+} as well as morphine-induced increases in mitochondrial ROS. These studies emphasize the link between opioids and endolysosomes as intracellular sources of iron that translocate into mitochondria leading to increased ROS and dysfunction.

Materials and Methods

Cell Culture

U87MG astrocytoma cells were cultured in 1x DMEM (Invitrogen) supplemented with 10% fetal calf serum and 1% penicillin/streptomycin (Invitrogen). Cells were grown to confluence in T75 flasks or to about 40% confluence in 35 mm^2 dishes in an environment of 5% CO_2 at 37°C. Cells were only used at passage numbers of 10 or less.

77

Endolysosome pH

As previously described (Chen et al., 2013, Hui et al., 2012a, Hui et al., 2012b), endolysosome pH was measured using a ratiometric indicator-dye, LysoSensor Yellow/Blue DND-160; a dual excitation dye that allows for the measurement of acidic organelles independent of dye loading efficiency. U87MG cells were loaded with 10 μM DND-160 for 5 minutes at 37°C. Post-incubation, dye-containing media was removed and PBS was added to the cells prior to them being taken for imaging. CellLight Lysosome-RFP (Thermosfisher), incubated in cells overnight, was used to label lysosomes in combination with LysoSensor DND-160 for selectivity of lysosomal labeling. Light emitted at 520 nm in response to excitation at 340 nm and 380 nm was measured for 2 msec every 10 seconds using a filter-based imaging system (Zeiss, Germany). The ratios of light excited (340/380 nm) versus light emitted (520 nm) were converted to pH using a calibration curve established with 10 μM of the H^+/Na^+ ionophore monensin, and 20 μM of the H^+/K^+ ionophore nigericin; both were dissolved in 20 mM 2-(N-morpholino) ethane sulfonic acid (MES), 110 mM KCl, and 20 mM NaCl adjusted to pH 3.0 to 7.0 with HCl/NaOH; the linear range was 4.5 to 6.0 pH.

Endolysosome Iron

FeRhonox-1 (10 μM) (Goryo Chemical), which is highly specific for Fe^{2+}, was incubated with cells for 1 h, washed with PBS, then measured using a confocal microscope at absorption and emission wavelengths 537 nm and 569 nm, respectively. Halcrow et el. (see Chapter 2) colocalized FeRhonox-1 with

endolysosomes in U87MG cells and primary neurons. Experiments were conducted on a LSM800 confocal laser-scanning microscope (ZEISS).

Cytosolic Iron

Cells were incubated with PhenGreen™ FL diacetate (10 µM) for 30 minutes at 37°C. Cells were washed with PBS and analyzed (Alexa Fluor 488) using a ThermoFisher Attune flow cytometry and an Axiovert 200M (Zeiss) microscope.

Mitochondrial Iron

Mitochondrial iron levels were measured using rhodamine B-[2,2'-bipyridine-4-yl)-aminocarbonyl]benzyl ester (RDA) dye (Squarix), a Fe^{2+} specific fluorescent sensor that is localized within mitochondria. Cells were treated with RDA (100 nM) for 10 minutes at 37°C, then washed with PBS followed by experiments conducted on a confocal laser scanning microscope (ZEISS).

Iron Chelator

Deferoxamine (50 µM), a Fe^{2+} chelator that is endocytosed (Doulias et al., 2003), was incubated in cells for 1 h prior to analysis and administering other compounds.

ROS Measurements

Cytosolic ROS was measured using H_2DCFDA, 2,7-dichlorodihydrofluoroscein diacetate (10 µM) (Thermofisher), and mitochondrial ROS was measured using MitoSox Red (5 µM) (Thermofisher).

Cells were incubated with the respective dyes at 37ºC for 30 minutes in serum-free media and then washed with PBS prior to analysis by flow cytometry.

Statistical Analysis

All results were expressed as mean ± SD. Data were analyzed using the software GraphPad Prism Version 6 (GraphPad Software, Inc., La Jolla, CA). Statistical significance between two groups was analyzed with a Student's t-test, and statistical significance among multiple groups was analyzed with one-way ANOVA plus a Tukey post-hoc test. $p<0.05$ was considered to be statistically significant.

<div align="center">

Results

</div>

Morphine De-acidified Endolysosome pH

Cultured U87MG cells were incubated with CellLight Lysosome-RFP and Lysosensor DND-160, which is a ratiometric excitation dye that allows for the measurement of pH in acidic organelles. Cells were treated with different concentrations of morphine (1 µM, 50 µM, and 100 µM). Morphine (10 µM) de-acidification of endolysosomes is a delayed response as shown in Figure 4.1A. Naloxone, a mu opioid antagonist, which did not by itself change endolysosome pH blocked the de-acidification of endolysosomes by morphine as shown in Figure 4.1B. In addition, the de-acidification of endolysosomes by morphine was dose-dependent (Figure 4.1C).

Morphine Releases Fe^{2+} from Endolysosomes into the Cytosol

The FeRhoNox-1 dye was previously determined to be highly specific for Fe^{2+} and endolysosomes (see Chapter 2). In addition, it has been shown that the

iron chelator DFO inhibits FeRhoNox-1 fluorescent intensity because it is endocytosed and chelates Fe^{2+} (see Chapter 2). U87MG cells were stained with FeRhoNox-1 for 1 h prior to experimentation. Also, these experiments were conducted from 0 min to 30 min, times consistent with rates of endolysosome de-acidification by morphine (Figure 4.1). In control cells treated with PBS, FeRhoNox-1 fluorescence intensity did not significantly change (Figure 4.2). Morphine significantly decreased FeRhoNox-1 fluorescence intensity, and naloxone inhibited the effects of morphine. Quantification of the FeRhoNox-1 within endolysosomes for control and morphine treated cells is shown in Figure 4.2D. To determine whether iron was released into the cytosol, Phen-Green FL was used; Phen-Green is a dye that quenches in the presence of metals such as zinc, copper, and ferrous iron. Because Phen-Green is a quenching stain, the reciprocal of the mean fluorescent intensity was calculated to illustrate an increase in cytosolic iron. Morphine treatment significantly quenched Phen Green, and naloxone blocked morphine-induced effects as shown in Figure 4.3A. Quantification of these effects are shown in Figure 4.3B. Deferoxamine is a ferrous iron chelator that is endocytosed (Doulias et al., 2003), and DFO significantly decreases the quenching of Phen Green, indicating there is a constitutive leak of Fe^{2+} from endolysosomes into the cytosol as shown in Figure 3C. Pretreatment with DFO prior to morphine treatment blocked the quenching of Phen Green, indicating a release of Fe^{2+} from endolysosomes into the cytosol by morphine as shown in Figure 4.3C by flow cytometry.

Endolysosome Iron is Taken up by Mitochondria

Rhodamine B 4-[(2,2'-bipyridin-4-yl)aminocarbonyl]benzyl ester (RDA) is a dye specific to Fe^{2+} and the mitochondria, and RDA fluorescence is stoichiometrically (3:1) quenched by Fe^{2+} ions (Rauen et al., 2007). U87MG cells were stained with RDA (100 nM), and the experiments were conducted from 0 min to 30 min, times consistent with the rate of endolysosome de-acidification by morphine (Figure 4.1) and the release of Fe^{2+} from endolysosomes (Figures 4.2 and 4.3). Control cells stained with RDA were treated with PBS which did not yield significant changes to RDA fluorescence (Figure 4.4). Morphine quenched RDA fluorescence as shown in Figure 4.4.

Morphine-induced Fe^{2+} Release from Endolysosomes Increases Mitochondrial ROS

Ferrous iron is a key reactant in the formation of the highly reactive hydroxyl radical and superoxide (Fenton, 1894). U87MG cells were stained with MitoSox, a mitochondrial measure of ROS. Morphine increased mitochondrial ROS, and DFO blocked morphine-induced mitochondrial ROS (Figure 4.5).

Schematic Diagram of Overall Cellular Mechanisms

The schematic diagram of the proposed cellular mechanisms involved in these studies was illustrated in Figure 4.6. Morphine de-acidifies the pH of endolysosomes, releases iron into the cytosol, and iron is up-taken into mitochondria. The iron released from endolysosomes leads to increased levels of ROS in the cytosol and in mitochondria. DFO chelates endolysosome iron and inhibits ROS induced by morphine.

Discussion

Although intracellular labile iron plays key roles in many cellular functions, excess iron has been implicated in promoting diseases and neurodegeneration (Padmanabhan et al., 2015, Rockfield et al., 2017). Moreover, a disrupted iron homeostasis has been established as a key factor in disease initiation and progression (Enns, 2003, Jellinger, 2009). Specifically, drugs of abuse have been observed to increase ROS and mitochondrial damage in the brain followed by a decrease in energy metabolism (Imam and Ali, 2000, Imam and Ali, 2001). Because iron is a key reactant in the formation of ROS and endolysosomes are major storage sites of ferrous iron, it was important to determine inter-organellar signaling between iron-rich endolysosomes and mitochondria (Fenton, 1894, Xu and Ren, 2015).

This study demonstrates that morphine, a drug of abuse, de-acidifies endolysosomes and releases Fe^{2+} into the cytosol. These findings are novel but are consistent with studies illustrating Ca^{2+} release with other de-acidifying agents (Christensen et al., 2002). Furthermore, this labile iron is translocated to the mitochondria resulting in increased ROS production and dysfunction. The morphine-induced formation of ROS is blocked with the iron chelator DFO, which emphasizes the significance of endolysosome iron.

In summary, these data confirm our hypothesis that endolysosome ferrous iron is an upstream event of morphine-induced mitochondrial ROS and dysfunction. DFO is a protectant from morphine-induced cytotoxicity, and emphasizes the importance of inter-organellar signaling of ferrous iron. Future

studies should include deferoxamine as a potential adjunctive strategy in the

treatment of opioid use disorders.
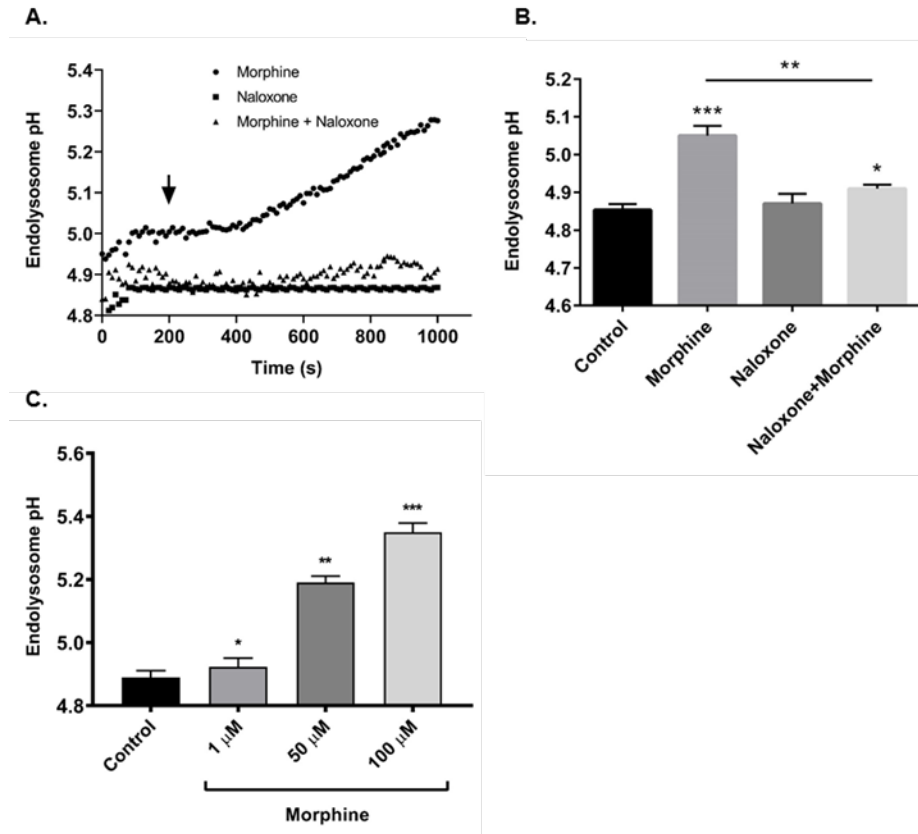
Figure 4. 1.   Morphine de-acidified endolysosomes.
(A) Morphine (10 µM) de-acidified endolysosome pH and
naloxone (50 µM) inhibited morphine de-acidification.
(B) Quantification of (A).
(C) Morphine dose-dependently de-acidified endolysosome pH.
Endolysosome de-acidification was measured using Lysosensor
DND-160.
(Vehicle for morphine and naloxone is PBS; n=30; * P < 0.05, **
P < 0.01, *** P < 0.001, **** P < 0.0001).
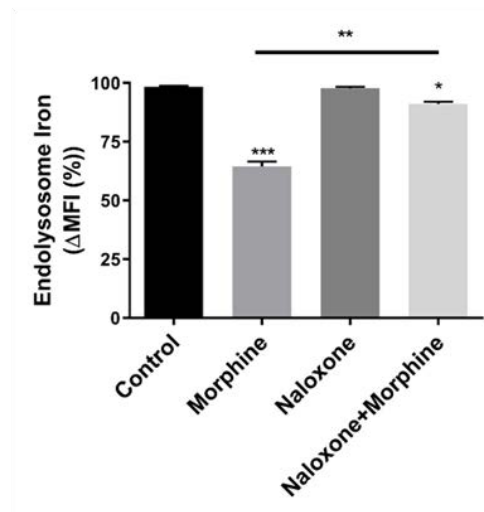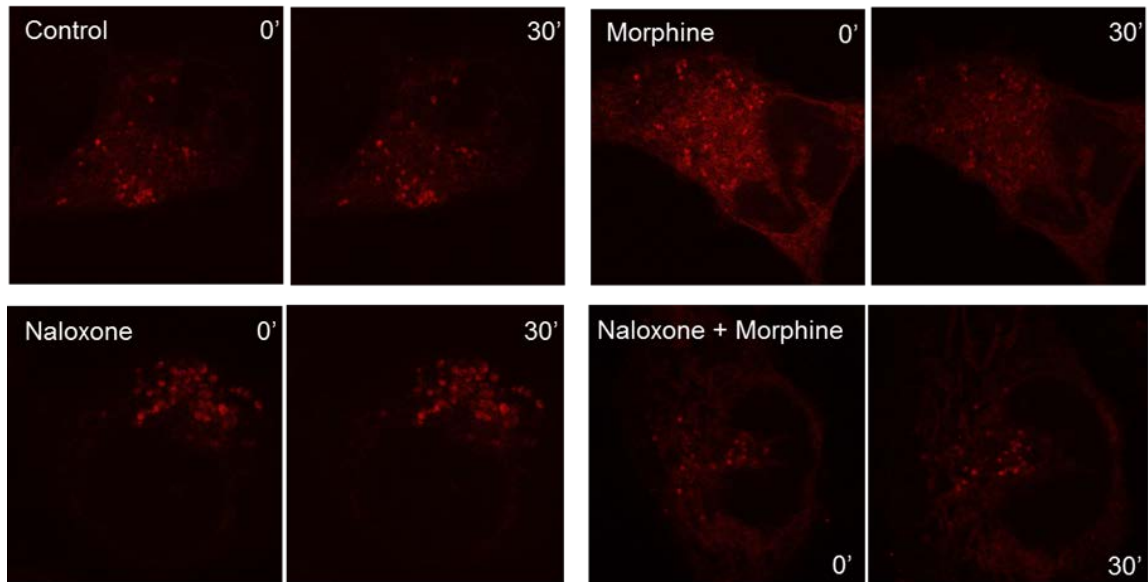
Figure 4. 2.   Morphine decreased endolysosome iron.
Morphine (10 µM) significantly decreased FeRhonox-1 fluorescence intensity at 30 minutes and naloxone (50 µM) inhibited morphine's effects. The change in fluorescence intensity was calculated as a percentage compared to the change in fluorescence intensity.
(n=30; * P < 0.05, ** P < 0.01, *** P < 0.001, **** P < 0.0001).
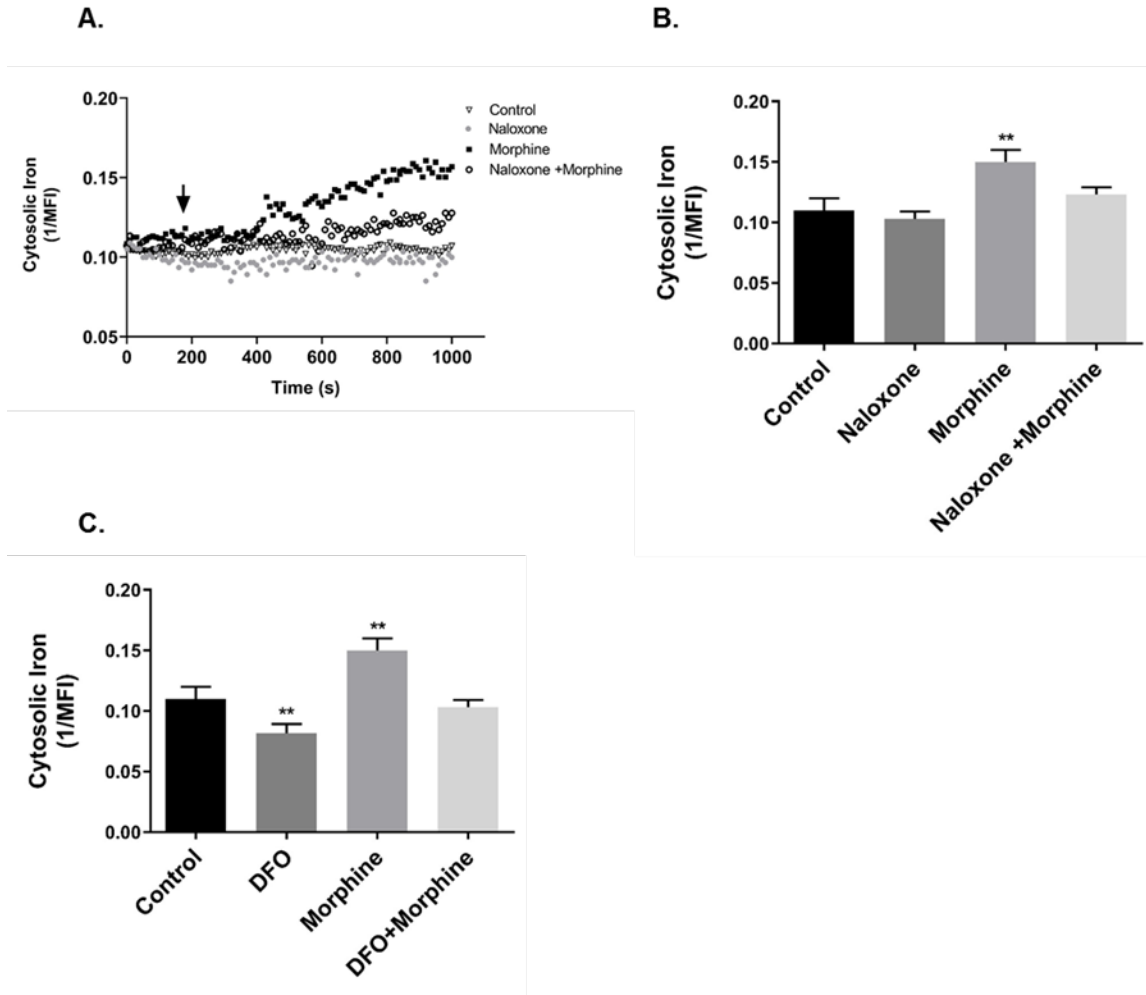
Figure 4. 3.　　Morphine increased cytosolic Fe^{2+}:
(A) Morphine (10 µM) quenched Phen-Green(the reciprocal of the Mean Fluorescent Intensity illustrates an increase in cytosolic iron), and naloxone (50 µM) inhibited morphine-induced iron release.
(B) Quantification of **(A)**.
(C) DFO blocked morphine-induced quenching of Phen-Green, and DFO alone suppressed Phen-Green quenching, which indicates a constitutive leak of Fe^{2+}.
(n=5; * $P < 0.05$, ** $P < 0.01$, *** $P < 0.001$, **** $P < 0.0001$).

Figure 4. 4.　　Morphine increased mitochondrial Fe^{2+}: Control cells stained with RDA and treated with PBS did not exhibit any significant changes in fluorescence intensity. Morphine (10 µM) quenched RDA fluorescence, and DFO inhibited morphine-induced RDA quenching.
(n=30; * $P < 0.05$, ** $P < 0.01$, *** $P < 0.001$, **** $P < 0.0001$).
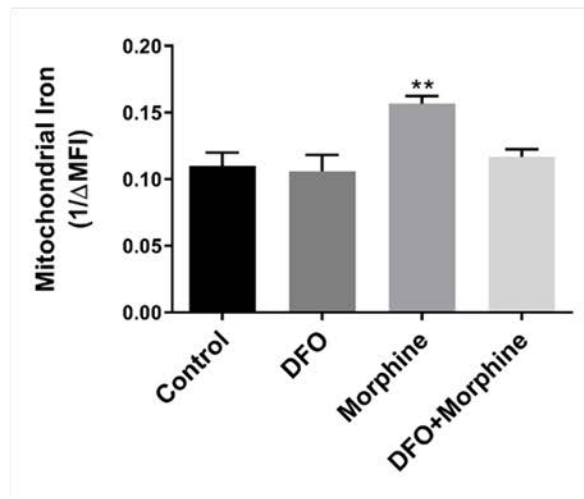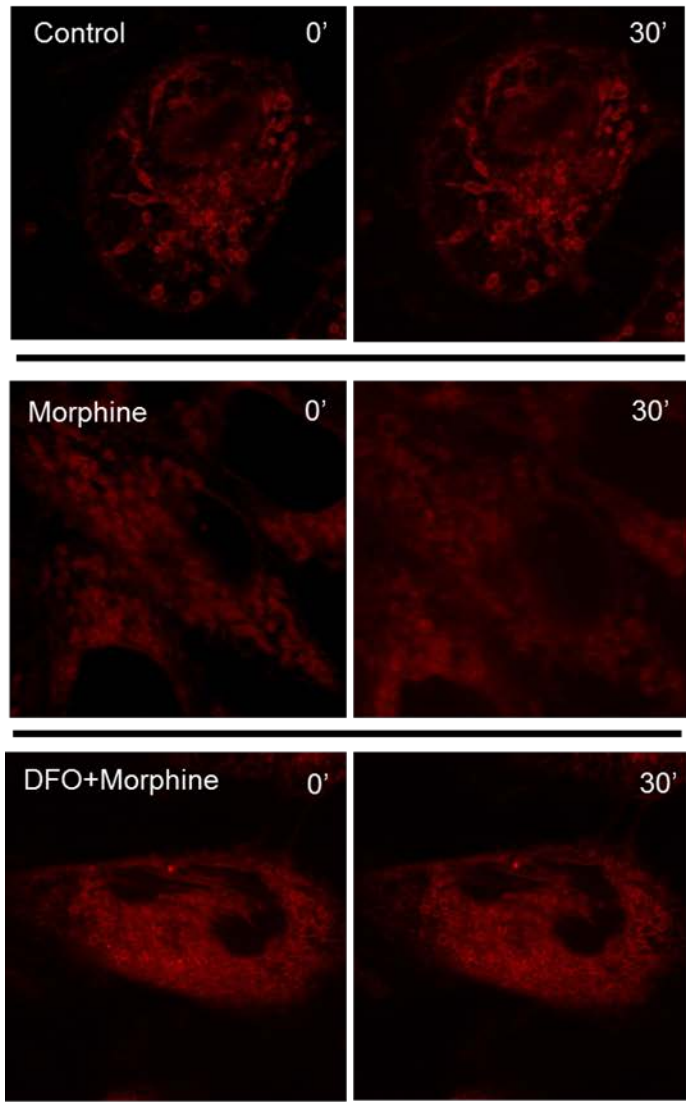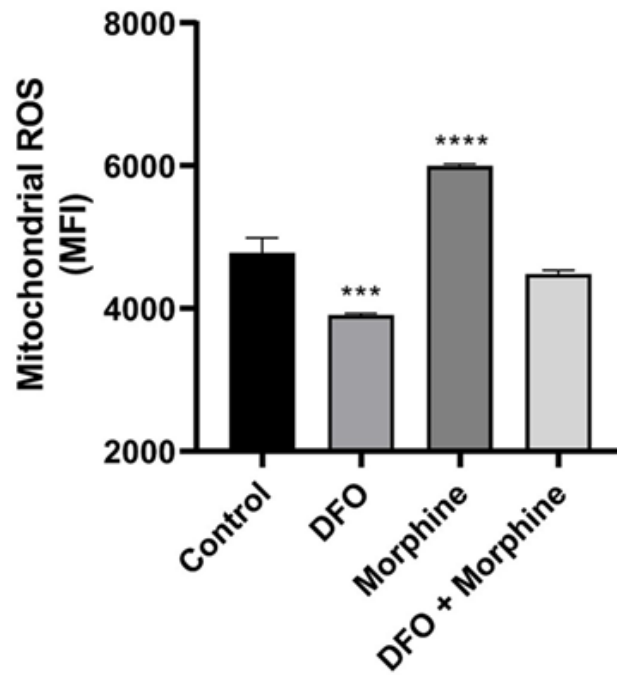
Figure 4. 5.   Chloroquine and bafilomycin A1 increased cytosolic ROS and mitochondrial ROS: Using MitoSox as a mitochondrial ROS measurement, morphine (10 µM) increased ROS, which was inhibited with DFO pretreatment.
(n=5; * P < 0.05, ** P < 0.01, *** P < 0.001, ****P<0.0001)
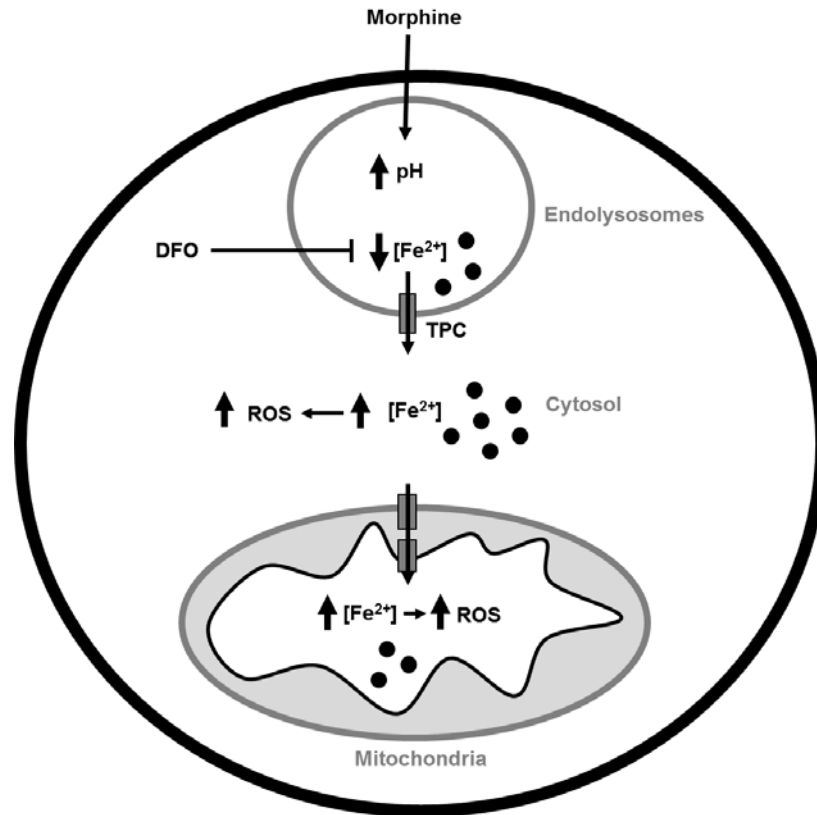
Figure 4. 6.   Schematic diagram of cellular mechanisms: Morphine-induced
de-acidification of endolysosomes causes ferrous iron in
endolysosomes to be released into the cytosol and into
mitochondria thereby resulting in mitochondrial dysfunction. DFO
chelated endolysosome iron and blocked morphine-induced
cytotoxicity.

References

ACIKGOZ, O., GONENC, S., KAYATEKIN, B. M., UYSAL, N., PEKCETIN, C., SEMIN, I. & GURE, A. 1998. Methamphetamine causes lipid peroxidation and an increase in superoxide dismutase activity in the rat striatum. *Brain Res,* 813**,** 200-2.

BINIENDA, Z., SIMMONS, C., HUSSAIN, S., SLIKKER, W., JR. & ALI, S. F. 1998. Effect of acute exposure to 3-nitropropionic acid on activities of endogenous antioxidants in the rat brain. *Neurosci Lett,* 251**,** 173-6.

BOVERIS, A. & CADENAS, E. 1975. Mitochondrial production of superoxide anions and its relationship to the antimycin insensitive respiration. *FEBS Lett,* 54**,** 311-4.

BREWER, G. J. 2007. Iron and copper toxicity in diseases of aging, particularly atherosclerosis and Alzheimer's disease. *Exp Biol Med (Maywood),* 232**,** 323-35.

CHEN, X., HUI, L., GEIGER, N. H., HAUGHEY, N. J. & GEIGER, J. D. 2013. Endolysosome involvement in HIV-1 transactivator protein-induced neuronal amyloid beta production. *Neurobiol Aging,* 34**,** 2370-8.

CHRIST, W. J., ASANO, O., ROBIDOUX, A. L., PEREZ, M., WANG, Y., DUBUC, G. R., GAVIN, W. E., HAWKINS, L. D., MCGUINNESS, P. D., MULLARKEY, M. A. & ET AL. 1995. E5531, a pure endotoxin antagonist of high potency. *Science,* 268**,** 80-3.

CHRISTENSEN, K. A., MYERS, J. T. & SWANSON, J. A. 2002. pH-dependent regulation of lysosomal calcium in macrophages. *J Cell Sci,* 115**,** 599-607.

DOULIAS, P. T., CHRISTOFORIDIS, S., BRUNK, U. T. & GALARIS, D. 2003. Endosomal and lysosomal effects of desferrioxamine: protection of HeLa cells from hydrogen peroxide-induced DNA damage and induction of cell-cycle arrest. *Free Radic Biol Med,* 35**,** 719-28.

ENNS, G. M. 2003. The contribution of mitochondria to common disorders. *Molecular Genetics and Metabolism,* 80**,** 11-26.

FENTON, H. J. H. 1894. LXXIII.—Oxidation of tartaric acid in presence of iron. *Journal of the Chemical Society, Transactions,* 65**,** 899-910.

FOSSLIEN, E. 2001. Mitochondrial medicine--molecular pathology of defective oxidative phosphorylation. *Ann Clin Lab Sci,* 31**,** 25-67.

MHUI, L., CHEN, X. & GEIGER, J. D. 2012a. Endolysosome involvement in LDL cholesterol-induced Alzheimer's disease-like pathology in primary cultured neurons. *Life Sci,* 91**,** 1159-68.

HUI, L., CHEN, X., HAUGHEY, N. J. & GEIGER, J. D. 2012b. Role of endolysosomes in HIV-1 Tat-induced neurotoxicity. *ASN Neuro,* 4**,** 243-52.

IMAM, S. Z. & ALI, S. F. 2000. Selenium, an antioxidant, attenuates methamphetamine-induced dopaminergic toxicity and peroxynitrite generation. *Brain Res,* 855**,** 186-91.

IMAM, S. Z. & ALI, S. F. 2001. Aging increases the susceptiblity to methamphetamine-induced dopaminergic neurotoxicity in rats: correlation with peroxynitrite production and hyperthermia. *J Neurochem,* 78**,** 952-9.

IMERYUZ, N., TAHAN, V., SONSUZ, A., EREN, F., URAZ, S., YUKSEL, M., AKPULAT, S., OZCELIK, D., HAKLAR, G., CELIKEL, C., AVSAR, E. & TOZUN, N. 2007. Iron preloading aggravates nutritional steatohepatitis in rats by increasing apoptotic cell death. *J Hepatol,* 47**,** 851-9.

JAESCHKE, H., GORES, G. J., CEDERBAUM, A. I., HINSON, J. A., PESSAYRE, D. & LEMASTERS, J. J. 2002. Mechanisms of hepatotoxicity. *Toxicol Sci,* 65**,** 166-76.

JELLINGER, K. A. 2009. Recent advances in our understanding of neurodegeneration. *J Neural Transm (Vienna),* 116**,** 1111-62.

KEHRER, J. P. 2000. The Haber-Weiss reaction and mechanisms of toxicity. *Toxicology,* 149**,** 43-50.

LOSCHEN, G., AZZI, A., RICHTER, C. & FLOHE, L. 1974. Superoxide radicals as precursors of mitochondrial hydrogen peroxide. *FEBS Lett,* 42**,** 68-72.

MENA, N. P., URRUTIA, P. J., LOURIDO, F., CARRASCO, C. M. & NÚÑEZ, M. T. 2015. Mitochondrial iron homeostasis and its dysfunctions in neurodegenerative disorders. *Mitochondrion,* 21**,** 92-105.

MINDELL, J. A. 2012. Lysosomal acidification mechanisms. *Annu Rev Physiol,* 74**,** 69-86.

PADMANABHAN, H., BROOKES, M. J. & IQBAL, T. 2015. Iron and colorectal cancer: evidence from in vitro and animal studies. *Nutr Rev,* 73**,** 308-17.

PERERA, R. M. & ZONCU, R. 2016. The Lysosome as a Regulatory Hub. *Annu Rev Cell Dev Biol,* 32**,** 223-253.

PETERSEN, D. R. 2005. Alcohol, iron-associated oxidative stress, and cancer. *Alcohol,* 35**,** 243-9.

PU, J., GUARDIA, C. M., KEREN-KAPLAN, T. & BONIFACINO, J. S. 2016. Mechanisms and functions of lysosome positioning. *Journal of cell science,* 129**,** 4329-4339.

RAUEN, U., SPRINGER, A., WEISHEIT, D., PETRAT, F., KORTH, H. G., DE GROOT, H. & SUSTMANN, R. 2007. Assessment of chelatable mitochondrial iron by using mitochondrion-selective fluorescent iron indicators with different iron-binding affinities. *Chembiochem,* 8**,** 341-52.

ROCKFIELD, S., RAFFEL, J., MEHTA, R., REHMAN, N. & NANJUNDAN, M. 2017. Iron overload and altered iron metabolism in ovarian cancer. *Biol Chem,* 398**,** 995-1007.

SCHWABE, R. F. & BRENNER, D. A. 2006. Mechanisms of Liver Injury. I. TNF-alpha-induced liver injury: role of IKK, JNK, and ROS pathways. *Am J Physiol Gastrointest Liver Physiol,* 290**,** G583-9.

SETTEMBRE, C., FRALDI, A., MEDINA, D. L. & BALLABIO, A. 2013. Signals from the lysosome: a control centre for cellular clearance and energy metabolism. *Nat Rev Mol Cell Biol,* 14**,** 283-96.

STEPHANS, S. E., WHITTINGHAM, T. S., DOUGLAS, A. J., LUST, W. D. & YAMAMOTO, B. K. 1998. Substrates of energy metabolism attenuate methamphetamine-induced neurotoxicity in striatum. *J Neurochem,* 71**,** 613-21.

SWANSON, C. A. 2003. Iron intake and regulation: implications for iron deficiency and iron overload. *Alcohol,* 30**,** 99-102.

VIDELA, L. A., FERNANDEZ, V., TAPIA, G. & VARELA, P. 2003. Oxidative stress-mediated hepatotoxicity of iron and copper: role of Kupffer cells. *Biometals,* 16**,** 103-11.

WEISS, F. H. A. J. 1934. The catalytic decomposition of hydrogen peroxide by iron salts. Royal Society.

XIONG, J. & ZHU, M. X. 2016. Regulation of lysosomal ion homeostasis by channels and transporters. *Science China. Life sciences,* 59**,** 777-791.

XU, H. & REN, D. 2015. Lysosomal Physiology. *Annual Review of Physiology,* 77**,** 57-80.

CHAPTER 5

HIV-1 GP120-INDUCED ENDOLYSOSOME DE-ACIDIFICATION CAUSES ENDOLYSOSOME IRON RELEASE AND INCREASED LEVELS OF REACTIVE OXYGEN SPECIES

Peter Halcrow, Koffi L. Lakpa, Nabab Khan, Nicole Miller, Zahra Afghah, Gaurav Datta, Xuesong Chen, and Jonathan D. Geiger*

Department of Biomedical Sciences
University of North Dakota School of Medicine and Health Sciences
Grand Forks, ND 58203, USA

Manuscript in preparation

Abstract

HIV-associated neurocognitive disorder (HAND) affects 50% of people living with HIV-1 despite viral suppression achieved by antiretroviral therapies. Pathologically, brain tissue from HAND patients has shown morphological changes to intracellular organelles including endolysosomes and mitochondria. Moreover, people living with HIV-1 show elevated iron serum levels and iron chelators have been suggested as an adjuvant therapy to antiretroviral therapeutics. Mechanistically, soluble factors including the HIV-1 coat protein gp120 have been implicated in HAND pathogenesis. Here, we tested the hypothesis that HIV-1 gp120-induced de-acidification of endolysosomes leads to an efflux of iron from endolysosomes and a subsequent increase in levels of cytosolic and mitochondrial reactive oxygen species (ROS). We used U87MG glioblastoma cells and time-lapse confocal microscopy to measure gp120-induced changes in endolysosome pH, endolysosome iron, cytosolic and mitochondrial iron, and ROS levels. HIV-1 gp120 de-acidified endolysosomes, reduced endolysosome iron levels, increased levels of cytosolic and mitochondrial iron, and increased levels of cytosolic and mitochondrial ROS. These effects were all attenuated significantly by the iron chelator deferoxamine that only enters cells via endocytosis. These results suggest that cellular and subcellular effects of HIV-1 gp120 can be downstream of its ability to de-acidify endolysosomes and increase the release of iron from endolysosomes. Thus, endolysosomes might represent an early and upstream target for therapeutic strategies against HAND.

Introduction

HIV-associated neurocognitive disorder (Bor et al.) affects about 50% of people living with HIV-1(PLWH) despite highly-effective viral suppression achieved using antiretroviral therapeutics (ART). Clinically, HAND is characterized by deficits in cognition, memory and motor function (Clifford and Ances, 2013); the severity of which varies from mild (asymptomatic) to severe (dementia) (Antinori et al., 2007). Pathologically, post mortem brain samples were found to exhibit decreased synaptodendritic arborization (Masliah et al., 1997) (Everall et al., 1999), Alzheimer's disease-like changes (Sacktor et al., 2002), and morphological changes in subcellular organelles including endolysosomes (Gelman et al., 2005), endoplasmic reticulum (Lindl et al., 2007), and mitochondria (Avdoshina et al., 2016). Molecular contributors to HAND pathogenesis include HIV-1 proteins (Ogishi and Yotsuyanagi, 2018, Scutari et al., 2017), oxidative stress (Turchan et al., 2003), and the ART themselves (Heaton et al., 2011). However, the full spectrum of underlying mechanisms of HAND still remain unclear.

Implicated in the pathogenesis of HAND are a number of soluble factors including HIV-1 transactivator of transcription protein (Tat) and the glycoprotein 120 (gp120) (Kovalevich and Langford, 2012). Tat and gp120 both are neurotoxic, decrease synaptodendritic arborization (Bruce-Keller et al., 2003, Toggas et al., 1996), and disrupt intracellular cation homeostasis (Haughey et al., 2001, Nath et al., 1995). Furthermore, Tat and gp120 are capable of affecting the

97

structure and function of subcellular organelles including endolysosomes and mitochondria (Hui et al., 2012b, Bae et al., 2014, Avdoshina et al., 2016).

Endolysosomes are acidic organelles that participate in the regulation of many important physiological functions including plasma membrane repair (Jaiswal et al., 2002), cell homeostasis, energy metabolism (McKenna et al., 2018), nutrient-dependent signal transduction (Zhang et al., 2016), and immune responses (Watts, 2012). Additionally, endolysosomes contain readily releasable stores of biologically-important cations including calcium and iron (Xiong and Zhu, 2016a). Efflux of calcium and iron from endolysosomes is induced when endolysosomes are de-acidified (Christensen et al., 2002, Fernández et al., 2016a), and when endolysosome membrane integrity is disrupted (Hui et al., 2012a, Hui et al., 2012b). Mitochondria too regulate a wide-variety of physiological functions, and when levels of calcium and iron are overloaded in mitochondria this results in increased levels of ROS (Brookes et al., 2004., Huang et al., 2017), toxic cellular responses, and cell death via apoptosis and ferroptosis (Dixon et al., 2012).

HIV-1 gp120 de-acidifies endolysosomes and increases levels of ROS (Viviani et al., 2001, Bae et al., 2014). The gp120-induced increases in cytosolic and mitochondrial ROS might result from endolysosome de-acidification-induced release of iron, increased iron accumulation in the cytoplasm and mitochondria, and formation of oxygen radicals mediated by the Fenton and Haber-Weiss reactions. Accordingly, we tested the hypothesis that gp120-induced de-acidification of endolysosomes leads to decreased levels of iron in

endolysosomes and increased levels of iron in cytoplasm and mitochondria, and that chelation of endolysosome iron can block downstream gp120-induced increases in cytosolic and mitochondrial ROS.

Materials and Methods

Cell Cultures

Glioblastoma (U87MG) cells were cultured in 1x DMEM (Invitrogen) containing 10% fetal bovine serum and 1% penicillin/streptomycin (Invitrogen). U87MG cells were grown in 35 mm^2 dishes to confluence in a 5% CO_2 incubator maintained at 37°C. Cells were not used past their tenth passage.

Endolysosome pH Measurements

As previously described (Hui et al.) (Liu et al., 2000), endolysosome pH was measured using a ratiometric indicator-dye, LysoSensor Yellow/Blue DND-160; a dual excitation dye that allows for pH measurements of acidic organelles that are independent of intracellular dye concentration. U87MG cells were loaded with 10 μM of DND-160 for 5 minutes at 37°C. Post-incubation, dye containing media was removed and fresh media was added to the cells just prior to them being taken for imaging. Light emitted at 520 nm in response to excitation for 2 msec at 340 nm and 380 nm was measured every 10 seconds using a filter-based imaging system (Zeiss, Germany). The ratios of light excited (340/380 nm) versus light emitted (520 nm) were converted to pH using a calibration curve established using 10 μM of the H^+/Na^+ ionophore monensin, and 20 μM of the H^+/K^+ ionophore nigericin; both were dissolved in a solution containing 20 mM

2-(N-morpholino) ethane sulfonic acid (MES), 110 mM KCl, and 20 mM NaCl, and the pH was adjusted to 3.0 to 7.0 with HCl/NaOH.

Endolysosome Iron Measurements

FeRhoNox-1 (Goryo Chemical), which stains specifically for Fe^{2+}, was added to cultured U87MG cells at a final concentration of 5 µM and cells were incubated at 37°C for 1 h after which they were washed twice with PBS. Following washing, fluorescence microscopy was used to visualize FeRhoNox-1 fluorescence at absorption and fluorescence wavelengths of 537 nm and 569 nm, respectively.

Cytosolic Iron Measurements

U87MG cells were incubated with PhenGreen™ SK diacetate at a concentration of 10 µM for 30 minutes at 37°C. Cells were then washed three-times with PBS and analyzed either with a ThermoFisher Attune flow cytometry (Alexa Fluor 488) or an Axiovert 200M (Zeiss) microscope-based system.

Mitochondrial Iron Measurements

Mitochondrial iron levels were measured using rhodamine B-[2,2'-bipyridine-4-yl)-aminocarbonyl]benzyl ester dye (RDA) (Squarix), a Fe^{2+}-specific fluorescence dye that localizes within mitochondria (Lindl et al.). Cells were incubated with RDA at a concentration of 100 nM for 10 minutes at 37°C. Cells were washed once with PBS followed by the addition of fresh DMEM media and then were examined using confocal scanning microscopy (Zeiss LSM800); changes in RDA mean fluorescence intensity were measured 30 minutes after gp120 was added. The red fluorescence intensity of RDA was captured using

absorption and emission wavelengths of 562 nm and 598 nm, respectively and captured images were analyzed using ImageJ software.

ROS Measurements in Cytosol and Mitochondria

Cytosolic ROS levels were measured using DCECF, 2,7-dichlorodihydrofluoroscein diacetate (10 µM) and mitochondrial ROS was measured using MitoSox Red (5 µM). U87MG cells were incubated with DCECF or MitoSox Red for 30 minutes at 37ºC in serum-free media and then washed twice with PBS prior to being analyzed using confocal scanning microscopy (Zeiss LSM800). For MitoSox Red, images were captured using absorption and emission wavelengths of 510 and 580 nm, respectively. For DCECF, images were captured using absorption and emission wavelengths of 495 and 529 nm, respectively. All images were analyzed using ImageJ software.

Cell Death Measurements

Cell death was measured using 20 ug/ml of propidium iodide (PI) staining (Sigma-Aldrich). U87MG cells were treated with gp120 (4 nM) in the absence or presence of DFO (100 µM) for 24-hours. Cells were then incubated with propidium iodide for 30 minutes and analyzed using an Attune NxT flow cytometer (ThermoFisher). PI-positive cells were identified using excitation and emission wavelengths of 493 and 636 nm, respectively. The percentage of PI-positive versus total number of cells was determined using Attune NxT software.

Cellular and Subcellular Morphology

Morphological features of U87MG cells and their subcellular organelles were determined by immunostaining for plasma membranes, nucleus, and

endolysosomes. Lysosomes were stained with an anti-LAMP1 antibody and an Alexa 488 anti-rabbit secondary antibody (Thermo Fisher. Plasma membranes were stained with an anti-beta1 sodium potassium ATPase antibody and an Alexa 594 anti-mouse antibody (Thermo Fischer). Nuclei were stained with DAPI (blue). Confocal scanning microscopy (Zeiss LSM800) was used to acquire images and when necessary Z-stack images were taken. Images were acquired and processed using Zen microscope imaging system software (Zeiss).

Reagents

All reagents were purchased from Thermo Fisher Scientific unless noted otherwise. HIV-1 gp120 IIIb was purchased from ABL Inc and aliquots were prepared and stored at -80°C to prevent freeze-thaw problems.

Statistics

All data were expressed as means and either S.D or S.E.M. Data analyses were completed using GraphPad Prism8 software. Statistical significance between two groups was determined using a Student's t test with a Welch's correction that did not include an assumption that both groups had the same SD. One-way ANOVA with Tukey's post-hoc tests were used to compare differences between multiple groups. $p \leq 0.05$ was designated to be statistically significant.

Results

Effects of gp120 on Cell Viability

The main focus of the studies reported on here was to determine the effects of HIV-1 gp120 on intracellular levels of Fe^{2+} and ROS. Because HIV-1

gp120 has the capacity to decrease cell viability, it was first necessary to determine whether gp120-induced cell death occurred under the experimental conditions used for our endolysosome morphological and functional studies. Using propidium iodide (PI) staining as a measure of cell death, we determined first the extent to which 30 min incubations with 4 nM gp120 decreased cell viability of U87MG cells. No statistically significant changes in cell viability were observed (see Supplemental Figure 5.A). Next, we determined the extent to which 24 h incubations with 4 nM gp120 decreased cell viability of U87MG cells and again observed no statistically significant changes in cell viability with either gp120 or the iron chelator DFO alone or in combination. Thus, under the conditions used we were not studying the effects of cell death on levels of Fe^{2+} and ROS.

Effects of gp120 on Endolysosome pH

Similar to our previously reported results on the effects of HIV-1 gp120 on endolysosome pH in primary cultures of rat hippocampal neurons (Bae et al., 2014), we found that gp120 at a concentration of 4 nM significantly increased endolysosome pH in U87MG cells from control values of 5.28 $\pm$ 0.05 pH units to values of 5.43 $\pm$ 0.04 pH units for gp120-treated cells (Figure 2, n=15; p<0.001). On average gp120 treatment increased endolysosome pH by 0.15 pH units; this equals a 32% reduction in endolysosomes proton concentrations as calculated using the formula pH = -log[H^+].

**Effects of gp120 on U87MG Cell Morphology and
Endolysosome Numbers and Volume**

Endolysosome deacidification has been shown by others and us to cause

changes in endolysosome morphology including their volume and numbers as

well as the distribution of endolysosomes within multiple cell types. To determine

the effects of gp120 on endolysosome morphology and number, we incubated

U87MG cells with 4 nM gp120 for 30 minutes and then measured changes in

LAMP1-positive endolysosomes. In Imaris reconstructed and confocal (inset)

images, it is visually apparent that endolysosomes are fewer in number but

greater in volume when exposed to gp120 or the v-ATPase inhibitor bafilomycin

that is known to de-acidify endolysosomes (Figure 5.2A). Quantitatively, gp120

significantly decreased significantly (p<0.0001) the number of endolysosomes

(average number of LAMP1-positive vesicles per cell), but significantly

(p<0.0001) increased the volume of LAMP1-positive endolysosomes

(Figure 5.2B).

gp120 Reduced the Levels of Iron within Endolysosomes

Next, we determined the degree to which gp120 released iron from

endolysosomes. U87MG cells were incubated with 5 µM FeRhoNox-1 and

fluorescence was measured 30-minutes after gp120 was added to the cells;

gp120 significantly (p<0.001) decreased endolysosome iron levels by 49%

(Figure 5.3).

gp120 Increased Iron Levels in the Cytosol

To determine the effects of gp120 on the labile pool of cytosolic iron, we

treated U87MG cells with PhenGreen SK (PG SK), which is a transition metal

indicator and a reported quenching probe for cytosolic iron (Petrat et al., 1999). First, we determined the extent to which gp120 increased levels of cytosolic iron and found that HIV-1 gp120 (4 nM) significantly ($p<0.001$) increased cytosolic iron levels (Figure 5.4). Next, we determined the extent to which the iron accumulating in the cytosol originated from endolysosomes. Using deferoxamine (DFO), an iron chelator that only enters cells by endocytosis (Cable and Lloyd, 1999, Lloyd et al., 1991a), we found that DFO significantly ($p<0.0001$) blocked gp120-induced increases in cytosolic iron to levels that were significantly ($p<0.05$) less than those in control cells (Figure 4). For ease of illustration, our fluorescence data were transformed as 1/MFI to illustrate more readily the gp120-induced increases in cytosolic iron.

gp120 Increased Mitochondrial Iron Levels

To determine the effects of gp120 on mitochondrial iron levels, we treated U87MG cells with rhodamine B-[2,2'-bipyridine-4-yl)-aminocarbonyl]benzyl ester dye (RDA; 100 nM) a dye whose fluorescence is quenched in the presence of mitochondrial ferrous iron (Rauen et al., 2007). For ease of illustration, our fluorescence data were transformed into 1/MFI to illustrate more readily the gp120-induced increases in mitochondrial iron. DFO by itself was found to cause a small but statistically significant ($p<0.01$) increase in levels of mitochondrial iron (Figure 5). gp120 (4 nM) significantly ($p<0.0001$) increased levels of mitochondrial iron (Figure 5.5). Pre-treatment of U87MG cells for 1hr with DFO significantly ($p<0.001$) blocked gp120-induced increases in mitochondrial iron level (Figure 5.5).

**gp120 Increased Reactive Oxygen Species (ROS) in
Cytosol and Mitochondria**

An increase of free labile iron levels is a catalyst for the production of ROS through the Haber-Weiss and/or the Fenton reactions. Because we observed that gp120 increased levels of cytosolic and mitochondrial iron, we next explored the effects of gp120 on levels of ROS in the cytosol and mitochondria. DFO alone significantly ($p<0.01$) reduced ROS levels in cytosol (Figure 6A), but not in mitochondria (Figure 6B). gp120 (4 nM) significantly increased cytosolic ($p<0.0001$) and mitochondrial ($p<0.001$) ROS (Figures 6A and 6B). Pretreatment of cells with DFO for 1 h prior to the addition of gp120 decreased significantly levels of ROS in cytosol ($p<0.001$) and in mitochondria ($p<0.01$).

Discussion

Over the past three decades, the development and use of effective antiretroviral therapeutics (ART) targeting HIV-1/AIDS has made this a manageable but chronic disease. Associated with HIV-1/AIDS in the ART-era is a high prevalence of neurological symptoms such has cognitive, motor, and behavioral problems that range in intensity from mild (asymptomatic) to severe (dementia) (13(Bhaskaran et al., 2008). Underlying the development of what has now been termed HIV-1 associated neurological disorders (HAND) are such pathological features as synaptodendritic damage, neuroinflammation, increased levels of oxidative stress, and damage to subcellular organelles (Everall et al., 1999). Current investigative efforts focused on determining mechanisms causing HAND include the involvement of soluble factors such as HIV-1 proteins as well as ART treatments themselves (Ogishi and Yotsuyanagi, 2018) (Gelman et al.,

2005) (Avdoshina et al., 2016) (Turchan et al., 2003) (Scutari et al., 2017). Here, we tested the hypothesis that HIV-1 gp120-induced de-acidification of endolysosomes leads to an efflux of iron from endolysosomes, an accumulation of iron in the cytosol and mitochondria, and a subsequent increase in levels of cytosolic and mitochondrial reactive oxygen species (ROS). The main findings of this work were that HIV-1 gp120 de-acidified endolysosomes, and that de-acidification led to increased efflux of ferrous iron out of endolysosomes. Further, the efflux of iron from endolysosomes led to increased accumulation of iron in cytoplasm and mitochondria; the result of which was increased levels of cytosolic and mitochondrial ROS. Together, these results suggest that cellular and subcellular effects of HIV-1 gp120 can be downstream of its ability to de-acidify endolysosomes and increase the release of iron from endolysosomes. Thus, endolysosomes might represent an early and upstream target for therapeutic strategies against HAND.

HIV-1 gp120 has been shown to affect endolysosomes (Bae et al., 2014) and mitochondria (Avdoshina et al., 2016), however virtually nothing is known about the extent to which gp120-induced endolysosome dysfunction causes mitochondrial dysfunction. In the current era of cell biology, there is an increased emphasis on better understanding physical and functional cross-talk between subcellular organelles and how these interactions help maintain cellular homeostasis (Bravo-Sagua et al., 2014). Indeed, inter-organellar signaling has been implicated in the pathogenesis of multiple diseases including cancer and

neurodegenerative diseases (Hughes and Gottschling, 2012, Plotegher and Duchen, 2017).

Oxidative stress has been implicated in the pathogenesis of neurodegenerative diseases including HAND (Scutari et al., 2017, Turchan et al., 2003), and the HIV-1 proteins gp120 and Tat have been shown by others and us to increase levels of ROS (Viviani et al., 2001). Implicated in the generation of ROS through the Fenton and Haber-Weiss reactions is iron and serum iron levels are elevated in PLWH (Nekhai et al., 2013). Ferric iron (Fe^{3+}) is endocytosed when bound to transferrin where it is reduced to redox-active ferrous iron (Fe^{2+}). Endolysosomes, which are acidic organelles, store ferrous iron and ferrous iron efflux is regulated by many factors including luminal pH and various cation channels (Fernández et al., 2016a). The iron released from endolysosomes can then accumulate in the cytoplasm and in mitochondria where it can generate ROS (Eaton and Qian, 2002).

Endolysosomes are dynamic organelles whose structure and function is closely regulated by changes in luminal pH. De-acidification of endolysosomes disrupts their trafficking, ability to degrade waste, and the maintenance of ion homeostasis (Christensen et al., 2002), (Fernández et al., 2016a). Previously, we reported that gp120 de-acidified neuronal endolysosomes (Bae et al., 2014). Here, we showed that gp120 de-acidified endolysosomes and increased their sizes while decreasing their numbers. The effects of gp120 are similar to the effects of HIV-1 Tat that we reported on previously; HIV-1 Tat disrupted endolysosome structure and increased endolysosome pH (Hui et al., 2012b). The

result of gp120-induced endolysosome de-acidification was increased release of ferrous iron from endolysosomes and the accumulation of ferrous iron in the cytosol and mitochondria. These effects were blocked completely by using the ferrous iron chelator deferoxamine that only enters cells by endocytosis (Doulias et al., 2003). Thus, it appears that gp120-induced ROS production is mediated upstream by endolysosome de-acidification and the release of their ferrous iron stores. Such a scenario where endolysosome iron might be transported into mitochondria was referred to as a "kiss and run" phenomenon (Hamdi et al., 2016).

It is important to note that the effects observed in these studies were not due to gp120-induced cell death. Under the conditions used here, we did not find any significant cell death with incubations of gp120 for either 30 min or 24-h. Others have shown that gp120 induced U87MG cell proliferation (Valentín-Guillama et al., 2018) by activation of glycolysis resulting in increased lipid and protein synthesis and cyto-protection by inducing GRP78 in astrocytomas (Lopez et al., 2017). However, it remains a possibility that over extended treatment intervals, gp120 by itself or in synergistic combination with other HIV-1 proteins could result in cell loss. Nevertheless, the effects of gp120 observed here were noted in the absence of measurable cell death. Thus, this study provides evidence that gp120 induces endolysosome de-acidification which leads to the efflux of iron from endolysosomes, the accumulation of iron in the cytosol and in mitochondria, and that the iron led to the increased production of cytosolic and mitochondrial ROS (Figure 5.7). This cross-talk between endolysosomes and

mitochondria might participate in the pathogenesis of HAND and endolysosomes

might represent early and upstream targets for therapeutic interventions against

HAND.
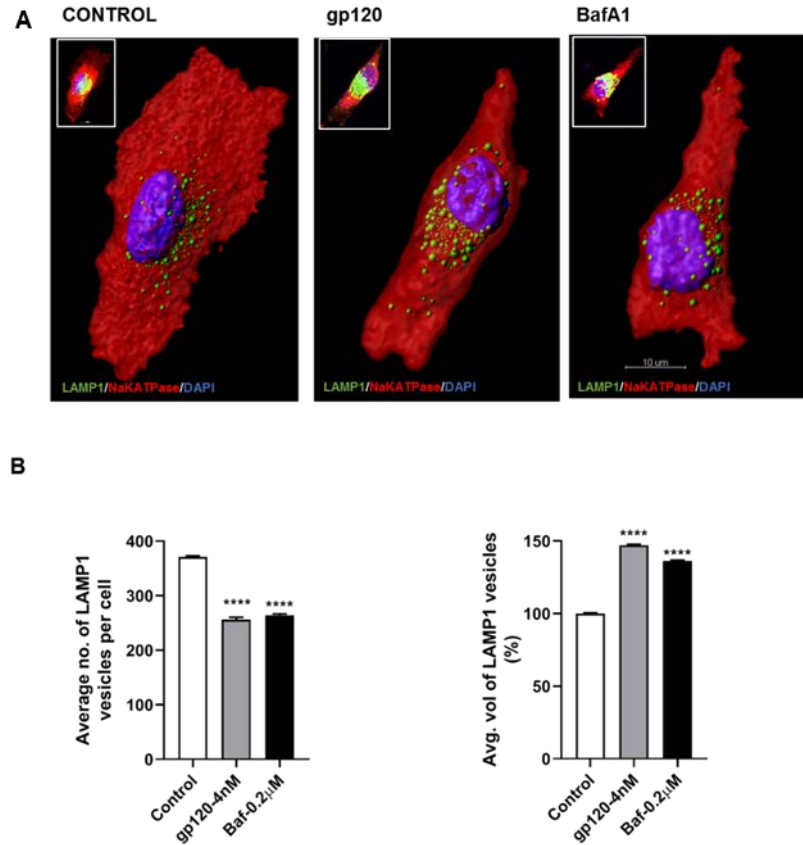
Figure 5. 1.   HIV-1 gp120 treatment affected lysosome number and
                morphology.
                (A) Representative Imaris reconstructed and confocal (inset)
                images of control and treated U87 cells with the lysosomes
                stained green(α-LAMP1), plasma membrane stained red (α-
                beta1 sodium ATPase) and nucleus blue (DAPI).
                (B) U87 glioblastoma cells treated with gp120 (4nM) for 30 min
                showed a significant decrease in average number and a
                simultaneous increase in volume of LAMP1 vesicles compared
                to control. Bafilomycin A1 (0.2µM, 30 min) served as positive
                control.
                Bar graph shows mean ± SD ($p<0.0001$, n=72).
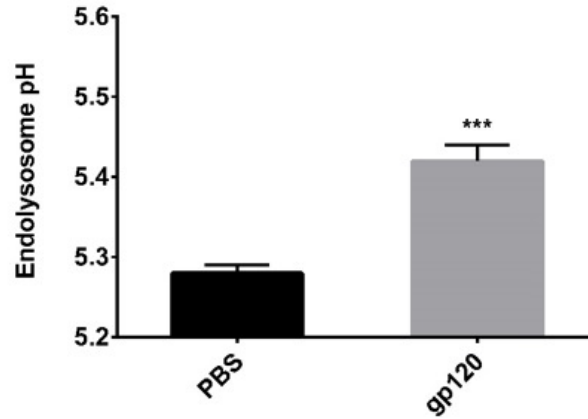
Figure 5. 2. HIV-1 gp120 increased endolysosome pH in U87MG cells. Treatment of U87MG cells with HIV-1 gp120 (4 nM) for 30 min caused statistically significant (n=15; ***p<0.001) increases in endolysosome pH when compared to phosphate-buffered saline vehicle (PBS) treated cells.
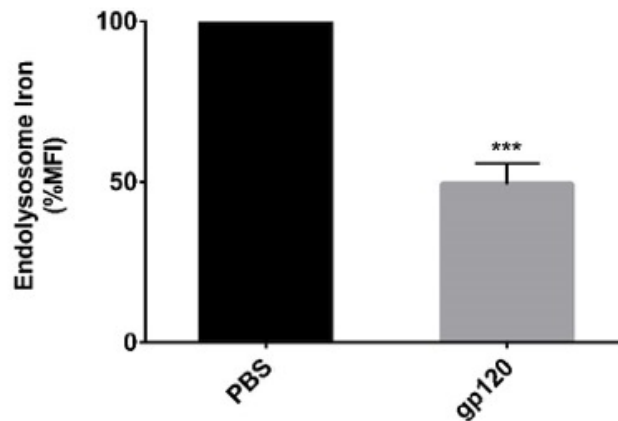
Figure 5. 3. HIV-1 gp120 reduced levels of iron in endolysosomes. HIV-1 gp120 (4 nM), but not phosphate buffered saline (PBS) vehicle significantly reduced the percentage mean fluorescence intensity (MFI) of FeRhoNox-1 staining for ferrous iron (Fe^{2+}) in endolysosomes of U87MG cells.
(n= 15; ***p<0.001).
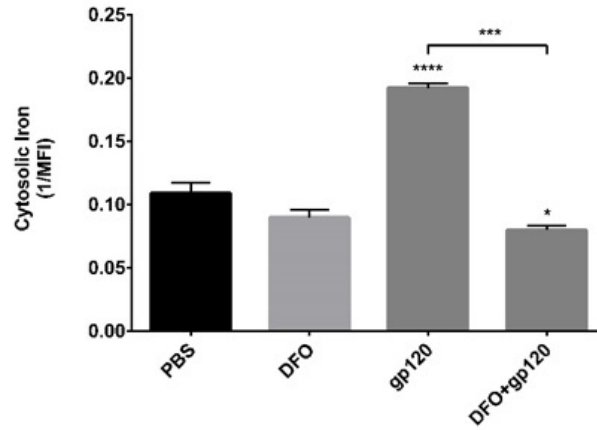
Figure 5. 4.   HIV-1 gp120 increased cytosolic iron levels. HIV-1 gp120 significantly (p<0.0001) decreased PhenGreen SK (PG SK) mean fluorescent intensity (MFI) in U87MG cells. Here, we transformed the data into 1/MFI to illustrate more clearly the gp120-induced increases in cytosolic iron (n=15; ****p<0.0001) because PhenGreen fluorescence quenches at high levels of iron. Deferoxamine (DFO, 100 μM) alone did not significantly affect PhenGreen MFI (n=15). Pretreatment of cells for 1 h with DFO (100 μM) followed by administration of gp120 (4 nM) significantly (***p<0.001) reduced the effects of gp120 on PhenGreen MFI (n=15).

113
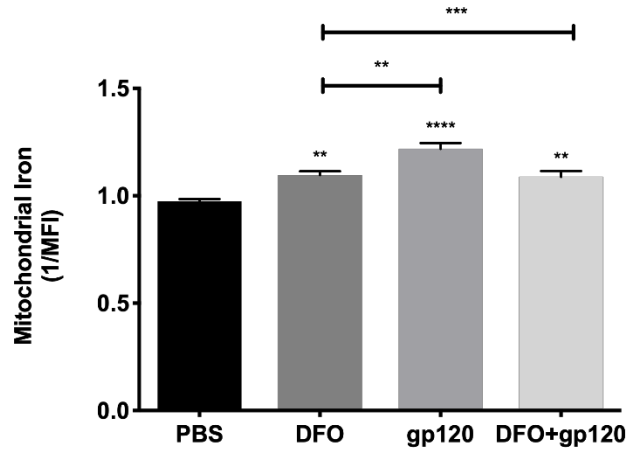
Figure 5. 5.   HIV-1 gp120 increased mitochondrial iron levels. HIV-1 gp120 at 4 nM significantly (****p<0.0001) increased mitochondrial iron levels (n=47), while DFO at 100 µM significantly (***p<0.001) reduced gp120-induced effects on mitochondrial iron levels (n=26). Deferoxamine (DFO, 100 µM) alone significantly (**p<0.01) increased levels of mitochondrial iron (n=15).
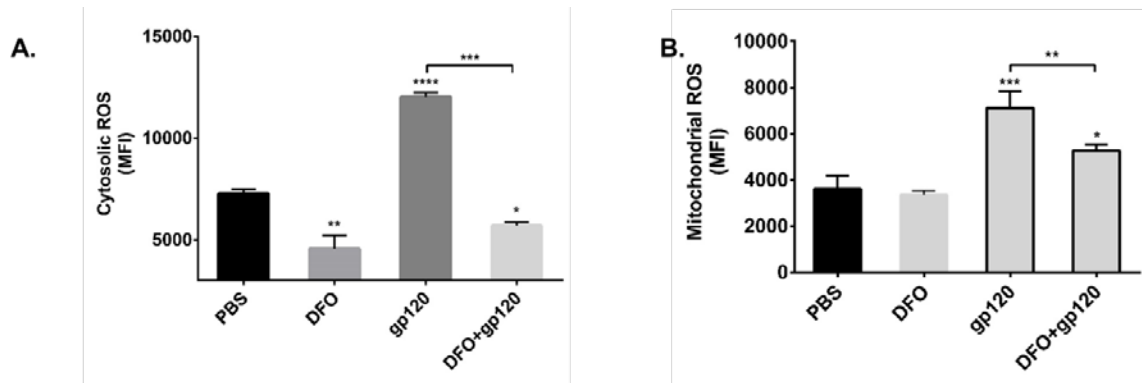
Figure 5. 6. HIV-1 gp120-induced increases in cytosolic and mitochondrial reactive oxygen species were blocked by deferoxamine (DFO). **(A)** HIV-1 gp120 treatment significantly increased the mean fluorescence intensity (MFI) of DCECF, 2,7-dichlorodihydrofluoroscein diacetate, a measure of cytosolic ROS (n=15; ****$p < 0.0001$). Treatment of cells with DFO alone significantly reduced levels of mitochondrial ROS (n=15; **$p < 0.01$). Treatment of cells with a combination of DFO and gp120 resulted in significantly (***$p < 0.001$) reduced MFI compared to gp120 (n=15).
(B) HIV-1 gp120 treatment significantly increased mitochondrial ROS. (n=15; ***$p < 0.001$). A combination of DFO and gp120 significantly (**$p < 0.01$) reduced mitochondrial ROS.
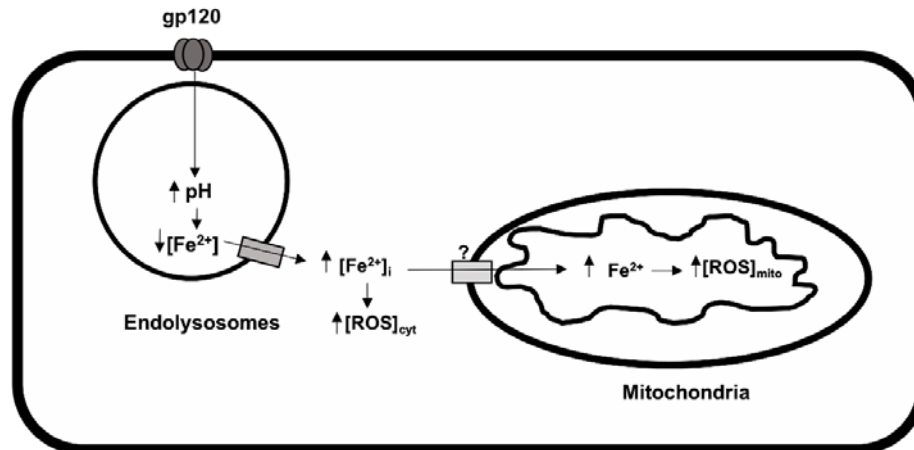
Figure 5. 7.   Schematic representation of the effects of gp120 on endolysosomes and mitochondria. Internalized gp120 within endolysosomes increases endolysosome pH, which then triggers a release of ferrous iron from endolysosomes. The released ferrous iron can accumulate in the cytosol and in mitochondria where it can be oxidized via the Fenton reaction to produce reactive oxygen species.
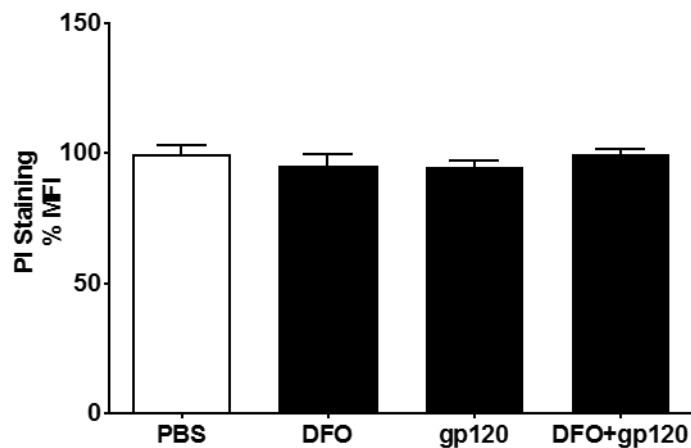
Figure 5. A.   *Supplemental Figure:* Effects of HIV-1 gp120 and DFO on cell death. Incubation of U87MG cells with HIV-1 gp120 (4 nM) for 30 min did cause statistically significant decreases in propidium iodide mean fluorescence intensity.
Incubation of U87MG cells for 24 h with HIV-1 gp120 (4 nM), DFO (100 μM), or gp120 in combination with DFO did cause statistically significant decreases in propidium iodide mean fluorescence intensity.

References

BOR DH, WOOLHANDLER S, NARDIN R, BRUSCH J, HIMMELSTEIN DU. Infective Endocarditis in the U.S., 1998–2009: A Nationwide Study. PLoS One. 82013.

CLIFFORD DB, ANCES BM. HIV-Associated Neurocognitive Disorder (HAND). Lancet Infect Dis. 2013;13(11):976-86.

ANTINORI A, ARENDT G, BECKER JT, BREW BJ, BYRD DA, CHERNER M, ET AL. Updated research nosology for HIV-associated neurocognitive disorders. Neurology. 2007;69(18):1789-99.

MASLIAH E, HEATON RK, MARCOTTE TD, ELLIS RJ, WILEY CA, MALLORY M, ET AL. Dendritic injury is a pathological substrate for human immunodeficiency virus-related cognitive disorders. HNRC Group. The HIV Neurobehavioral Research Center. Ann Neurol. 1997;42(6):963-72.

EVERALL IP, HEATON RK, MARCOTTE TD, ELLIS RJ, MCCUTCHAN JA, ATKINSON JH, ET AL. Cortical synaptic density is reduced in mild to moderate human immunodeficiency virus neurocognitive disorder. HNRC Group. HIV Neurobehavioral Research Center. Brain pathology (Zurich, Switzerland). 1999;9(2):209-17.

SACKTOR N, MCDERMOTT MP, MARDER K, SCHIFITTO G, SELNES OA, MCARTHUR JC, ET AL. HIV-associated cognitive impairment before and after the advent of combination therapy. J Neurovirol. 2002;8(2):136-42.

GELMAN BB, SOUKUP VM, HOLZER CE, 3RD, FABIAN RH, SCHUENKE KW, KEHERLY MJ, ET AL. Potential role for white matter lysosome expansion in HIV-associated dementia. J Acquir Immune Defic Syndr. 2005;39(4):422-5.

LINDL KA, AKAY C, WANG Y, WHITE MG, JORDAN-SCIUTTO KL. Expression of the endoplasmic reticulum stress response marker, BiP, in the central nervous system of HIV-positive individuals. Neuropathology and applied neurobiology. 2007;33(6):658-69.

AVDOSHINA V, FIELDS JA, CASTELLANO P, DEDONI S, PALCHIK G, TREJO M, ET AL. The HIV Protein gp120 Alters Mitochondrial Dynamics in Neurons. Neurotox Res. 2016;29(4):583-93.

OGISHI M, YOTSUYANAGI H. Prediction of HIV-associated neurocognitive disorder (HAND) from three genetic features of envelope gp120 glycoprotein. Retrovirology. 2018;15(1):12.

SCUTARI R, ALTERI C, PERNO CF, SVICHER V, AQUARO S. The Role of HIV Infection in Neurologic Injury. Brain Sci. 2017;7(4).

TURCHAN J, POCERNICH CB, GAIROLA C, CHAUHAN A, SCHIFITTO G, BUTTERFIELD DA, ET AL. Oxidative stress in HIV demented patients and protection ex vivo with novel antioxidants. Neurology. 2003;60(2):307-14.

HEATON RK, FRANKLIN DR, ELLIS RJ, MCCUTCHAN JA, LETENDRE SL, LEBLANC S, ET AL. HIV-associated neurocognitive disorders before and during the era of combination antiretroviral therapy: differences in rates, nature, and predictors. J Neurovirol. 2011;17(1):3-16.

KOVALEVICH J, LANGFORD D. Neuronal toxicity in HIV CNS disease. Future Virol. 2012;7(7):687-98.

BRUCE-KELLER AJ, CHAUHAN A, DIMAYUGA FO, GEE J, KELLER JN, NATH A. Synaptic transport of human immunodeficiency virus-Tat protein causes neurotoxicity and gliosis in rat brain. The Journal of neuroscience : the official journal of the Society for Neuroscience. 2003;23(23):8417-22.

TOGGAS SM, MASLIAH E, MUCKE L. Prevention of HIV-1 gp120-induced neuronal damage in the central nervous system of transgenic mice by the NMDA receptor antagonist memantine. Brain Res. 1996;706(2):303-7.

HAUGHEY NJ, NATH A, MATTSON MP, SLEVIN JT, GEIGER JD. HIV-1 Tat through phosphorylation of NMDA receptors potentiates glutamate excitotoxicity. J Neurochem. 2001;78(3):457-67.

NATH A, PADUA RA, GEIGER JD. HIV-1 coat protein gp120-induced increases in levels of intrasynaptosomal calcium. Brain Res. 1995;678(1-2):200-6.

HUI L, CHEN X, HAUGHEY NJ, GEIGER JD. Role of endolysosomes in HIV-1 Tat-induced neurotoxicity. ASN Neuro. 2012;4(4):243-52.

BAE M, PATEL N, XU H, LEE M, TOMINAGA-YAMANAKA K, NATH A, ET AL. Activation of TRPML1 clears intraneuronal Abeta in preclinical models of HIV infection. The Journal of neuroscience : the official journal of the Society for Neuroscience. 2014;34(34):11485-503.

JAISWAL JK, ANDREWS NW, SIMON SM. Membrane proximal lysosomes are the major vesicles responsible for calcium-dependent exocytosis in nonsecretory cells. J Cell Biol. 2002;159(4):625-35.

MCKENNA MC, SCHUCK PF, FERREIRA GC. Fundamentals of CNS energy metabolism and alterations in lysosomal storage diseases. J Neurochem. 2018.

ZHANG X, CHENG X, YU L, YANG J, CALVO R, PATNAIK S, ET AL. MCOLN1 is a ROS sensor in lysosomes that regulates autophagy. Nat Commun. 2016;7:12109.

WATTS C. The endosome-lysosome pathway and information generation in the immune system. Biochim Biophys Acta. 2012;1824(1):14-21.

XIONG J, ZHU MX. Regulation of lysosomal ion homeostasis by channels and transporters. Sci China Life Sci. 2016;59(8):777-91.

CHRISTENSEN KA, MYERS JT, SWANSON JA. pH-dependent regulation of lysosomal calcium in macrophages. J Cell Sci. 2002;115(Pt 3):599-607.

FERNÁNDEZ B, FDEZ E, GÓMEZ-SUAGA P, GIL F, MOLINA-VILLALBA I, FERRER I, ET AL. Iron overload causes endolysosomal deficits modulated by NAADP-regulated 2-pore channels and RAB7A. Autophagy. 122016. p. 1487-506.

HUI L, CHEN X, GEIGER JD. Endolysosome involvement in LDL cholesterol-induced Alzheimer's disease-like pathology in primary cultured neurons. Life Sci. 2012;91(23-24):1159-68.

BROOKES PS, YOON Y, ROBOTHAM JL, ANDERS MW, SHEU SS. Calcium, ATP, and ROS: a mitochondrial love-hate triangle. Am J Physiol Cell Physiol. 2004;287(4):C817-33.

HUANG H, CHEN J, LU H, ZHOU M, CHAI Z, HU Y. Iron-induced generation of mitochondrial ROS depends on AMPK activity. Biometals. 2017;30(4): 623-8.

DIXON SJ, LEMBERG KM, LAMPRECHT MR, SKOUTA R, ZAITSEV EM, GLEASON CE, ET AL. Ferroptosis: an iron-dependent form of nonapoptotic cell death. Cell. 2012;149(5):1060-72.

VIVIANI B, CORSINI E, BINAGLIA M, GALLI CL, MARINOVICH M. Reactive oxygen species generated by glia are responsible for neuron death induced by human immunodeficiency virus-glycoprotein 120 in vitro. Neuroscience. 2001;107(1):51-8.

LIU Y, JONES M, HINGTGEN CM, BU G, LARIBEE N, TANZI RE, ET AL. Uptake of HIV-1 tat protein mediated by low-density lipoprotein receptor-related protein disrupts the neuronal metabolic balance of the receptor ligands. Nat Med. 2000;6(12):1380-7.

PETRAT F, RAUEN U, DE GROOT H. Determination of the chelatable iron pool of isolated rat hepatocytes by digital fluorescence microscopy using the fluorescent probe, phen green SK. Hepatology. 1999;29(4):1171-9.

CABLE H, LLOYD JB. Cellular uptake and release of two contrasting iron chelators. J Pharm Pharmacol. 1999;51(2):131-4.

LLOYD JB, CABLE H, RICE-EVANS C. Evidence that desferrioxamine cannot enter cells by passive diffusion. Biochem Pharmacol. 1991;41(9):1361-3.

RAUEN U, SPRINGER A, WEISHEIT D, PETRAT F, KORTH HG, DE GROOT H, ET AL. Assessment of chelatable mitochondrial iron by using mitochondrion-selective fluorescent iron indicators with different iron-binding affinities. Chembiochem : a European journal of chemical biology. 2007;8(3):
341-52.

BHASKARAN K, HAMOUDA O, SANNES M, BOUFASSA F, JOHNSON AM, LAMBERT PC, ET AL. Changes in the risk of death after HIV seroconversion compared with mortality in the general population. JAMA. 2008;300(1):51-9.

CYSIQUE LA, BAIN MP, BREW BJ, MURRAY JM. The burden of HIV-associated neurocognitive impairment in Australia and its estimates for the future. Sex Health. 2011;8(4):541-50.

NEKHAI S, KUMARI N, DHAWAN S. Role of cellular iron and oxygen in the regulation of HIV-1 infection. Future Virol. 2013;8(3):301-11.

NATH A, HAUGHEY NJ, JONES M, ANDERSON C, BELL JE, GEIGER JD. Synergistic neurotoxicity by human immunodeficiency virus proteins Tat and gp120: protection by memantine. Ann Neurol. 2000;47(2):186-94.

EATON JW, QIAN M. Molecular bases of cellular iron toxicity. Free Radic Biol Med. 2002;32(9):833-40.

BRAVO-SAGUA R, TORREALBA N, PAREDES F, MORALES PE, PENNANEN C, LOPEZ-CRISOSTO C, ET AL. Organelle communication: signaling crossroads between homeostasis and disease. Int J Biochem Cell Biol. 2014;50:55-9.

HUGHES AL, GOTTSCHLING DE. An early age increase in vacuolar pH limits mitochondrial function and lifespan in yeast. Nature. 2012;492(7428):
261-5.

PLOTEGHER N, DUCHEN MR. Mitochondrial Dysfunction and Neurodegeneration in Lysosomal Storage Disorders. Trends Mol Med. 2017;23(2):116-34.

DOULIAS PT, CHRISTOFORIDIS S, BRUNK UT, GALARIS D. Endosomal and lysosomal effects of desferrioxamine: protection of HeLa cells from hydrogen peroxide-induced DNA damage and induction of cell-cycle arrest. Free Radic Biol Med. 2003;35(7):719-28.

FOGA IO, NATH A, HASINOFF BB, GEIGER JD. Antioxidants and dipyridamole inhibit HIV-1 gp120-induced free radical-based oxidative damage to human monocytoid cells. Journal of acquired immune deficiency syndromes and human retrovirology : official publication of the International Retrovirology Association. 1997;16(4):223-9.

HAMDI A, ROSHAN TM, KAHAWITA TM, MASON AB, SHEFTEL AD, PONKA P. Erythroid cell mitochondria receive endosomal iron by a "kiss-and-run" mechanism. Biochim Biophys Acta. 2016;1863(12):2859-67.

VALENTÍN-GUILLAMA G, LÓPEZ S, KUCHERYAVYKH YV, CHORNA NE, PÉREZ J, ORTIZ-RIVERA J, ET AL. HIV-1 Envelope Protein gp120 Promotes Proliferation and the Activation of Glycolysis in Glioma Cell. Cancers (Basel). 102018.

LOPEZ SN, RODRIGUEZ-VALENTIN M, RIVERA M, RODRIGUEZ M, BABU M, CUBANO LA, ET AL. HIV-1 Gp120 clade B/C induces a GRP78 driven cytoprotective mechanism in astrocytoma. Oncotarget. 2017;8(40): 68415-38.

CHAPTER 6

GENERAL DISCUSSION

After ferric iron is released from enterocytes and macrophages into the bloodstream it binds to transferrin (Tf), which is an abundant plasma glycoprotein able to bind two atoms of iron with very high affinity (Aisen et al., 1978, Morgan, 1981). Consequently, very little toxic iron is in the bloodstream (Anderson and Vulpe, 2009). Furthermore, the circulating Tf-Fe complex binds to the plasma membrane transferrin receptor 1 and the complex is endocytosed (Richardson and Ponka, 1997). Within endolysosomes ferric iron is reduced to ferrous iron by STEAP3, a metalloreductase (Ohgami et al., 2006). Therefore, it is well established that ferrous iron resides within endolysosomes (Starke and Farber, 1985, Kurz et al., 2011). However, the concentration of ferrous iron within endolysosomes has yet to be determined. This study determined the level of ferrous iron concentration within endolysosomes as well as inter-organellar signaling of ferrous iron from endolysosomes to mitochondria. This present study was initiated under Dr. Geiger, who had returned from a conference where he discussed the effects of iron on mitochondria at a poster session. It was uncertain at the time where iron was coming from that might be leading to mitochondrial dysfunction. Thus, we began to look at the literature to further

123

investigate and study endolysosome iron as an upstream effect of mitochondrial dysfunction.

The present study, outlined in Chapter 2, was initiated by looking for a probe specific to Fe^{2+} and endolysosomes. About five years ago, the fluorescence 'turn-on' probe FeRhoNox-1 was found to have pronounced specificity for Fe^{2+} versus other biologically relevant metal ions (Mukaide, Hattori et al. 2014). It was also shown that FeRhoNox-1 labels Fe^{2+} stores in acidic Golgi organelles at least in some cells (Hirayama, Okuda et al. 2013). However, prior to our work, no reports have appeared determining whether FeRhoNox-1 labels Fe^{2+} in endolysosomes and whether FeRhoNox-1 can be used to quantitatively measure levels of Fe^{2+} in endolysosomes. Here, we found that FeRhoNox-1 was highly specific for Fe^{2+} versus other cations such as calcium, magnesium, copper and zinc. Further, FeRhoNox-1 positive stores were selectively localized in endolysosomes. FeRhonox-1 colocalized with LysoTracker with a high Pearson Correlation Coefficient of 0.84. FeRhonox-1 colocalized with EEA1-positive endolysosomes with a Pearson correlation coefficient of 0.86, and FeRhonox-1 colocalized with LAMP1-positive late endosomes/lysosomes with a Pearson correlation coefficient of 0.56.

As a proof of principle for quantitative measurements of labile iron stores, endolysosome Fe^{2+} stores were increased with ferric ammonium citrate supplementation and were decreased with the iron chelator deferoxamine. Control levels of Fe^{2+} were 36.3 ± 13.6 μM in endolysosomes, and stores of Fe^{2+} in endolysosomes increased to 75 ± 15.7 μM when cells were incubated with

ferric ammonium citrate and decreased to 0.08 ± 0.05 µM when cells were

incubated with the iron chelator deferoxamine. It is likely that FeRhoNox-1 will

find extensive use for better understanding the physiological relevance and

pathological significance of Fe^{2+} in living cells. Our findings demonstrate the

utility of using FeRhoNox-1 to measure Fe^{2+} stores in endolysosomes and

suggest that this probe will find important uses in better understanding cellular

events downstream of released endolysosome Fe^{2+}.

Endolysosomes are storage sites for readily-releasable ions including H^+,

Na^+, K^+, Cl^-, Ca^{2+}, Zn^{2+}, Fe^{3+}, and Fe^{2+} (Xu and Ren, 2015, Xiong and Zhu,

2016b) as they integrate and digest materials compartmentalized by endocytosis,

phagocytosis or autophagy. Further, studies have shown that drug-induced de-

acidification of the endolysosome lumen causes an efflux of cations such as Ca^{2+}

from endolysosomes into the cytosol (Christensen et al., 2002, Fernández et al.,

2016b). With this knowledge, the study, outlined in Chapter 3, was to determine

whether chloroquine and bafilomycin A1 would act like controls and release iron

from endolysosomes as they both de-acidify endolysosome pH. It was

determined that ferrous iron is released from endolysosomes upon treatment with

chloroquine and bafilomycin A1. We determined that ferrous iron enters into the

cytosol via two-pore channels and it is taken up by the mitochondria via

mitochondrial permeability transition pores. The iron that enters the cytosol

increases ROS levels and the iron that enters the mitochondria increases the

ROS levels. These findings were further confirmed with the use of deferoxamine,

which is an iron chelator that is cell impermeable and is taken up into cells by

endocytosis. DFO pretreatment chelated endolysosome iron and significantly

blocked chloroquine- and bafilomycin A1-induced cytosolic and mitochondrial

ROS levels.

Taken together, these findings demonstrate the importance of

endolysosome ferrous iron as an upstream event of mitochondrial iron overload

and dysfunction. Under pharmacological conditions such as chloroquine and

bafilomycin A1, which de-acidify endolysosomes, ferrous iron accumulated in

mitochondrial, increased mitochondrial ROS, and caused cell death. Since

mitochondrial iron overload has been implicated in numerous diseases, these

results open up new understandings of the role of endolysosome iron.

The study, as outlined in Chapter 4, was an extension of the previous

Chapter 3 study. Morphine is a drug of abuse, and drugs of abuse have been

associated with neurological diseases. More specifically, evidence shows that

drugs of abuse increase free radicals and mitochondrial dysfunction such as

decreased cellular energy production followed by toxicity (Imam and Ali, 2000,

Imam and Ali, 2001, Stephans et al., 1998, Cunha-Oliveira et al., 2013, Xu et al.,

2011). Neuronal degeneration is associated with failed ATP production due to an

increase in ROS and nitrogen species (Acikgoz et al., 1998, Binienda et al.,

1998), and studies have shown that neurotoxicity induced by drugs of abuse can

be protected by antioxidants such as selenium and melatonin (Fosslien, 2001,

Imam and Ali, 2000). However, the increase in mitochondrial ROS production

induced by drugs of abuse remains uncertain. Our study demonstrated that

morphine increased endolysosome pH, released ferrous iron into the cytosol, and

increased ferrous iron in mitochondria. Not surprisingly, morphine increased mitochondrial ROS levels. Furthermore, morphine effects were blocked by DFO. These results taken together shows that endolysosome iron is an upstream event of mitochondrial iron overload and dysfunction, and drugs of abuse, like morphine, affect mitochondrial function through inter-organellar signaling of ferrous iron.

The last study, Chapter 5, determined the effects of the HIV-1 protein gp120 on endolysosome iron and mitochondrial dysfunction. People living with HIV-1 show elevated iron serum levels and iron chelators have been suggested as an adjuvant therapy to antiretroviral therapeutics. Mechanistically, soluble factors including the HIV-1 coat protein gp120 have been implicated in HAND pathogenesis. Here, we determined that gp120 de-acidified endolysosomes, released iron into the cytosol, which is then taken up by the mitochondria. gp120 lead to increased cytosolic ROS and mitochondrial ROS. DFO blocked gp120-induced ROS and mitochondrial iron overload. These results suggest that cellular and subcellular effects of HIV-1 gp120 can be downstream of its ability to de-acidify endolysosomes and increase the release of iron from endolysosomes, and that DFO might serve as adjunctive therapy.

The main mechanisms underlying these studies demonstrate some of the roles of ferrous iron within endolysosomes in inter-organellar signaling with mitochondria. Endolysosome ferrous iron plays an upstream role in mitochondrial iron overload, dysfunction, and cell death. These studies outline the key mechanisms of inter-organellar signaling and stress the significance that DFO

might serve as adjunctive therapy in protecting mitochondria from iron overload

and dysfunction. With the probe of FeRhoNox-1 and the results within this

dissertation, future studies should key on endolysosome ferrous iron and the

roles this redox-active molecule has on normal cellular processes as well as

cellular dysfunction and cell death.

REFERENCES

ACIKGOZ, O., GONENC, S., KAYATEKIN, B. M., UYSAL, N., PEKCETIN, C., SEMIN, I. & GURE, A. 1998. Methamphetamine causes lipid peroxidation and an increase in superoxide dismutase activity in the rat striatum. *Brain Res,* 813**,** 200-2.

AISEN, P., LEIBMAN, A. & ZWEIER, J. 1978. Stoichiometric and site characteristics of the binding of iron to human transferrin. *Journal of Biological Chemistry,* 253**,** 1930-1937.

ANDERSEN, H. H., JOHNSEN, K. B. & MOOS, T. 2014. Iron deposits in the chronically inflamed central nervous system and contributes to neurodegeneration. *Cell Mol Life Sci,* 71**,** 1607-22.

ANDERSON, G. J. & VULPE, C. D. 2009. Mammalian iron transport. *Cellular and molecular life sciences : CMLS,* 66**,** 3241-3261.

ANDREYEV, A. Y., KUSHNAREVA, Y. E. & STARKOV, A. A. 2005. Mitochondrial metabolism of reactive oxygen species. *Biochemistry (Mosc),* 70**,** 200-14.

ANTINORI, A., ARENDT, G., BECKER, J. T., BREW, B. J., BYRD, D. A., CHERNER, M., CLIFFORD, D. B., CINQUE, P., EPSTEIN, L. G., GOODKIN, K., GISSLEN, M., GRANT, I., HEATON, R. K., JOSEPH, J., MARDER, K., MARRA, C. M., MCARTHUR, J. C., NUNN, M., PRICE, R. W., PULLIAM, L., ROBERTSON, K. R., SACKTOR, N., VALCOUR, V. & WOJNA, V. E. 2007. Updated research nosology for HIV-associated neurocognitive disorders. *Neurology,* 69**,** 1789-99.

AVDOSHINA, V., FIELDS, J. A., CASTELLANO, P., DEDONI, S., PALCHIK, G., TREJO, M., ADAME, A., ROCKENSTEIN, E., EUGENIN, E., MASLIAH, E. & MOCCHETTI, I. 2016. The HIV Protein gp120 Alters Mitochondrial Dynamics in Neurons. *Neurotox Res,* 29**,** 583-593.

BAE, M., PATEL, N., XU, H., LEE, M., TOMINAGA-YAMANAKA, K., NATH, A., GEIGER, J., GOROSPE, M., MATTSON, M. P. & HAUGHEY, N. J. 2014. Activation of TRPML1 clears intraneuronal Abeta in preclinical models of HIV infection. *J Neurosci,* 34**,** 11485-503.

BALABAN, R. S., NEMOTO, S. & FINKEL, T. 2005. Mitochondria, oxidants, and aging. *Cell,* 120**,** 483-95.

BALLAS, S. K., ZEIDAN, A. M., DUONG, V. H., DEVEAUX, M. & HEENEY, M. M. 2018. The effect of iron chelation therapy on overall survival in sickle cell disease and β-thalassemia: A systematic review. *American Journal of Hematology,* 93**,** 943-952.

BERG, T. O., STRØMHAUG, P. E., LØVDAL, T., SEGLEN, P. O. & BERG, T. 1994. Use of glycyl-l-phenylalanine 2-naphthylamide, a lysosome-disrupting cathepsin C substrate, to distinguish between lysosomes and prelysosomal endocytic vacuoles. *Biochemical Journal,* 300**,** 229.

BHASKARAN, K., HAMOUDA, O., SANNES, M., BOUFASSA, F., JOHNSON, A. M., LAMBERT, P. C., PORTER, K. & COLLABORATION, C. 2008. Changes in the risk of death after HIV seroconversion compared with mortality in the general population. *JAMA,* 300**,** 51-9.

BINIENDA, Z., SIMMONS, C., HUSSAIN, S., SLIKKER, W., JR. & ALI, S. F. 1998. Effect of acute exposure to 3-nitropropionic acid on activities of endogenous antioxidants in the rat brain. *Neurosci Lett,* 251**,** 173-6.

BOCCACCIO, A., SCHOLZ-STARKE, J., HAMAMOTO, S., LARISCH, N., FESTA, M., GUTLA, P. V., COSTA, A., DIETRICH, P., UOZUMI, N. & CARPANETO, A. 2014. The phosphoinositide PI(3,5)P(2) mediates activation of mammalian but not plant TPC proteins: functional expression of endolysosomal channels in yeast and plant cells. *Cell Mol Life Sci,* 71**,** 4275-83.

BOR, D. H., WOOLHANDLER, S., NARDIN, R., BRUSCH, J. & HIMMELSTEIN, D. U. 2013. Infective Endocarditis in the U.S., 1998–2009: A Nationwide Study. *PLoS One.*

BORDET, T., BERNA, P., ABITBOL, J.-L. & PRUSS, R. M. 2010. Olesoxime (TRO19622): A Novel Mitochondrial-Targeted Neuroprotective Compound. *Pharmaceuticals (Basel, Switzerland),* 3**,** 345-368.

BOVERIS, A. & CADENAS, E. 1975. Mitochondrial production of superoxide anions and its relationship to the antimycin insensitive respiration. *FEBS Lett,* 54**,** 311-4.

BRAVO-SAGUA, R., TORREALBA, N., PAREDES, F., MORALES, P. E., PENNANEN, C., LOPEZ-CRISOSTO, C., TRONCOSO, R., CRIOLLO, A., CHIONG, M., HILL, J. A., SIMMEN, T., QUEST, A. F. & LAVANDERO, S. 2014. Organelle communication: signaling crossroads between homeostasis and disease. *Int J Biochem Cell Biol,* 50**,** 55-9.

BRENDA, C. 1898. *"Ueber die Spermatogenese der Vertebraten und höherer Evertebraten. II. Theil: Die Histiogenese der Spermien. Arch. Anal. Physiol.*

BREWER, G. J. 2007. Iron and copper toxicity in diseases of aging, particularly atherosclerosis and Alzheimer's disease. *Exp Biol Med (Maywood),* 232**,** 323-35.

BREWER, G. J., TORRICELLI, J. R., EVEGE, E. K. & PRICE, P. J. 1993. Optimized survival of hippocampal neurons in B27-supplemented Neurobasal, a new serum-free medium combination. *J Neurosci Res,* 35**,** 567-76.

BROOKES, P. S., YOON, Y., ROBOTHAM, J. L., ANDERS, M. W. & SHEU, S. S. 2004. Calcium, ATP, and ROS: a mitochondrial love-hate triangle. *Am J Physiol Cell Physiol,* 287**,** C817-33.

BRUCE-KELLER, A. J., CHAUHAN, A., DIMAYUGA, F. O., GEE, J., KELLER, J. N. & NATH, A. 2003. Synaptic transport of human immunodeficiency virus-Tat protein causes neurotoxicity and gliosis in rat brain. *J Neurosci,* 23**,** 8417-22.

BYSTROM, L. M., GUZMAN, M. L. & RIVELLA, S. 2014. Iron and reactive oxygen species: friends or foes of cancer cells? *Antioxidants & redox signaling,* 20**,** 1917-1924.

CABLE, H. & LLOYD, J. B. 1999. Cellular uptake and release of two contrasting iron chelators. *J Pharm Pharmacol,* 51**,** 131-4.

CALCRAFT, P. J., RUAS, M., PAN, Z., CHENG, X., ARREDOUANI, A., HAO, X., TANG, J., RIETDORF, K., TEBOUL, L., CHUANG, K. T., LIN, P., XIAO, R., WANG, C., ZHU, Y., LIN, Y., WYATT, C. N., PARRINGTON, J., MA, J., EVANS, A. M., GALIONE, A. & ZHU, M. X. 2009. NAADP mobilizes calcium from acidic organelles through two-pore channels. *Nature,* 459**,** 596-600.

CANG, C., ARANDA, K., SEO, Y. J., GASNIER, B. & REN, D. 2015. TMEM175 Is an Organelle K(+) Channel Regulating Lysosomal Function. *Cell,* 162**,** 1101-12.

CAO, Q., ZHONG, X. Z., ZOU, Y., ZHANG, Z., TORO, L. & DONG, X. P. 2015. BK Channels Alleviate Lysosomal Storage Diseases by Providing Positive Feedback Regulation of Lysosomal Ca2+ Release. *Dev Cell,* 33**,** 427-41.

CARROLL, C. B., ZEISSLER, M. L., CHADBORN, N., GIBSON, K., WILLIAMS, G., ZAJICEK, J. P., MORRISON, K. E. & HANEMANN, C. O. 2011. Changes in iron-regulatory gene expression occur in human cell culture models of Parkinson's disease. *Neurochemistry International,* 59**,** 73-80.

CHANCE, B., SIES, H. & BOVERIS, A. 1979. Hydroperoxide metabolism in mammalian organs. *Physiol Rev,* 59**,** 527-605.

CHAVEZ-CROOKER, P., GARRIDO, N. & AHEARN, G. A. 2001. Copper transport by lobster hepatopancreatic epithelial cells separated by centrifugal elutriation: measurements with the fluorescent dye Phen Green. *J Exp Biol,* 204**,** 1433-44.

CHEN, X., HUI, L., GEIGER, N. H., HAUGHEY, N. J. & GEIGER, J. D. 2013. Endolysosome involvement in HIV-1 transactivator protein-induced neuronal amyloid beta production. *Neurobiol Aging,* 34**,** 2370-8.

CHENG, X., ZHANG, X., GAO, Q., ALI SAMIE, M., AZAR, M., TSANG, W. L., DONG, L., SAHOO, N., LI, X., ZHUO, Y., GARRITY, A. G., WANG, X., FERRER, M., DOWLING, J., XU, L., HAN, R. & XU, H. 2014. The intracellular Ca2+ channel MCOLN1 is required for sarcolemma repair to prevent muscular dystrophy. *Nature Medicine,* 20**,** 1187.

CHRIST, W. J., ASANO, O., ROBIDOUX, A. L., PEREZ, M., WANG, Y., DUBUC, G. R., GAVIN, W. E., HAWKINS, L. D., MCGUINNESS, P. D., MULLARKEY, M. A. & ET AL. 1995. E5531, a pure endotoxin antagonist of high potency. *Science,* 268**,** 80-3.

CHRISTENSEN, K. A., MYERS, J. T. & SWANSON, J. A. 2002. pH-dependent regulation of lysosomal calcium in macrophages. *J Cell Sci,* 115**,** 599-607.

CLIFFORD, D. B. & ANCES, B. M. 2013. HIV-Associated Neurocognitive Disorder (HAND). *Lancet Infect Dis,* 13**,** 976-86.

COLACURCIO, D. J. & NIXON, R. A. 2016. Disorders of lysosomal acidification-The emerging role of v-ATPase in aging and neurodegenerative disease. *Ageing Res Rev,* 32**,** 75-88.

CONNER, S. D. & SCHMID, S. L. 2003. Regulated portals of entry into the cell. *Nature,* 422**,** 37-44.

CUNHA-OLIVEIRA, T., SILVA, L., SILVA, A. M., MORENO, A. J., OLIVEIRA, C. R. & SANTOS, M. S. 2013. Mitochondrial complex I dysfunction induced by cocaine and cocaine plus morphine in brain and liver mitochondria. *Toxicology Letters,* 219**,** 298-306.

DE DUVE, C. 2005. The lysosome turns fifty. *Nature Cell Biology,* 7**,** 847.

DEFELICE, L. J. & GOSWAMI, T. 2007. Transporters as channels. *Annu Rev Physiol,* 69**,** 87-112.

DI FIORE, P. P. & VON ZASTROW, M. 2014. Endocytosis, signaling, and beyond. *Cold Spring Harb Perspect Biol,* 6.

DIXON, S. J., LEMBERG, K. M., LAMPRECHT, M. R., SKOUTA, R., ZAITSEV, E. M., GLEASON, C. E., PATEL, D. N., BAUER, A. J., CANTLEY, A. M., YANG, W. S., MORRISON, B., 3RD & STOCKWELL, B. R. 2012. Ferroptosis: an iron-dependent form of nonapoptotic cell death. *Cell,* 149**,** 1060-72.

DONG, X. P., CHENG, X., MILLS, E., DELLING, M., WANG, F., KURZ, T. & XU, H. 2008. The type IV mucolipidosis-associated protein TRPML1 is an endolysosomal iron release channel. *Nature,* 455**,** 992-6.

DONG, X. P., WANG, X. & XU, H. 2010. TRP channels of intracellular membranes. *J Neurochem,* 113**,** 313-28.

DORN, G. W., 2ND, VEGA, R. B. & KELLY, D. P. 2015. Mitochondrial biogenesis and dynamics in the developing and diseased heart. *Genes Dev,* 29**,** 1981-91.

DOULIAS, P. T., CHRISTOFORIDIS, S., BRUNK, U. T. & GALARIS, D. 2003. Endosomal and lysosomal effects of desferrioxamine: protection of HeLa cells from hydrogen peroxide-induced DNA damage and induction of cell-cycle arrest. *Free Radic Biol Med,* 35**,** 719-28.

EATON, J. W. & QIAN, M. 2002. Molecular bases of cellular iron toxicity. *Free Radic Biol Med,* 32**,** 833-40.

EICHELSDOERFER, J. L., EVANS, J. A., SLAUGENHAUPT, S. A. & CUAJUNGCO, M. P. 2010. Zinc dyshomeostasis is linked with the loss of mucolipidosis IV-associated TRPML1 ion channel. *J Biol Chem,* 285**,** 34304-8.

ENNS, G. M. 2003. The contribution of mitochondria to common disorders. *Molecular Genetics and Metabolism,* 80**,** 11-26.

ERNSTER, L. & SCHATZ, G. 1981. Mitochondria: a historical review. *The Journal of cell biology,* 91**,** 227s-255s.

EVERALL, I. P., HEATON, R. K., MARCOTTE, T. D., ELLIS, R. J., MCCUTCHAN, J. A., ATKINSON, J. H., GRANT, I., MALLORY, M. & MASLIAH, E. 1999. Cortical synaptic density is reduced in mild to moderate human immunodeficiency virus neurocognitive disorder. HNRC Group. HIV Neurobehavioral Research Center. *Brain Pathol,* 9**,** 209-17.

FENTON, H. J. H. 1894. LXXIII.—Oxidation of tartaric acid in presence of iron. *Journal of the Chemical Society, Transactions,* 65**,** 899-910.

FERNÁNDEZ, B., FDEZ, E., GÓMEZ-SUAGA, P., GIL, F., MOLINA-VILLALBA, I., FERRER, I., PATEL, S., CHURCHILL, G. C. & HILFIKER, S. 2016a. Iron overload causes endolysosomal deficits modulated by NAADP-regulated 2-pore channels and RAB7A. *Autophagy.*

FERNÁNDEZ, B., FDEZ, E., GÓMEZ-SUAGA, P., GIL, F., MOLINA-VILLALBA, I., FERRER, I., PATEL, S., CHURCHILL, G. C. & HILFIKER, S. 2016b. Iron overload causes endolysosomal deficits modulated by NAADP-regulated 2-pore channels and RAB7A. *Autophagy,* 12**,** 1487-1506.

FESTA, L., GUTOSKEY, C. J., GRAZIANO, A., WATERHOUSE, B. D. & MEUCCI, O. 2015. Induction of Interleukin-1beta by Human Immunodeficiency Virus-1 Viral Proteins Leads to Increased Levels of Neuronal Ferritin Heavy Chain, Synaptic Injury, and Deficits in Flexible Attention. *J Neurosci,* 35**,** 10550-61.

FORGAC, M. 2007. Vacuolar ATPases: rotary proton pumps in physiology and pathophysiology. *Nat Rev Mol Cell Biol,* 8**,** 917-29.

FOSSLIEN, E. 2001. Mitochondrial medicine--molecular pathology of defective oxidative phosphorylation. *Ann Clin Lab Sci,* 31**,** 25-67.

FUTTER, C. E., PEARSE, A., HEWLETT, L. J. & HOPKINS, C. R. 1996. Multivesicular endosomes containing internalized EGF-EGF receptor complexes mature and then fuse directly with lysosomes. *The Journal of Cell Biology,* 132**,** 1011.

GELMAN, B. B., SOUKUP, V. M., HOLZER, C. E., 3RD, FABIAN, R. H., SCHUENKE, K. W., KEHERLY, M. J., RICHEY, F. J. & LAHART, C. J. 2005. Potential role for white matter lysosome expansion in HIV-associated dementia. *J Acquir Immune Defic Syndr,* 39**,** 422-5.

GOLDSTEIN, J. L. & BROWN, M. S. 2015. A century of cholesterol and coronaries: from plaques to genes to statins. *Cell,* 161**,** 161-172.

GRIFFITHS, K. K. & LEVY, R. J. 2017. Evidence of Mitochondrial Dysfunction in Autism: Biochemical Links, Genetic-Based Associations, and Non-Energy-Related Mechanisms. *Oxid Med Cell Longev,* 2017**,** 4314025.

HAMDI, A., ROSHAN, T. M., KAHAWITA, T. M., MASON, A. B., SHEFTEL, A. D. & PONKA, P. 2016. Erythroid cell mitochondria receive endosomal iron by a "kiss-and-run" mechanism. *Biochim Biophys Acta,* 1863**,** 2859-2867.

HAUGHEY, N. J., NATH, A., MATTSON, M. P., SLEVIN, J. T. & GEIGER, J. D. 2001. HIV-1 Tat through phosphorylation of NMDA receptors potentiates glutamate excitotoxicity. *J Neurochem,* 78**,** 457-67.

HEATON, R. K., FRANKLIN, D. R., ELLIS, R. J., MCCUTCHAN, J. A., LETENDRE, S. L., LEBLANC, S., CORKRAN, S. H., DUARTE, N. A., CLIFFORD, D. B., WOODS, S. P., COLLIER, A. C., MARRA, C. M., MORGELLO, S., MINDT, M. R., TAYLOR, M. J., MARCOTTE, T. D., ATKINSON, J. H., WOLFSON, T., GELMAN, B. B., MCARTHUR, J. C., SIMPSON, D. M., ABRAMSON, I., GAMST, A., FENNEMA-NOTESTINE, C., JERNIGAN, T. L., WONG, J., GRANT, I., GROUP, C. & GROUP, H. 2011. HIV-associated neurocognitive disorders before and during the era of combination antiretroviral therapy: differences in rates, nature, and predictors. *J Neurovirol,* 17**,** 3-16.

HIRAYAMA, T. 2018. Development of Chemical Tools for Imaging of Fe(II) Ions in Living Cells: A Review. *Acta Histochem Cytochem,* 51**,** 137-143.

HIRAYAMA, T., OKUDA, K. & NAGASAWA, H. 2013. *A highly selective turn-on fluorescent probe for iron(II) to visualize labile iron in living cells.*

HUANG, H., CHEN, J., LU, H., ZHOU, M., CHAI, Z. & HU, Y. 2017. Iron-induced generation of mitochondrial ROS depends on AMPK activity. *Biometals,* 30**,** 623-628.

HUGHES, A. L. & GOTTSCHLING, D. E. 2012. An early age increase in vacuolar pH limits mitochondrial function and lifespan in yeast. *Nature,* 492**,** 261-5.

HUI, L., CHEN, X. & GEIGER, J. D. 2012a. Endolysosome involvement in LDL cholesterol-induced Alzheimer's disease-like pathology in primary cultured neurons. *Life Sci,* 91**,** 1159-68.

HUI, L., CHEN, X., HAUGHEY, N. J. & GEIGER, J. D. 2012b. Role of endolysosomes in HIV-1 Tat-induced neurotoxicity. *ASN Neuro,* 4**,** 243-52.

HUI, L., GEIGER, N. H., BLOOR-YOUNG, D., CHURCHILL, G. C., GEIGER, J. D. & CHEN, X. 2015. Release of calcium from endolysosomes increases calcium influx through N-type calcium channels: Evidence for acidic store-operated calcium entry in neurons. *Cell Calcium,* 58**,** 617-27.

IMAM, S. Z. & ALI, S. F. 2000. Selenium, an antioxidant, attenuates methamphetamine-induced dopaminergic toxicity and peroxynitrite generation. *Brain Res,* 855**,** 186-91.

IMAM, S. Z. & ALI, S. F. 2001. Aging increases the susceptiblity to methamphetamine-induced dopaminergic neurotoxicity in rats: correlation with peroxynitrite production and hyperthermia. *J Neurochem,* 78**,** 952-9.

IMERYUZ, N., TAHAN, V., SONSUZ, A., EREN, F., URAZ, S., YUKSEL, M., AKPULAT, S., OZCELIK, D., HAKLAR, G., CELIKEL, C., AVSAR, E. & TOZUN, N. 2007. Iron preloading aggravates nutritional steatohepatitis in rats by increasing apoptotic cell death. *J Hepatol,* 47**,** 851-9.

ISHIBASHI, K., SUZUKI, M. & IMAI, M. 2000. Molecular cloning of a novel form (two-repeat) protein related to voltage-gated sodium and calcium channels. *Biochem Biophys Res Commun,* 270**,** 370-6.

ISHIDA, Y., NAYAK, S., MINDELL, J. A. & GRABE, M. 2013. A model of lysosomal pH regulation. *J Gen Physiol,* 141**,** 705-20.

JAESCHKE, H., GORES, G. J., CEDERBAUM, A. I., HINSON, J. A., PESSAYRE, D. & LEMASTERS, J. J. 2002. Mechanisms of hepatotoxicity. *Toxicol Sci,* 65**,** 166-76.

JAISWAL, J. K., ANDREWS, N. W. & SIMON, S. M. 2002. Membrane proximal lysosomes are the major vesicles responsible for calcium-dependent exocytosis in nonsecretory cells. *J Cell Biol,* 159**,** 625-35.

JELLINGER, K. A. 2009. Recent advances in our understanding of neurodegeneration. *J Neural Transm (Vienna),* 116**,** 1111-62.

JENSEN, P. K. 1966. Antimycin-insensitive oxidation of succinate and reduced nicotinamide-adenine dinucleotide in electron-transport particles. I. pH dependency and hydrogen peroxide formation. *Biochim Biophys Acta,* 122**,** 157-66.

JEZEGOU, A., LLINARES, E., ANNE, C., KIEFFER-JAQUINOD, S., O'REGAN, S., AUPETIT, J., CHABLI, A., SAGNE, C., DEBACKER, C., CHADEFAUX-VEKEMANS, B., JOURNET, A., ANDRE, B. & GASNIER, B. 2012. Heptahelical protein PQLC2 is a lysosomal cationic amino acid exporter underlying the action of cysteamine in cystinosis therapy. *Proc Natl Acad Sci U S A,* 109**,** E3434-43.

JOHRI, A. & BEAL, M. F. 2012. Mitochondrial dysfunction in neurodegenerative diseases. *J Pharmacol Exp Ther,* 342**,** 619-30.

KALINOWSKI, D. S. & RICHARDSON, D. R. 2007. Future of toxicology--iron chelators and differing modes of action and toxicity: the changing face of iron chelation therapy. *Chem Res Toxicol,* 20**,** 715-20.

KASPER, D., PLANELLS-CASES, R., FUHRMANN, J. C., SCHEEL, O., ZEITZ, O., RUETHER, K., SCHMITT, A., POET, M., STEINFELD, R., SCHWEIZER, M., KORNAK, U. & JENTSCH, T. J. 2005. Loss of the chloride channel ClC-7 leads to lysosomal storage disease and neurodegeneration. *Embo j,* 24**,** 1079-91.

KAUR, J. & DEBNATH, J. 2015. Autophagy at the crossroads of catabolism and anabolism. *Nat Rev Mol Cell Biol,* 16**,** 461-72.

KEBERLE, H. 1964. THE BIOCHEMISTRY OF DESFERRIOXAMINE AND ITS RELATION TO IRON METABOLISM. *Ann N Y Acad Sci,* 119**,** 758-68.

KEHRER, J. P. 2000. The Haber-Weiss reaction and mechanisms of toxicity. *Toxicology,* 149**,** 43-50.

KISELYOV, K., COLLETTI, G. A., TERWILLIGER, A., KETCHUM, K., LYONS, C. W., QUINN, J. & MUALLEM, S. 2011. TRPML: transporters of metals in lysosomes essential for cell survival? *Cell Calcium,* 50**,** 288-94.

KOPPENOL, W. H. 2001. The Haber-Weiss cycle – 70 years later. *Redox Report,* 6**,** 229-234.

KOVALEVICH, J. & LANGFORD, D. 2012. Neuronal toxicity in HIV CNS disease. *Future Virol,* 7**,** 687-698.

KTISTAKIS, N. T. & TOOZE, S. A. 2016. Digesting the Expanding Mechanisms of Autophagy. *Trends Cell Biol,* 26**,** 624-635.

KUMFU, S., CHATTIPAKORN, S., FUCHAROEN, S. & CHATTIPAKORN, N. 2012. Mitochondrial calcium uniporter blocker prevents cardiac mitochondrial dysfunction induced by iron overload in thalassemic mice. *Biometals,* 25**,** 1167-75.

KURZ, T., EATON, J. W. & BRUNK, U. T. 2011. The role of lysosomes in iron metabolism and recycling. *Int J Biochem Cell Biol,* 43**,** 1686-97.

LAFOURCADE, C., SOBO, K., KIEFFER-JAQUINOD, S., GARIN, J. & VAN DER GOOT, F. G. 2008. Regulation of the V-ATPase along the Endocytic Pathway Occurs through Reversible Subunit Association and Membrane Localization. *PLOS ONE,* 3**,** e2758.

LANGE, P. F., WARTOSCH, L., JENTSCH, T. J. & FUHRMANN, J. C. 2006. ClC-7 requires Ostm1 as a beta-subunit to support bone resorption and lysosomal function. *Nature,* 440**,** 220-3.

LELLOUCH, A. 1993. [Metchnikoff (1845-1916) and aging]. *Hist Sci Med,* 27**,** 13-22.

LESNEFSKY, E. J., MOGHADDAS, S., TANDLER, B., KERNER, J. & HOPPEL, C. L. 2001. Mitochondrial Dysfunction in Cardiac Disease: Ischemia–Reperfusion, Aging, and Heart Failure. *Journal of Molecular and Cellular Cardiology,* 33**,** 1065-1089.

LINDL, K. A., AKAY, C., WANG, Y., WHITE, M. G. & JORDAN-SCIUTTO, K. L. 2007. Expression of the endoplasmic reticulum stress response marker, BiP, in the central nervous system of HIV-positive individuals. *Neuropathol Appl Neurobiol,* 33**,** 658-69.

LIU, B., DU, H., RUTKOWSKI, R., GARTNER, A. & WANG, X. 2012. LAAT-1 is the lysosomal lysine/arginine transporter that maintains amino acid homeostasis. *Science,* 337**,** 351-4.

LIU, Y., JONES, M., HINGTGEN, C. M., BU, G., LARIBEE, N., TANZI, R. E., MOIR, R. D., NATH, A. & HE, J. J. 2000. Uptake of HIV-1 tat protein mediated by low-density lipoprotein receptor-related protein disrupts the neuronal metabolic balance of the receptor ligands. *Nat Med,* 6**,** 1380-7.

LIU, Z. D. & HIDER, R. C. 2002. Design of clinically useful iron(III)-selective chelators. *Med Res Rev,* 22**,** 26-64.

LLOYD, J. B., CABLE, H. & RICE-EVANS, C. 1991a. Evidence that desferrioxamine cannot enter cells by passive diffusion. *Biochem Pharmacol,* 41**,** 1361-3.

LLOYD, J. B., CABLE, H. & RICE-EVANS, C. 1991b. Evidence that desferrioxamine cannot enter cells by passive diffusion. *Biochemical Pharmacology,* 41**,** 1361-1363.

LLOYD-EVANS, E., MORGAN, A. J., HE, X., SMITH, D. A., ELLIOT-SMITH, E., SILLENCE, D. J., CHURCHILL, G. C., SCHUCHMAN, E. H., GALIONE, A. & PLATT, F. M. 2008. Niemann-Pick disease type C1 is a sphingosine storage disease that causes deregulation of lysosomal calcium. *Nat Med,* 14**,** 1247-55.

LOPEZ, S. N., RODRIGUEZ-VALENTIN, M., RIVERA, M., RODRIGUEZ, M., BABU, M., CUBANO, L. A., XIONG, H., WANG, G., KUCHERYAVYKH, L. & BOUKLI, N. M. 2017. HIV-1 Gp120 clade B/C induces a GRP78 driven cytoprotective mechanism in astrocytoma. *Oncotarget,* 8**,** 68415-68438.

LOSCHEN, G., AZZI, A., RICHTER, C. & FLOHE, L. 1974. Superoxide radicals as precursors of mitochondrial hydrogen peroxide. *FEBS Lett,* 42**,** 68-72.

LUZIO, J. P., BRIGHT, N. A. & PRYOR, P. R. 2007. The role of calcium and other ions in sorting and delivery in the late endocytic pathway. *Biochem Soc Trans,* 35**,** 1088-91.

LUZIO, J. P., ROUS, B. A., BRIGHT, N. A., PRYOR, P. R., MULLOCK, B. M. & PIPER, R. C. 2000. Lysosome-endosome fusion and lysosome biogenesis. *J Cell Sci,* 113 (Pt 9)**,** 1515-24.

MACKENZIE, B. & ERICKSON, J. D. 2004. Sodium-coupled neutral amino acid (System N/A) transporters of the SLC38 gene family. *Pflugers Arch,* 447**,** 784-95.

MASLIAH, E., HEATON, R. K., MARCOTTE, T. D., ELLIS, R. J., WILEY, C. A., MALLORY, M., ACHIM, C. L., MCCUTCHAN, J. A., NELSON, J. A., ATKINSON, J. H. & GRANT, I. 1997. Dendritic injury is a pathological substrate for human immunodeficiency virus-related cognitive disorders. HNRC Group. The HIV Neurobehavioral Research Center. *Ann Neurol,* 42**,** 963-72.

MCBRIDE, H. M., NEUSPIEL, M. & WASIAK, S. 2006. Mitochondria: more than just a powerhouse. *Curr Biol,* 16**,** R551-60.

MCKENNA, M. C., SCHUCK, P. F. & FERREIRA, G. C. 2018. Fundamentals of CNS energy metabolism and alterations in lysosomal storage diseases. *J Neurochem*.

MEDINA, D. L., FRALDI, A., BOUCHE, V., ANNUNZIATA, F., MANSUETO, G., SPAMPANATO, C., PURI, C., PIGNATA, A., MARTINA, J. A., SARDIELLO, M., PALMIERI, M., POLISHCHUK, R., PUERTOLLANO, R. & BALLABIO, A. 2011. Transcriptional activation of lysosomal exocytosis promotes cellular clearance. *Dev Cell,* 21**,** 421-30.

MELLMAN, I. 1996. ENDOCYTOSIS AND MOLECULAR SORTING. *Annual Review of Cell and Developmental Biology,* 12**,** 575-625.

MENA, N. P., URRUTIA, P. J., LOURIDO, F., CARRASCO, C. M. & NÚÑEZ, M. T. 2015. Mitochondrial iron homeostasis and its dysfunctions in neurodegenerative disorders. *Mitochondrion,* 21**,** 92-105.

MILLS, E., DONG, X. P., WANG, F. & XU, H. 2010. Mechanisms of brain iron transport: insight into neurodegeneration and CNS disorders. *Future Med Chem,* 2**,** 51-64.

MINDELL, J. A. 2012a. Lysosomal acidification mechanisms. *Annu Rev Physiol,* 74**,** 69-86.

MINDELL, J. A. 2012b. Lysosomal Acidification Mechanisms. *Annual Review of Physiology,* 74**,** 69-86.

MIZUSHIMA, N. & KOMATSU, M. 2011. Autophagy: renovation of cells and tissues. *Cell,* 147**,** 728-41.

MOBARRA, N., SHANAKI, M., EHTERAM, H., NASIRI, H., SAHMANI, M., SAEIDI, M., GOUDARZI, M., POURKARIM, H. & AZAD, M. 2016. A Review on Iron Chelators in Treatment of Iron Overload Syndromes. *International journal of hematology-oncology and stem cell research,* 10**,** 239-247.

MORGAN, A. J., PLATT, F. M., LLOYD-EVANS, E. & GALIONE, A. 2011. Molecular mechanisms of endolysosomal Ca2+ signalling in health and disease. *Biochem J,* 439**,** 349-74.

MORGAN, E. H. 1981. Transferrin, biochemistry, physiology and clinical significance. *Molecular Aspects of Medicine,* 4**,** 1-123.

MOTULSKY, A. G. 1986. The 1985 Nobel Prize in physiology or medicine. *Science,* 231**,** 126-9.

MUKAIDE, T., HATTORI, Y., MISAWA, N., FUNAHASHI, S., JIANG, L., HIRAYAMA, T., NAGASAWA, H. & TOYOKUNI, S. 2014. Histological detection of catalytic ferrous iron with the selective turn-on fluorescent probe RhoNox-1 in a Fenton reaction-based rat renal carcinogenesis model. *Free Radic Res,* 48**,** 990-5.

MULLER, F. 2000. The nature and mechanism of superoxide production by the electron transport chain: Its relevance to aging. *J Am Aging Assoc,* 23**,** 227-53.

MURPHY, M. P. 2009. How mitochondria produce reactive oxygen species. *The Biochemical journal,* 417**,** 1-13.

NATH, A., PADUA, R. A. & GEIGER, J. D. 1995. HIV-1 coat protein gp120-induced increases in levels of intrasynaptosomal calcium. *Brain Res,* 678**,** 200-6.

NEKHAI, S., KUMARI, N. & DHAWAN, S. 2013. Role of cellular iron and oxygen in the regulation of HIV-1 infection. *Future Virol,* 8**,** 301-11.

NIWA, M., HIRAYAMA, T., OKUDA, K. & NAGASAWA, H. 2014. A new class of high-contrast Fe(II) selective fluorescent probes based on spirocyclized scaffolds for visualization of intracellular labile iron delivered by transferrin. *Org Biomol Chem,* 12**,** 6590-7.

OGISHI, M. & YOTSUYANAGI, H. 2018. Prediction of HIV-associated neurocognitive disorder (HAND) from three genetic features of envelope gp120 glycoprotein. *Retrovirology,* 15**,** 12.

OHGAMI, R. S., CAMPAGNA, D. R., MCDONALD, A. & FLEMING, M. D. 2006. The Steap proteins are metalloreductases. *Blood,* 108**,** 1388.

PADMANABHAN, H., BROOKES, M. J. & IQBAL, T. 2015. Iron and colorectal cancer: evidence from in vitro and animal studies. *Nutr Rev,* 73**,** 308-17.

PELIZZONI, I., MACCO, R., MORINI, M. F., ZACCHETTI, D., GROHOVAZ, F. & CODAZZI, F. 2011. Iron handling in hippocampal neurons: activity-dependent iron entry and mitochondria-mediated neurotoxicity. *Aging Cell,* 10**,** 172-83.

PERERA, R. M. & ZONCU, R. 2016. The Lysosome as a Regulatory Hub. *Annu Rev Cell Dev Biol,* 32**,** 223-253.

PETERSEN, D. R. 2005. Alcohol, iron-associated oxidative stress, and cancer. *Alcohol,* 35**,** 243-9.

PETRAT, F., DE GROOT, H., SUSTMANN, R. & RAUEN, U. 2002. The chelatable iron pool in living cells: a methodically defined quantity. *Biol Chem,* 383**,** 489-502.

PETRAT, F., RAUEN, U. & DE GROOT, H. 1999. Determination of the chelatable iron pool of isolated rat hepatocytes by digital fluorescence microscopy using the fluorescent probe, phen green SK. *Hepatology,* 29**,** 1171-9.

PITCHER, J., ABT, A., MYERS, J., HAN, R., SNYDER, M., GRAZIANO, A., FESTA, L., KUTZLER, M., GARCIA, F., GAO, W. J., FISCHER-SMITH, T., RAPPAPORT, J. & MEUCCI, O. 2014. Neuronal ferritin heavy chain and drug abuse affect HIV-associated cognitive dysfunction. *J Clin Invest,* 124**,** 656-69.

PLOTEGHER, N. & DUCHEN, M. R. 2017. Mitochondrial Dysfunction and Neurodegeneration in Lysosomal Storage Disorders. *Trends Mol Med,* 23**,** 116-134.

PU, J., GUARDIA, C. M., KEREN-KAPLAN, T. & BONIFACINO, J. S. 2016. Mechanisms and functions of lysosome positioning. *Journal of cell science,* 129**,** 4329-4339.

RAUEN, U., SPRINGER, A., WEISHEIT, D., PETRAT, F., KORTH, H. G., DE GROOT, H. & SUSTMANN, R. 2007. Assessment of chelatable mitochondrial iron by using mitochondrion-selective fluorescent iron indicators with different iron-binding affinities. *Chembiochem,* 8**,** 341-52.

RICHARDSON, D. R., KALINOWSKI, D. S., LAU, S., JANSSON, P. J. & LOVEJOY, D. B. 2009. Cancer cell iron metabolism and the development of potent iron chelators as anti-tumour agents. *Biochim Biophys Acta,* 1790**,** 702-17.

RICHARDSON, D. R. & PONKA, P. 1997. The molecular mechanisms of the metabolism and transport of iron in normal and neoplastic cells. *Biochimica et Biophysica Acta - Reviews on Biomembranes,* 1331**,** 1-40.

RIGOBELLO, M. P., SCUTARI, G., BOSCOLO, R. & BINDOLI, A. 2002. Induction of mitochondrial permeability transition by auranofin, a gold(I)-phosphine derivative. *British journal of pharmacology,* 136**,** 1162-1168.

RIVERO-RIOS, P., FERNANDEZ, B., MADERO-PEREZ, J., LOZANO, M. R. & HILFIKER, S. 2016. Two-Pore Channels and Parkinson's Disease: Where's the Link? *Messenger (Los Angel),* 5**,** 67-75.

ROCKFIELD, S., RAFFEL, J., MEHTA, R., REHMAN, N. & NANJUNDAN, M. 2017. Iron overload and altered iron metabolism in ovarian cancer. *Biol Chem,* 398**,** 995-1007.

RONG, Y., LIU, M., MA, L., DU, W., ZHANG, H., TIAN, Y., CAO, Z., LI, Y., REN, H., ZHANG, C., LI, L., CHEN, S., XI, J. & YU, L. 2012. Clathrin and phosphatidylinositol-4,5-bisphosphate regulate autophagic lysosome reformation. *Nat Cell Biol,* 14**,** 924-34.

ROUAULT, T. A. & TONG, W.-H. 2005. Iron–sulphur cluster biogenesis and mitochondrial iron homeostasis. *Nature Reviews Molecular Cell Biology,* 6**,** 345-351.

SACKTOR, N., MCDERMOTT, M. P., MARDER, K., SCHIFITTO, G., SELNES, O. A., MCARTHUR, J. C., STERN, Y., ALBERT, S., PALUMBO, D., KIEBURTZ, K., DE MARCAIDA, J. A., COHEN, B. & EPSTEIN, L. 2002. HIV-associated cognitive impairment before and after the advent of combination therapy. *J Neurovirol,* 8**,** 136-42.

SAGNE, C., AGULHON, C., RAVASSARD, P., DARMON, M., HAMON, M., EL MESTIKAWY, S., GASNIER, B. & GIROS, B. 2001. Identification and characterization of a lysosomal transporter for small neutral amino acids. *Proc Natl Acad Sci U S A,* 98**,** 7206-11.

SAITO, M., HANSON, P. I. & SCHLESINGER, P. 2007. Luminal chloride-dependent activation of endosome calcium channels: patch clamp study of enlarged endosomes. *J Biol Chem,* 282**,** 27327-33.

SCHWABE, R. F. & BRENNER, D. A. 2006. Mechanisms of Liver Injury. I. TNF-alpha-induced liver injury: role of IKK, JNK, and ROS pathways. *Am J Physiol Gastrointest Liver Physiol,* 290**,** G583-9.

SCUTARI, R., ALTERI, C., PERNO, C. F., SVICHER, V. & AQUARO, S. 2017. The Role of HIV Infection in Neurologic Injury. *Brain Sci,* 7.

SENGUPTA, R., BURBASSI, S., SHIMIZU, S., CAPPELLO, S., VALLEE, R. B., RUBIN, J. B. & MEUCCI, O. 2009. Morphine increases brain levels of ferritin heavy chain leading to inhibition of CXCR4-mediated survival signaling in neurons. *J Neurosci,* 29**,** 2534-44.

SETTEMBRE, C. & BALLABIO, A. 2013. New targets for old diseases: lessons from mucolipidosis type II. *EMBO Mol Med,* 5**,** 1801-3.

SETTEMBRE, C., FRALDI, A., MEDINA, D. L. & BALLABIO, A. 2013. Signals from the lysosome: a control centre for cellular clearance and energy metabolism. *Nat Rev Mol Cell Biol,* 14**,** 283-96.

SHIMIZU, S., ABT, A. & MEUCCI, O. 2011. Bilaminar co-culture of primary rat cortical neurons and glia. *J Vis Exp.*

SIEKEVITZ, P. 1957. Powerhouse of the Cell. *Scientific American,* 197**,** 131-144.

SRIPETCHWANDEE, J., KENKNIGHT, S. B., SANIT, J., CHATTIPAKORN, S. & CHATTIPAKORN, N. 2014. Blockade of mitochondrial calcium uniporter prevents cardiac mitochondrial dysfunction caused by iron overload. *Acta Physiol (Oxf),* 210**,** 330-41.

STARKE, P. E. & FARBER, J. L. 1985. Ferric iron and superoxide ions are required for the killing of cultured hepatocytes by hydrogen peroxide. Evidence for the participation of hydroxyl radicals formed by an iron-catalyzed Haber-Weiss reaction. *J Biol Chem,* 260**,** 10099-104.

STAUBER, T. & JENTSCH, T. J. 2013. Chloride in vesicular trafficking and function. *Annu Rev Physiol,* 75**,** 453-77.

STEHLING, O., MASCARENHAS, J., VASHISHT, AJAY A., SHEFTEL, ALEX D., NIGGEMEYER, B., RÖSSER, R., PIERIK, ANTONIO J., WOHLSCHLEGEL, JAMES A. & LILL, R. 2013. Human CIA2A-FAM96A and CIA2B-FAM96B Integrate Iron Homeostasis and Maturation of Different Subsets of Cytosolic-Nuclear Iron-Sulfur Proteins. *Cell Metabolism,* 18**,** 187-198.

STEINBERG, B. E., HUYNH, K. K., BRODOVITCH, A., JABS, S., STAUBER, T., JENTSCH, T. J. & GRINSTEIN, S. 2010. A cation counterflux supports lysosomal acidification. *J Cell Biol,* 189**,** 1171-86.

STEINMAN, R. M., MELLMAN, I. S., MULLER, W. A. & COHN, Z. A. 1983. Endocytosis and the recycling of plasma membrane. *J Cell Biol,* 96**,** 1-27.

STEPHANS, S. E., WHITTINGHAM, T. S., DOUGLAS, A. J., LUST, W. D. & YAMAMOTO, B. K. 1998. Substrates of energy metabolism attenuate methamphetamine-induced neurotoxicity in striatum. *J Neurochem,* 71**,** 613-21.

STOORVOGEL, W., STROUS, G. J., GEUZE, H. J., OORSCHOT, V. & SCHWARTZT, A. L. 1991. Late endosomes derive from early endosomes by maturation. *Cell,* 65**,** 417-427.

SWANSON, C. A. 2003. Iron intake and regulation: implications for iron deficiency and iron overload. *Alcohol,* 30**,** 99-102.

TAPIERO, H. & TEW, K. D. 2003. Trace elements in human physiology and pathology: zinc and metallothioneins. *Biomed Pharmacother,* 57**,** 399-411.

TAPPER, H. & SUNDLER, R. 1995. Bafilomycin A1 inhibits lysosomal, phagosomal, and plasma membrane H(+)-ATPase and induces lysosomal enzyme secretion in macrophages. *J Cell Physiol,* 163**,** 137-44.

THOMAS, F., SERRATRICE, G., BEGUIN, C., AMAN, E. S., PIERRE, J. L., FONTECAVE, M. & LAULHERE, J. P. 1999. Calcein as a fluorescent probe for ferric iron. Application to iron nutrition in plant cells. *J Biol Chem,* 274**,** 13375-83.

TOGGAS, S. M., MASLIAH, E. & MUCKE, L. 1996. Prevention of HIV-1 gp120-induced neuronal damage in the central nervous system of transgenic mice by the NMDA receptor antagonist memantine. *Brain Res,* 706**,** 303-7.

TURCHAN, J., POCERNICH, C. B., GAIROLA, C., CHAUHAN, A., SCHIFITTO, G., BUTTERFIELD, D. A., BUCH, S., NARAYAN, O., SINAI, A., GEIGER, J., BERGER, J. R., ELFORD, H. & NATH, A. 2003. Oxidative stress in HIV demented patients and protection ex vivo with novel antioxidants. *Neurology,* 60**,** 307-14.

UCHIYAMA, A., KIM, J. S., KON, K., JAESCHKE, H., IKEJIMA, K., WATANABE, S. & LEMASTERS, J. J. 2008. Translocation of iron from lysosomes into mitochondria is a key event during oxidative stress-induced hepatocellular injury. *Hepatology,* 48**,** 1644-54.

URRUTIA, P. J., MENA, N. P. & NUNEZ, M. T. 2014. The interplay between iron accumulation, mitochondrial dysfunction, and inflammation during the execution step of neurodegenerative disorders. *Front Pharmacol,* 5**,** 38.

VALENTÍN-GUILLAMA, G., LÓPEZ, S., KUCHERYAVYKH, Y. V., CHORNA, N. E., PÉREZ, J., ORTIZ-RIVERA, J., INYUSHIN, M., MAKAROV, V., VALENTÍN-ACEVEDO, A., QUINONES-HINOJOSA, A., BOUKLI, N. & KUCHERYAVYKH, L. Y. 2018. HIV-1 Envelope Protein gp120 Promotes Proliferation and the Activation of Glycolysis in Glioma Cell. *Cancers (Basel).*

VIDELA, L. A., FERNANDEZ, V., TAPIA, G. & VARELA, P. 2003. Oxidative stress-mediated hepatotoxity of iron and copper: role of Kupffer cells. *Biometals,* 16**,** 103-11.

VIVIANI, B., CORSINI, E., BINAGLIA, M., GALLI, C. L. & MARINOVICH, M. 2001. Reactive oxygen species generated by glia are responsible for neuron death induced by human immunodeficiency virus-glycoprotein 120 in vitro. *Neuroscience,* 107**,** 51-8.

WANG, S., TSUN, Z. Y., WOLFSON, R. L., SHEN, K., WYANT, G. A., PLOVANICH, M. E., YUAN, E. D., JONES, T. D., CHANTRANUPONG, L., COMB, W., WANG, T., BAR-PELED, L., ZONCU, R., STRAUB, C., KIM, C., PARK, J., SABATINI, B. L. & SABATINI, D. M. 2015. Metabolism. Lysosomal amino acid transporter SLC38A9 signals arginine sufficiency to mTORC1. *Science,* 347**,** 188-94.

WANG, X., ZHANG, X., DONG, X. P., SAMIE, M., LI, X., CHENG, X., GOSCHKA, A., SHEN, D., ZHOU, Y., HARLOW, J., ZHU, M. X., CLAPHAM, D. E., REN, D. & XU, H. 2012. TPC proteins are phosphoinositide- activated sodium-selective ion channels in endosomes and lysosomes. *Cell,* 151**,** 372-83.

WATTS, C. 2012. The endosome-lysosome pathway and information generation in the immune system. *Biochim Biophys Acta,* 1824**,** 14-21.

WEISIGER, R. A. & FRIDOVICH, I. 1973. Superoxide dismutase. Organelle specificity. *J Biol Chem,* 248**,** 3582-92.

WEISS, F. H. A. J. 1934. The catalytic decomposition of hydrogen peroxide by iron salts. Royal Society.

WONG, C. O., LI, R., MONTELL, C. & VENKATACHALAM, K. 2012. Drosophila TRPML is required for TORC1 activation. *Curr Biol,* 22**,** 1616-21.

XIONG, J. & ZHU, M. X. 2016a. Regulation of lysosomal ion homeostasis by channels and transporters. *Sci China Life Sci,* 59**,** 777-91.

XIONG, J. & ZHU, M. X. 2016b. Regulation of lysosomal ion homeostasis by channels and transporters. *Science China. Life sciences,* 59**,** 777-791.

XU, H. & REN, D. 2015. Lysosomal Physiology. *Annual Review of Physiology,* 77**,** 57-80.

XU, J., TIAN, W., MA, X., GUO, J., SHI, Q., JIN, Y., XI, J. & XU, Z. 2011. The Molecular Mechanism Underlying Morphine-Induced Akt Activation: Roles of Protein Phosphatases and Reactive Oxygen Species. *Cell Biochemistry and Biophysics,* 61**,** 303-311.

YOSHIMORI, T., YAMAMOTO, A., MORIYAMA, Y., FUTAI, M. & TASHIR, Y. 1991. Bafilomycin AI, a Specific Inhibitor of Vacuolar-type H+-ATPase, Inhibits Acidification and Protein Degradation in Lysosomes of Cultured Cells. THE JOURNAL OF BIOLOGICAL CHEMISTRY
.
ZECCA, L., YOUDIM, M. B., RIEDERER, P., CONNOR, J. R. & CRICHTON, R. R. 2004. Iron, brain ageing and neurodegenerative disorders. *Nat Rev Neurosci,* 5**,** 863-73.

ZHANG, X., CHENG, X., YU, L., YANG, J., CALVO, R., PATNAIK, S., HU, X., GAO, Q., YANG, M., LAWAS, M., DELLING, M., MARUGAN, J., FERRER, M. & XU, H. 2016. MCOLN1 is a ROS sensor in lysosomes that regulates autophagy. *Nat Commun,* 7**,** 12109.

ZHARKICH, I. L., NADEEV, A. D., TSITRIN, E. B., GONCHAROV, N. V. & AVDONIN, P. V. 2016. Suppression of Histamine-Induced Relaxation of Rat Aorta and Calcium Signaling in Endothelial Cells by Two-Pore Channel Blocker trans-NED19 and Hydrogen Peroxide. *Izv Akad Nauk Ser Biol*, 430-438.

APPENDIX

Abbreviations

ATP	Adenosine Triphosphate
AF	Auranofin
BAF	Bafilomycin A1
CSA	Cyclosporin A
CQ	Chloroquine
DFO	Deferoxamine
DMEM	Dulbecco's Modified Eagle's Medium
EEA1	Early Endolysosomes
FAC	Ferric Ammonium Citrate
Fe^{2+}	Ferrous Iron
Fe^{3+}	Ferric Iron
GPN	Glycyl-l-Phenylalanine 2-Naphthylamide
Gp120	Glycoprotein 120
HAND	HIV-Associated Neurocognitive Disorders
HO	Hydroxyl Radical
H_2O_2	Hydrogen Peroxide

ISC	Iron-Sulfur Clusters
LAMP1	Late Endosomes/Lysosomes
MFI	Mean Fluorescent Intensity
MnSOD	Manganese Superoxide Dismutase
MOR	Morphine
MPTP	Mitochondrial Permeability Transition Pores
NAADP	Nicotinic Acid Adenine Dinucleotide Phosphate
O_2	Oxygen
O_2^-	Superoxide
PI	Propidium Iodide
RDA	Rhodamine B 4-[(2,2'-bipyridin-4-yl)Aminocarbonyl]Benzyl Ester
ROS	Reactive Oxygen Species
SOD	Superoxide Dismutase
TPC	Two-Pore Channls
TAT	Trans-activator of Transcription Protein
TRPML	Transient Receptor Potential Mucolipin
U87MG	Glioblastoma